AD_____

Award Number: DAMD17-99-1-9490

TITLE: Anti-Excitotoxic and Antioxidant TGF-Beta Family Neurotrophic Factors: In Vitro Screening Models of Motor Neuron Degeneration

PRINCIPAL INVESTIGATOR: Jeffrey D. Rothstein, M.D., Ph.D.

CONTRACTING ORGANIZATION: The Johns Hopkins University
Baltimore, Maryland 21205

REPORT DATE: July 2002

TYPE OF REPORT: Final

PREPARED FOR: U.S. Army Medical Research and Materiel Command
Fort Detrick, Maryland 21702-5012

REPORT DOCUMENTATION PAGE

Form Approved
OMB No. 074-0188

1. AGENCY USE ONLY (Leave blank)	2. REPORT DATE	3. REPORT TYPE AND DATES COVERED
	July 2002	Final (1 Jun 99 - 31 May 02)

4. TITLE AND SUBTITLE
Anti-Excitotoxic and Antioxidant TGF-Beta Family Neurotrophic Factors: In Vitro Screening Models of Motor Neuron Degeneration

5. FUNDING NUMBERS
DAMD17-99-1-9490

6. AUTHOR(S)
Jeffrey D. Rothstein, M.D., Ph.D.

7. PERFORMING ORGANIZATION NAME(S) AND ADDRESS(ES)

The Johns Hopkins University
Baltimore, Maryland 21205

E-Mail: jrothste@welchlink.welch.jhu.edu

8. PERFORMING ORGANIZATION REPORT NUMBER

9. SPONSORING / MONITORING AGENCY NAME(S) AND ADDRESS(ES)

U.S. Army Medical Research and Materiel Command
Fort Detrick, Maryland 21702-5012

10. SPONSORING / MONITORING AGENCY REPORT NUMBER

11. SUPPLEMENTARY NOTES

12a. DISTRIBUTION / AVAILABILITY STATEMENT

Approved for Public Release; Distribution Unlimited

12b. DISTRIBUTION CODE

13. ABSTRACT ***(Maximum 200 Words)***

TGFß-like trophic factors have been shown to be protective in acute neuronal injury paradigms. In the current studies, we analyzed and compared members of this growing family, including GDNF, neurturin, nodal, persephin, TGFß1 as well as neuroimmunophilin ligand GPI-1046, for protection against chronic glutamate toxicity and the mechanisms for protection. In parallel, we developed a novel organotypic spinal cord culture system to study the ability of these factors to promote motor axon outgrowth. Using these systems, we were able to differentiate the neuroprotective effect of the TGFß-like factors from their motor axon outgrowth-promoting activity. GDNF, neurturin, persephin, and nodal all protect against excitotoxic motor neuron degeneration. Low amounts of GDNF (1 ng/ml) and high concentrations of neurturin induced vigorous motor axon outgrowth. In contrast, nodal, persephin and TGFß1 did not induce motor axon outgrowth. Finally, we have ascertained that the neuroprotective properties of some of these compounds (GDNF and GPI-1046) may lie in their ability to induce rapidly synthesis of the glutamate transporter EAAT2.

14. SUBJECT TERMS	15. NUMBER OF PAGES
neurotoxin, acute neuronal injury paradigms, organotypic spinal cord culture system, motor axon outgrowth	70
	16. PRICE CODE

17. SECURITY CLASSIFICATION OF REPORT	18. SECURITY CLASSIFICATION OF THIS PAGE	19. SECURITY CLASSIFICATION OF ABSTRACT	20. LIMITATION OF ABSTRACT
Unclassified	Unclassified	Unclassified	Unlimited

FOREWORD

Opinions, interpretations, conclusions and recommendations are those of the author and are not necessarily endorsed by the U.S. Army.

_X__ Where copyrighted material is quoted, permission has been obtained to use such material.

__X_ Where material from documents designated for limited distribution is quoted, permission has been obtained to use the material.

___ Citations of commercial organizations and trade names in this report do not constitute an official Department of Army endorsement or approval of the products or services of these organizations.

X In conducting research using animals, the investigator(s) adhered to the "Guide for the Care and Use of Laboratory Animals," prepared by the Committee on Care and use of Laboratory Animals of the Institute of Laboratory Resources, national Research Council (NIH Publication No. 86-23, Revised 1985).

N/A For the protection of human subjects, the investigator(s) adhered to policies of applicable Federal Law 45 CFR 46.

N/A In conducting research utilizing recombinant DNA technology, the investigator(s) adhered to current guidelines promulgated by the National Institutes of Health.

N/A In the conduct of research utilizing recombinant DNA, the investigator(s) adhered to the NIH Guidelines for Research Involving Recombinant DNA Molecules.

N/A In the conduct of research involving hazardous organisms, the investigator(s) adhered to the CDC-NIH Guide for Biosafety in Microbiological and Biomedical Laboratories.

PI - Signature Date

Table of Contents

Introduction

We will use two in vitro models relevant to neurodegeneration to investigate the neuroprotective potential of new TGF trophic factors and new synthetic immunophilin ligands. These agents will be studied in a model of chronic *excitotoxicity* and chronic *oxidative stress* using organotypic spinal cord cultures and in cultures prepared from transgenic mice with human SOD1 mutations. To date, this model has been relatively accurate in predicting agents with clinical efficacy in the fatal neurodegenerative disease amyotrophic lateral sclerosis (ALS; Lou Gehrig's disease). Furthermore, these models will enable the detection of new agents capable of inducing rapid motor axon growth.

Body

The original Aims for years 1-3 of the proposal included the following:

Aim 1. Neuroprotection: excitotoxicity. To determine if selected members of the TGF family of neurotrophic factors (neurturin, nodal, and GDNF) or other potent neurotrophic factors (e.g., carditropin-1) or small molecule synthetic factors (e.g. GPI-1046;Gilford) can prevent motor neuron degeneration in a model of chronic excitotoxicity.

A. To investigate the effects of selected TGF family trophic factors, GPI-1046 and carditropin-1 on motor neuron growth and survival in organotypic spinal cord cultures

B. To evaluate the neuroprotective properties of selected TGF family trophic factors, GPI-1046 and carditropin on motor neurons in a model of chronic excitotoxicity.

C. To investigate the mechanisms by which TGF trophic factors protect against excitotoxic motor neuron degeneration: alterations in glutamate receptor subunits that modulate calcium permeability (GluR2), and glutamate transporters.

Significance: These studies could serve as indicators of potent neuroprotectants and motor axon growth stimulation that have the potential to alter the course of ALS and/or repair motor axons after injury.

Aim 2. Neuroprotection: mutant SOD1. To determine if selected members of the TGFβ family of neurotrophic factors (neurturin, nodal, and GDNF) or other potent neurotrophic factors (e.g., carditropin-1) or small molecule synthetic factors (e.g. GPI-1046;Gilford) can prevent degeneration of motor neurons cultured from mice transgenic for mutant SOD1.

A. To investigate the effects of selected TGFβ family trophic factors, GPI-1046 and carditropin-1 on altering, in vitro, motor neuron degeneration from mice with human SOD1 mutations.
B. To investigate the mechanisms by which TGFβ trophic factors protect against motor neuron degeneration associated with the SOD1 mutations: modulation of

oxidative stress-induction of antioxidant protection systems and/or alterations in glutamate receptor subunits that modulate calcium permeability (GluR2).

Most of Aim 1 projects were addressed in the first year of this grant proposal, recently resulting in a publication[1] , and presentations at National meetings[2].

In Year two of the grant (this years report), the original proposal outlined plans to evaluate aims Aim 1C, Aim 2A, and Aim 2B. Most of the studies in those Aims were completed during the year and some of those results were presented at National meetings [2-6]. A manuscript based on that data is now being prepared for peer-review publication.

Neuroprotection in ALS Models and Excitotoxicity

In the first 2 years of this project we demonstrated that a novel nonimmunosuppressive immunophilin ligand, GPI-1046 was highly protective of motor neurons in an in-vitro model of excitotoxicity. The mechanism of this neuroprotective effect was unknown. We went on to show that the neuroprotective properties of GPI-1046 were due, in part, to up regulation of the glutamate transporter GLT-1.

As described last year, excessive accumulation of extracellular glutamate results in neuronal death. Termination of synaptic glutamate transmission and the prevention of excitotoxicity depend on rapid removal of glutamate by high affinity transporters. Of the 5 transporters expressed in the mammalian brain, EAAT2 (GLT-1) is the most abundant and responsible for the bulk of all glutamate transport, accounting for 80-95% of all transport activity (varying by brain region). This transporter plays a crucial role in the prevention of chronic glutamate neurotoxicity, and is markedly decreased in amyotrophic lateral sclerosis (ALS). Additional studies suggest abnormalities of EAAT2 may exist, to a lesser degree in Alzheimer's disease and Huntington's disease.

Induction of GLT1/EAAT2 by GPI-1046 and GDNF. Recent studies have shown that GLT-1 expression can be induced in-vitro by various factors. The immunophilin ligand GPI-1046 (3-(3-pyridyl)-1-propyl (2S)-1-(3,3-dimethyl-1,2-dioxopentyl)-2-pyrrolidinecarboxylate) is a synthetic, non-immunosuppressive derivative of FK506. In the spinal cord organotypic culture model of chronic excitotoxicity GPI-1046 exerts a potent neuroprotective effect on motor neuron survival. We found that in the same organotypic model GPI-1046 increases GLT-1 immunoreactivity by over 100%, and causes a similar increase in DHK-sensitive Na+-dependent glutamate uptake. We further demonstrated induction of GLT-1 expression and function in-vivo, by both, oral-dosing, and intraventricular infusion of rodents with this neuroimmunophilin ligand. We hypothesize that the neuroprotective properties of this agent may be due, in part, to stimulation of glutamate transporter expression and activity, and that such an induction may become a valuable therapeutic approach against excitotoxicity. In a similar fashion we were also able to show that GDNF induced GLT-1 expression by over 100%. We further demonstrated specific inductions in GLT-1 levels in several brain regions of male, Sprague Dawley rats following intraventricular infusion with GDNF. These studies are now being written up for publication

The glutamate transporter EAAT2 has been shown to be deficient in ALS and antisense knockdown of EAAT2 leads to motor neuron degeneration. As described above, our preliminary data suggested that GPI-1046 may increase expression of EAAT2 protein and function. We therefore studied the effect of GPI-1046 on survival and motor performance in the G93A transgenic mouse model of familial ALS. Two lines of transgenic mice, a high expresser (G1H+) and a low expresser (G1L/+) were used.

G1H/+ transgenic mice received a subcutaneous injection of either 20 mg/kg or 40 mg/kg of body weight of GPI-1046 on 5 days out of 7 from the age of 50 days. G1L/+ transgenic mice received an oral administration of 50 mg/kg of body weight of GPI1046 twice a day from the age of 150 days. The oral administration of GPI-1046 was able to significantly delay the onset of motor impairment (quantified by failure on rotorod) from 212.2+/-12.47 (n=14) to 234.1+/-10.65 (n=15) days of age (P= 0.048; one tail T-test) and thus extend the survival by approximately 12%. No significant changes were observed compared' with the control group in the high expressor line of mice. GPI-1046 may therefore have therapeutic potential in neurological diseases such as ALS, Alzheimer's disease, Parkinson's disease and stroke.

Glutamate Transporter Interacter Proteins. Since glutamate transport may be an important process to minimize glutamate toxicity, and the drugs described above provide one means to modulate this important protein, we have developed a program to identify proteins that interact and modify glutamate transporter activity. We recently completed such a screen and identified two such proteins, GTRAP (glutamate transporter associated proteins) that can potently stimulate neuronal glutamate transporters. This data is included in our recent publication[7-9].

FDA Screen- Drugs screen to identify Drugs capable of Stimulating Transporter Synthesis. Although not originally included in this grant proposal, identification of a range of drugs capable of stimulating EAAT2 synthesis may be useful therapeutically. Under the initiation of a short term project by NINDS, we recently completed a c=screen of 1040 FDA approved drugs and nutritional supplements The assay, based on slice cultures ofd spinal cord, was designed to determine if a particular agent, at a fixed concentration, could induce synthesis of EAAT2. The screen was completed in 6 months. From this assay, we detected 10 drugs capable of stimulating EAAT2 protein 3 to 6.5 fold compared to untreated controls. We will soon be examining whether these drugs induce transporter activity and can be neuroprotective in vitro in animal models of neurological disease (e.g. ALS transgenic ice). If we are successful, many of these compounds could readily be used clinically and could be examined in other models of neurodegenerative disease. (this work largely funded by NIH Supplement grant)[10-11]

Identification, Cloning and Analysis of the EAAT2 promoter. We have identified typical putative promoter elements that include CCAAT boxes, Sp 1 binding sites (GGGGCGGGG or CCCCGCCCC), E-box motifs (CACCTG, CAYGTG or CANNTG), binding sites for elements from the GATA family of transcription factors

(motifs that can affect kidney tissue expression), NF-κB, and binding sites for WT1 (GNGGGNGNG). Nucleotide repeat regions, poly(dA:dT) and poly(dG:dT), that are thought to affect transcription through conformational changes in the DNA structure were also found in the flanking sequence. Notably, cyclic AMP response elements (CREB binding domains) were also identified in this first 2.8 kb fragment. GLT-1/EAAT2 is known to be upregulated by cyclic AMP, which typically activates transcription thru cyclic AMP response elements (CREB). Several possible CREB promoter motifs were also found within the EAAT2 promoter.

Three regions from the 5' EAAT2 flanking region of the promoter were amplified by PCR and cloned into a promoterless luciferase reporter vector (pGL3, Promega). The constructs were transiently transfected into various cell lines eg. HEK 293T, COS7, C6 glioma, and luciferase activity was measured. The highest level of expression was obtained from COS7 cells. To control for transfection efficiency luciferase activities will be normalized with Renilla luciferase activity or β-galactosidase activity. All three fragment showed activity, with the greatest activity from the full length construct. In preliminary studies to determine if the promoter can drive expression of EAAT2, we packaged the 2.8 upstream fragment along with the EAAT2 cDNA. In transient transfection, EAAT2 protein can be measured from COS-7 cells containing this construct. (This work largely funded by patient donated gifts).

Overall Key Research Accomplishments:

- Identification of new TGFß1 neuroprotective factors (GDNF) for motor neuron toxicity.
- New methods to prevent motor neuron degeneration
- New agents to enhance motor axon growth- GDNF, Neurturin
- A new method to screen for drugs/factors capable of enhancing motor nerve growth (organotypic cultures)
- Extended survival in a transgenic mouse model of ALS by the neuroimmunophilin GPI-1046
- Identification of GTRAP41 and GTRAP48- positive modulators of glutamate transport.
- Development of a model to screen for dugs capable of inducing EAAT2/GLT-1 synthesis
- Identification of 10 related FDA approved drugs that potently stimulate EAAT2 synthesis.
- Identification of the EAAT2 Promoter

Reportable outcomes

1. TGFß-like trophic factors induce synthesis of glutamate transporter proteins. This discovery provides one possible mechanism for action of these agents in their neuroprotective profile discovered in our earlier work[1].

2. Neuroimmunophilin compounds are capable of inducing the synthesis of the predominant glutamate transporter EAAT2. This can occur even with oral delivery.

3. Neuroimmunophilin GPI-1046 can increase survival in an ALS transgenic model.

4. GTRAP41 and GTRAP48 are novel potent stimulators of cerebellar specific glutamate transport protein EAAT4.

Conclusions to date

Members of TGFß-like trophic factors family including GDNF, neurturin, persephin, nodal andTGFß1 can protect motor neurons against chronic glutamate toxicity. However, only GDNF and neurturin can induce motor axon outgrowth and this effect appears to be mediated through the RET receptor and the MAP kinase/PIK3 pathways. We have now learned that the neuroprotection afforded by these compounds may be due to their ability to induce the synthesis and activation of glutamate transporters. These compounds may be useful as potential therapeutic agents in treating neurodegenerative diseases such as ALS, Parkinson's disease and other disease in which glutamate excess may be a contributing factor. The axon growth stimulation of some of these compounds, as reported last year, may also have relevance in peripheral nerve injuries and spinal cord injury.

Compounds and proteins have been identified that can stimulate/regulate glutamate transporter function. These agents, in the future could serve as useful therapeutics to prevent neural degeneration associated with excess glutamate. Such diseases include Amyotrophic lateral sclerosis, Parkinson's disease, Alzheimer's disease. At least some of these compounds might sub serve other therapeutics- such as antiepileptics[12] and drugs capable of slowing brain tumor growth.

Final Conclusions- This study identified several different classes of drugs that can increase glutamate transporter protein and function. These drugs could prove very useful as a treatment to **slow down disease** in a number if neurological conditions including:

ALS
Parkinson's disease

Indirect additional benefits form some of these drugs could include:

Brain tumor (glioblastoma)
Epilepsy

References

1. Ho,T.W. *et al.* TGFbeta trophic factors differentially modulate motor axon outgrowth and protection from excitotoxicity. *Exp. Neurol* **161**, 664-675 (2000).

2. Ganel,R. *et al.* Excitotoxicity and neurodegeneration - a novel therapeutic approach. *Society for Neuroscience* **24**, 2069 (825.19) (1998).

3. R. Ganel, C. Coccia, J. Steiner, JD Rothstein. The neuroimmunophilin ligand GPI-1056 induces expression of the glutamate transporter EAAT2 (GLT-1) subtype. *Society for Neuroscience*, 25, Abstract 170.1 (1999)

4. C. Coccia, R. Ganel, JD Rothstein. GDNF induces an increase in EAAT2 (GLT-1) expression. *Society for Neuroscience*, 25, Abstract 170.2 (1999)

5. JD Rothstein, M. Jackson, C. Sakal, Dm Spicer, BD Kim, JP Steiner. GPI-1046, a novel non-immunosurpressant immunophilin ligand, delays the appearance of motor defifict in a transgenic mouse model of familial amyotrophic lateral sclersosis. *Society for Neuroscience*, 25, Abstract 638.5 (1999)

6. Ganel R *et al.* The neuroimmunophilin ligand GPI-1046 increases glutamate uptake and GLT-1 immunoreactivity in vitro and in vivo. *Society for Neuroscience* **26**,Abstract 539.3(2000)

7. Lin CLG, Orlov I, Ruggiero AM, Dykes-Hoberg M, Lee A, and Rothstein JD. Modulation of the neuronal glutamate transporter EAAC1 by an interacting protein GTRAP3-18. Nature, 2001, 410:84-88

8. Jackson M., Song W., Liu MY, Jin L., Dykes-Hoberg M., Lin CLG, Bowers WJ, Federoff HJ, Sternweis PC, Rothstein JD. Modulation of the neuronal glutamate transporter EAAT4 by two interacting proteins. Nature, 2001, 401:89-93.

9. CD Wells, MY Liu, M Jackson, S Gutowski, PM Sternweis, JD Rothstein, T Kozasa, PC Sternweis, Mechanisms for Reversible Regulation between G13 and Rho Exchange Factors. J. Biol. Chem., In Press. 2002.

10. Drachman,D.B., Rothstein,J.D. Inhibition of cyclooxygenase-2 protects motor neurons in an organotypic model of amyotrophic lateral sclerosis., Ann.Neurol 2000:792-795.

11. Melone M., Vitellaro Zuccarello L, Vallejo-Illarramendi A., Pérez-Samartin A., Matute C., Cozzi A., Pellegrini-Giampietro DE, Rothstein JD, and Conti F., The expression of glutamate transporter GLT-1 in the rat cerebral cortex is down-regulated by the antipsychotic drug clozapine. Molecular Psychiatry, July 2001, Vol. 6, No. 4 pp.380-386.

12. JP Sepkuty , AS Cohen, C Eccles, A Rafik, K Behar, R Ganel, DA Coulter, JD Rothstein. A neuronal glutamate transporter contributes to neurotransmitter GABA synthesis and epilepsy. In Press, J. Neuroscience

List Of Personnel Receiving Pay from this Proposal:

Jeffrey D. Rothstein- Principal Investigator

Carol Coccia- Technician

Raquelli Ganel- Post Doc

Appendix

1. Lin CLG, Orlov I, Ruggiero AM, Dykes-Hoberg M, Lee A, and Rothstein JD. Modulation of the neuronal glutamate transporter EAAC1 by an interacting protein GTRAP3-18. Nature, 2001, 410:84-88

2. Jackson M., Song W., Liu MY, Jin L., Dykes-Hoberg M., Lin CLG, Bowers WJ, Federoff HJ, Sternweis PC, Rothstein JD. Modulation of the neuronal glutamate transporter EAAT4 by two interacting proteins. Nature, 2001, 401:89-93.

3. CD Wells, MY Liu, M Jackson, S Gutowski, PM Sternweis, JD Rothstein, T Kozasa, PC Sternweis, Mechanisms for Reversible Regulation between G13 and Rho Exchange Factors. J. Biol. Chem., In Press. 2002.

4. Drachman,D.B., Rothstein,J.D. Inhibition of cyclooxygenase-2 protects motor neurons in an organotypic model of amyotrophic lateral sclerosis., Ann.Neurol 2000:792-795.

5. Melone M., Vitellaro Zuccarello L, Vallejo-Illarramendi A., Pérez-Samartin A., Matute C., Cozzi A., Pellegrini-Giampietro DE, Rothstein JD, and Conti F., The expression of glutamate transporter GLT-1 in the rat cerebral cortex is down-regulated by the antipsychotic drug clozapine. Molecular Psychiatry, July 2001, Vol. 6, No. 4 pp.380-386.

6. JP Sepkuty , AS Cohen, C Eccles, A Rafik, K Behar, R Ganel, DA Coulter, JD Rothstein. A neuronal glutamate transporter contributes to neurotransmitter GABA synthesis and epilepsy. In Press, J. Neuroscience

Molecular Psychiatry (2001) 6, 380–386

www.nature.com/mp

ORIGINAL RESEARCH ARTICLE

The expression of glutamate transporter GLT-1 in the rat cerebral cortex is down-regulated by the antipsychotic drug clozapine

M Melone[1], L Vitellaro-Zuccarello[2], A Vallejo-Illarramendi[3], A Pérez-Samartin[3], C Matute[3], A Cozzi[4], DE Pellegrini-Giampietro[4], JD Rothstein[5] and F Conti[1]

[1]*Istituto di Fisiologia Umana, Università di Ancona, Via Tronto 10/A, Torrette di Ancona, 60020 Ancona, Italy;* [2]*Dipartimento di Fisiologia e Biochimica Generali, Università di Milano, Via Celoria 26, 20133 Milan, Italy;* [3]*Departamento de Neurociencias, Universidad del Pais Vasco, 48940-Leioa, Vizcaya, Spain;* [4]*Dipartimento di Farmacologia Preclinica e Clinica, Università degli Studi di Firenze, Viale G Pieraccini 6, 50139 Firenze, Italy;* [5]*Department of Neurology, The Johns Hopkins University, Baltimore, MD 21287–7519, USA*

We show here that clozapine, a beneficial antipsychotic, down-regulates the expression of the glutamate transporter GLT-1 in the rat cerebral cortex, thereby reducing glutamate transport and raising extracellular glutamate levels. Clozapine treatment (25–35 mg kg^{-1} day^{-1} orally) reduced GLT-1 immunoreactivity in several brain regions after 3 weeks; this effect was most prominent after 9 weeks and most evident in the frontal cortex. GLT-1 protein levels were reduced in the cerebral cortex of treated rats compared with controls and were more severely affected in the anterior (71.9 ± 4.5%) than in the posterior (53.2 ± 15.4%) cortex. L-[^{3}H]-glutamate uptake in *Xenopus laevis* oocytes injected with mRNA extracted from the anterior cerebral cortex of rats treated for 9 weeks was remarkably reduced (to 30.6 ± 8.6%) as compared to controls. In addition, electrophysiological recordings from oocytes following application of glutamate revealed a strong reduction in glutamate uptake currents (46.3 ± 10.2%) as compared to controls. Finally, clozapine treatment led to increases in both the mean basal (8.1 ± 0.7 μM) and the KCl-evoked (28.7 ± 7.7 μM) output of glutamate that were 3.1 and 3.5, respectively, higher than in control rats. These findings indicate that clozapine may potentiate glutamatergic synaptic transmission by regulating glutamate transport. *Molecular Psychiatry* (2001) **6**, 380–386.

Keywords: glutamate; glutamate uptake; neuroleptics; transporter regulation; synaptic transmission; schizophrenia

Introduction

Several studies suggest that glutamatergic hypofunction mediated by alterations of *N*-methyl-D-aspartate (NMDA) glutamate receptors may explain some features of schizophrenia.[1–8] Indeed, the psychotomimetic drug phencyclidine blocks the NMDA channel[9] and mice expressing low levels of the NMDAR1 subunit display behaviors related to schizophrenia that are ameliorated by antipsychotic treatment.[6]

Defective glutamatergic signaling, however, may also result from other mechanisms. High-affinity glutamate transporters (GluTs) play a pivotal role in the regulation of glutamatergic transmission, as they contribute to shaping excitatory postsynaptic responses and are essential for maintaining physiological levels of glutamate.[10] Among the five GluTs that have been characterized in the mammalian CNS, GLT-1, a GluT localized to distal astrocytic processes, exhibits the highest level of expression, it is responsible for the greatest proportion of total glutamate transport and its functional inactivation raises extracellular glutamate levels.[11,12] We therefore examined whether chronic oral administration[13] of the widely used and highly effective antipsychotic clozapine[14,15] (25–35 mg kg^{-1} day^{-1} in the drinking water) reduces the expression of GLT-1 in rats.

Correspondence: F Conti, Istituto di Fisiologia Umana, Università di Ancona, Via Tronto 10/A, Torrette di Ancona, 1–60020 Ancona, Italy. E-mail: f.conti@popcsi.unian.it
Received 11 October 2000; revised 8 January 2001; accepted 10 January 2001

Materials and methods

Animals

Eighty-eight adult Sprague–Dawley rats (initial weight 190–220 g) were used. Their care and handling were approved by the Ethical Committee for Animal Research of the University of Ancona. Animals were housed 2–3 per cage, kept under a 12 h light-dark cycle (lights on at 6 am) and permitted food and water *ad libitum*. Experimental animals ($n = 44$) received cloza-

pine for one ($n = 4$), three ($n = 4$), six ($n = 5$), nine ($n = 27$) or 12 ($n = 4$) weeks. Each group was matched to a group of control animals of the same age ($n = 44$).

Treatment regimen, doses and length of treatment were as in Fitzgerald *et al*,[13] and were based on previous dosing strategies in rats[16,17] that have been extrapolated from human clinical dosages.[13,18] Oral clozapine administration provides more stable and continuous levels, given the reported rapid elimination of the drug[13] and its inability to accumulate in the brain.[19,20] Clozapine (Sandoz, Basel, Switzerland) was diluted in the drinking water at 0.5 mg ml^{-1} (pH 6.0) as described by See and Ellison.[16] Daily dosage, calculated from drinking water intake, was between 25 and 35 mg kg^{-1}; based on previous studies in rats,[21,22] it can be estimated that clozapine plasma levels in these experimental series ranged from 20 to 60 ng ml^{-1}. Daily examination revealed no observable behavioral or neurological changes besides a slight sedation during the first week of treatment. Control rats received water adjusted with diluted acetic acid to match the pH of the drug solution.

Immunohistochemistry and Western blotting

For immunohistochemistry, rats were anesthetized with chloral hydrate (300 mg kg^{-1}, i.p.) and perfused by transcardial perfusion with 4% paraformaldehyde. Brains were cut in 30-μm thick sections with a Vibratome; one hemisphere of each brain was cut coronally, the other parasagittally. From the former hemispheres, sections were collected from +5.2 to –6.3, and from the latter from lateral 1.4 to lateral 4.0–4.5.[23] Free-floating sections from control and experimental animals were processed as described previously[24] using affinity-purified polyclonal antibodies (0.06–0.08 μg ml^{-1}) against GLT-1.[25] Sections from control and treated animals were processed in parallel to minimize possible variations.

For immunoblotting, rats were perfused with cold 4 mM Tris-HCl (pH 7.4) containing 0.32 M sucrose, 1 mM EDTA, 0.5 mM phenylmethylsulphonyl fluoride (PMSF), and 0.5 mM N-ethylmaleimide (NEM). The cortical regions lying rostral to the bregma were separated from those caudal to it. The anterior and posterior cortical regions of four clozapine-treated and four control rats were separately homogenized with a glass-Teflon homogenizer in 10 vol of ice-cold buffer (4 mM Tris-HCl, pH 7.4; 0.32 M sucrose; 1 mM EDTA; and 0.25 mM dithiothreitol). Homogenate processing, protein concentration determination, and protein electroblotting onto nitrocellulose filters (0.22 μm) probed with antiGLT-1 antibodies (0.025 μg ml^{-1}) were performed as described previously.[26] Optical densities of the bands were determined using the 1.61 NIH Image analysis software. Results were normalized to GLT-1 levels in controls prepared in parallel and loaded onto the same gel. Statistical significance was evaluated by ANOVA.

Glutamate transport measurements

Messenger RNA was extracted using the guanidinium/phenol/chloroform method[27] and purified by oligo (dT)-cellulose chromatography. *Xenopus* oocyte harvesting, injection (50 ng per 50 nl per oocyte), collagenase treatment and electrophysiological recordings were as described previously.[28] L-[^{3}H]-glutamate uptake (1 μM; specific activity 46 Ci $mmol^{-1}$; Amersham) was measured 4–5 days after injection by incubating oocytes for 1 h in frog's Ringer containing the radioisotope, at room temperature following a procedure described in a previous work.[29] Glutamate transport was calculated by subtracting the total amount of radioactivity incorporated into oocytes from that measured in the presence of the glutamate transporter inhibitor L-transpyrrolidine-2,4-dicarboxylate (500 μM). Glutamate transport-induced currents were recorded 4–5 days after mRNA injection by perfusion with glutamate (1–10 mM) in the presence of the glutamate receptor antagonists D-2-amino-5-phosphonopentanoic acid (D-AP-5, 100 μM), 6-cyano-7-nitroquinoxaline-2,3-dione (CNQX; 100 μM) and RS-α-methyl-4-carboxyphenylglycine (MCPG; 1 mM). All drugs were purchased from Tocris.

Microdialysis and measurement of extracellular glutamate

Rats were anesthetized with chloral hydrate (300 mg kg^{-1}, i.p.) and placed in a stereotaxic frame for the implantation of a transcerebral microdialysis tube across the frontal cortex (coordinates for fiber in- and out-let: 2.2 mm from the bregma and 1.9 mm from the skull surface). After at least 24 h recovery, the membranes were perfused with an iso-osmotic solution (in mM: NaCl 155, KCl 3.0, $CaCl_2$ 2.3; pH 7.2) at a flow rate of 3.5 μl min^{-1}. After a washout period of approximately 2 h, eight fractions were collected every 10 min to determine the basal output. The glutamate recovered in the probes was approximately 45%. The membranes were then perfused for 10 min with a solution containing 100 mM KCl (with equimolar replacement of NaCl) and then again with the control solution to monitor the recovery of basal output. At the end of the experiments, rats were anesthetized with chloral hydrate (300 mg kg^{-1}, i.p.) and perfused transcardially with approximately 150 ml of 4% paraformaldehyde. Brains were removed and the placement of the tubing and the presence of extensive damage was assessed on parasagittal sections. Rats displaying: (i) incorrect placement of the tubing; (ii) gross histological lesions in areas surrounding the probe path, and/or (iii) no significant increase in basal glutamate output following perfusion with 100 mM KCl were discarded from the study. Microdialysis samples were kept on ice during the collection period and stored at –20°C until assayed. Glutamate was measured by HPLC separation and fluorometric detection after precolumn derivatization with *o*-phthalaldehyde and ethylmercaptan, as previously described.[30] Statistical significance was evaluated by performing ANOVA followed by Tukey's *w* test for multiple comparisons.

Results

Robust GLT-1 immunoreactivity (ir) was observed in the gray matter of control animals in most brain regions (Figure 1, left column) as dense punctate structures (Figure 2a and b). In the cerebral cortex, it was present throughout the cortical mantle with a variable patchy pattern, more evident in the frontal cortex (Figure 1, left column).

GLT-1 ir was slightly reduced in several brain regions after 3 weeks of clozapine treatment (Figure 1, second row) and more evidently in the animals treated for 6 weeks (Figure 1, third row). Clozapine produced the strongest effect after 9 weeks (Figure 1, fourth row). In rats treated for 12 weeks, clozapine-induced reduction of GLT-1 ir appeared less intense than in those treated for 9 weeks (Figure 1, fifth row). The loss of immunostaining seemed to result from an increase of GLT-1-poor patches (Figure 2c and d) and was most evident in the cerebral cortex, although the caudate-putamen, hippocampus and thalamus were also slightly affected (Figure 1).

These data indicate that clozapine's effects on GLT-1 immunoreactivity are stronger in the cerebral cortex than in other brain regions and that they are strongest in the rats treated for 9 weeks. We therefore directed our subsequent experiments to the cerebral cortex of rats treated with clozapine for 9 weeks.

The reduction in GLT-1 immunoreactivity was

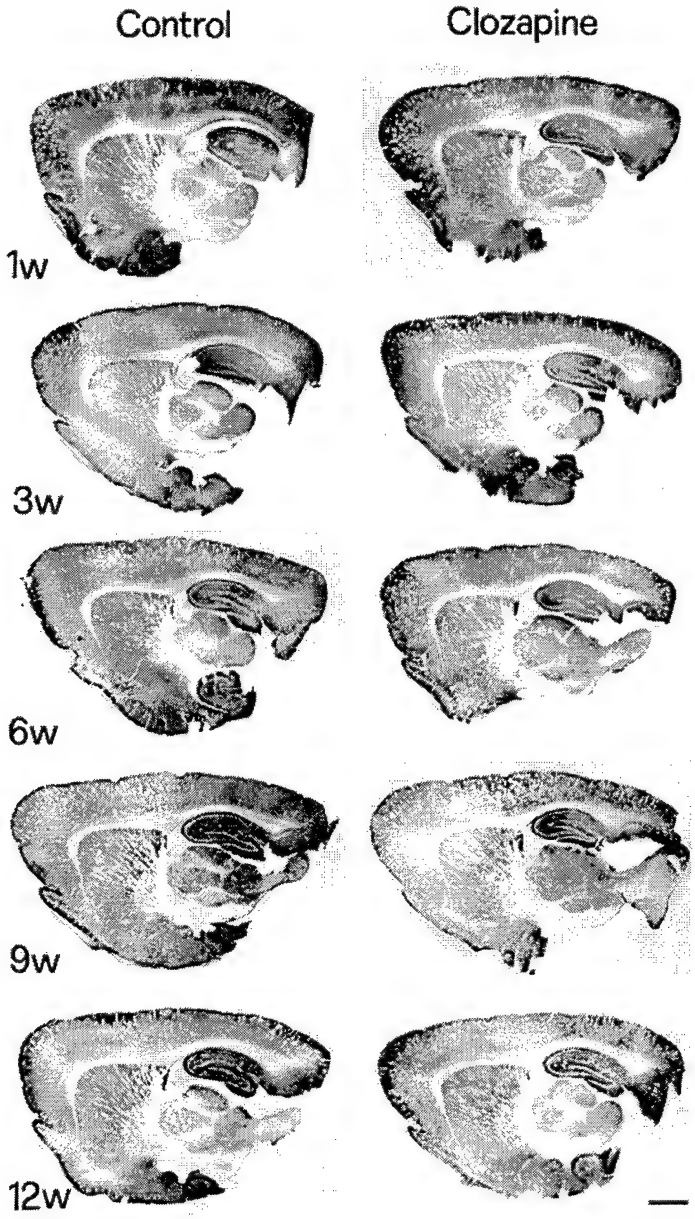

Figure 1 GLT-1 is reduced in clozapine-treated rats. Parasagittal sections from control and clozapine-treated rats showing the time course of clozapine effects on GLT-1 immunoreactivity. Bar: 2 mm.

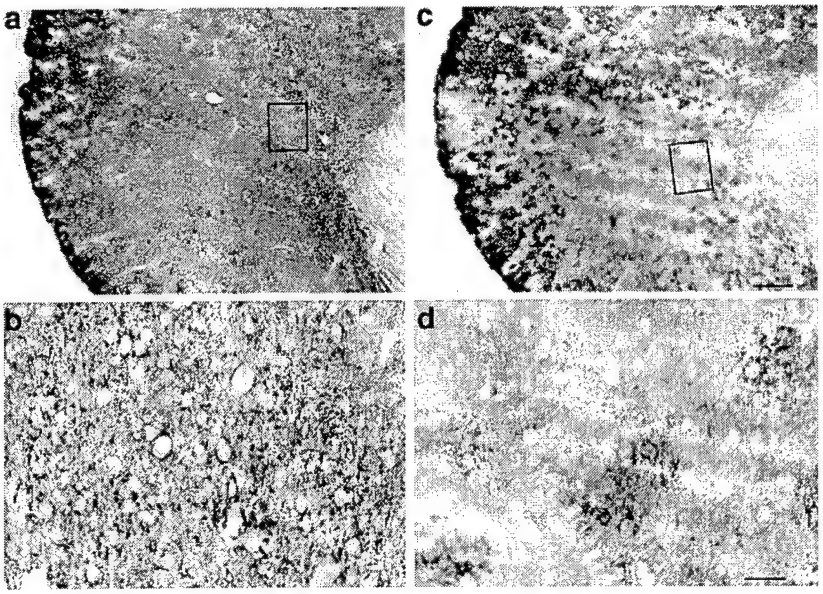

Figure 2 High magnification photomicrographs showing the remarkable reduction of GLT-1 labeling in the frontal cortex of rats treated for 9 weeks with clozapine (c and d) as compared to control animals (a and b). Framed regions in the top panels are enlarged in the corresponding bottom panels. Bar: 300 μm for (a) and (c), 50 μm for (b) and (d).

intense in the frontal cortex, moderate in the fronto-parietal somatic sensory and motor cortices and striate cortex (Figure 1), and from barely detectable to absent in the auditory, cortical-amygdaloid, cingulate and retrosplenial cortices (data not shown). Immunoblotting of samples from clozapine-treated rats and from controls showed that the antiGLT-1 antibody recognized a protein with the molecular weight of about 70 kDa (Figure 3a), consistent with the known molecular weight of GLT-1.[31] Since the observations on cortical sections suggested a stronger reduction in fronto-parietal regions, the cortical regions lying rostral to the bregma were separated from those caudal to it, and the two resulting blocks were defined anterior and posterior cortex, respectively. Densitometric analysis showed that GLT-1 protein levels were remarkably reduced in the cerebral cortex of treated rats compared to controls (Figure 3a and b) and that they were more severely affected in the anterior (rostral to the bregma; $71.9 \pm 4.5\%$) than in the posterior (caudal to the bregma; $53.2 \pm 15.4\%$) cortex (Figure 3b). One way ANOVA analysis showed that $P < 0.001$ in samples from the anterior cortex and <0.05 in those from the posterior cortex.

To obtain an indirect measure of glutamate transport we injected *Xenopus laevis* oocytes with mRNA extracted from the anterior cerebral cortex and we evaluated the amount of L-[^{3}H]-glutamate uptake. These experiments showed that in all the samples examined glutamate transport was consistently reduced in oocytes injected with extracts from rats treated for 9 weeks as compared to control animals ($30.6 \pm 8.6\%$; range 8.8–64%; seven rats; Figure 4). Statistical significance, determined by Fisher's protected least significant difference (PLSD) following ANOVA, was <0.01 in two out of the seven cases stud-

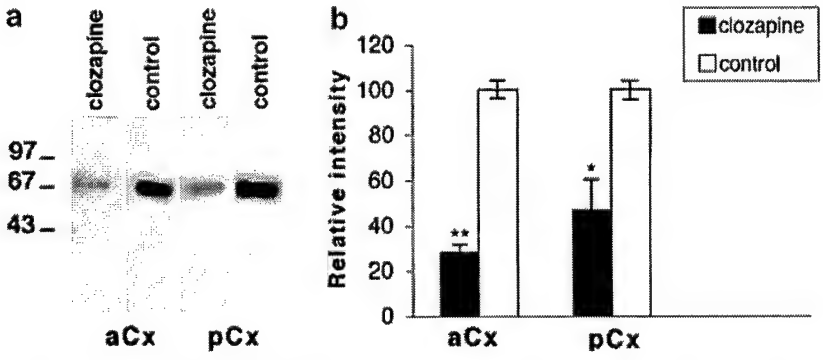

Figure 3 Representative immunoblots of GLT-1 in the anterior (aCx) and posterior (pCx) cerebral cortex of clozapine-treated and control rats (a), and densitometric analysis of GLT-1 protein levels in immunoblots of clozapine-treated and control animals (b). Results are expressed as percentage of control (mean ± SEM). $^{**}P < 0.001$; $^{*}P < 0.05$ (one way ANOVA).

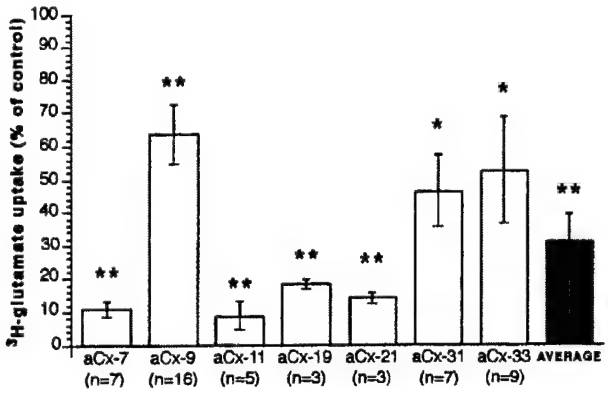

Figure 4 L-[^{3}H]-glutamate uptake into oocytes injected with mRNA from the anterior cortex of clozapine-treated rats is considerably reduced. Values are from 3–16 oocytes in each of the seven treated and seven control rats examined (total number of oocytes assayed 100). $*P < 0.01$; $**P < 0.001$ (one way ANOVA; Fisher PDLS test). aCx-7–aCx-33, animal code.

ied and <0.001 in the remaining five (Figure 4). To confirm these results, we also measured the currents generated by glutamate in *Xenopus laevis* oocytes injected with mRNA extracted from the anterior cerebral cortex of both clozapine-treated and control animals. Electrophysiological recordings from oocytes following application of glutamate (1–10 mM) in the presence of ionotropic and metabotropic glutamate receptor antagonists revealed a strong reduction in glutamate uptake currents ($46.3 \pm 10.2\%$; range 16–62%; four rats; Figure 5a and b). Fisher PDLS test following one way ANOVA showed that $P < 0.005$. Altogether these results show that the efficacy of glutamate transport in rats treated with clozapine for 9 weeks is severely reduced in the anterior cortex.

We then used transverse microdialysis to study the output of glutamate from the anterior cortex of rats treated for 9 weeks with clozapine and of age-matched controls. In control rats ($n = 5$, 490 ± 20 g), the mean basal glutamate output (2.6 ± 0.2 μM) increased to 8.1 ± 2.1 μM when rats were perfused with an isoosmotic solution containing 100 mM KCl and it returned to basal levels 20 min later (Figure 6). In clozapine-treated rats ($n = 5$, 501 ± 18 g), both the mean basal (8.1 ± 0.7 μM) and the KCl-evoked (28.7 ± 7.7 μM) output of glutamate were significantly elevated as compared with controls (Figure 6); following KCl stimulation, glutamate initially returned to the elevated basal values but, after approximately 30 min, glutamate increased again and remained elevated (at 16.5 ± 2.8 μM) until the end of the experiments (Figure 6). All differences were statistically significant (see legend to Figure 6). These results indicate that the extracellular concentrations of glutamate under basal and depolarizing conditions are elevated in the frontal cortex of rats treated with clozapine and suggest a late impairment of glutamate reuptake following depolarization.

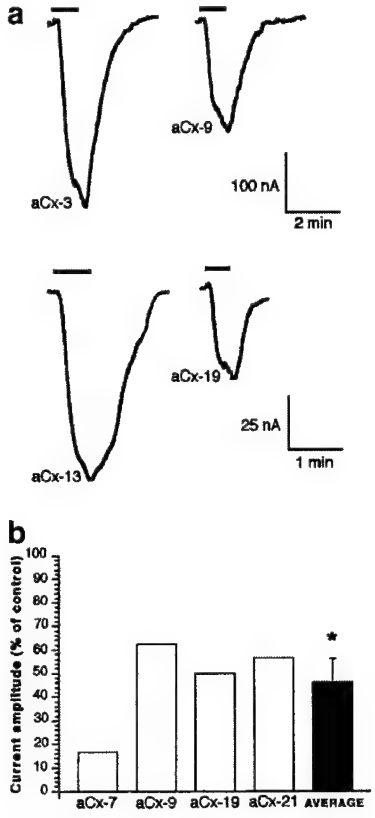

Figure 5 Glutamate uptake currents are strongly reduced in clozapine-treated rats. (a) Currents recorded, following application of 10 mM glutamate (plus ionotropic and metabotropic glutamate receptor antagonists) during the time indicated with a bar, show a lower amplitude in oocytes injected with mRNA from clozapine-treated animals (traces in the right) than from control animals (traces in the left). (b) Averages of GluT-mediated current amplitudes are reduced in clozapine-treated animals. Values are from 3–7 oocytes for each of the four treated and four control rats examined. $*P < 0.005$ (one way ANOVA; Fisher PDLS test). aCx-3–aCx-21, animal code.

Discussion

Clozapine is highly effective in the treatment of schizophrenic patients, but the full spectrum of its effects has not been detailed. Clozapine blocks several dopamine and serotonin receptors[14,32] and facilitates NMDA receptor activity.[33] Our results demonstrate a novel effect, ie, down-regulation of GLT-1 protein expression and increase in extracellular glutamate levels in the cerebral cortex.

The temporal profile of clozapine-induced changes in GLT-1 cortical expression shows that they decline after 12 weeks of treatment. This may be related to adaptive changes occuring at glutamatergic synapses or reflect the relative reduction of clozapine levels secondary to the physiological weight gain occuring over the 9 weeks of treatment and/or, most likely, to that induced by clozapine itself.[34–37]

This study shows that the reduction in GLT-1 expression is uneven, with the strongest reduction

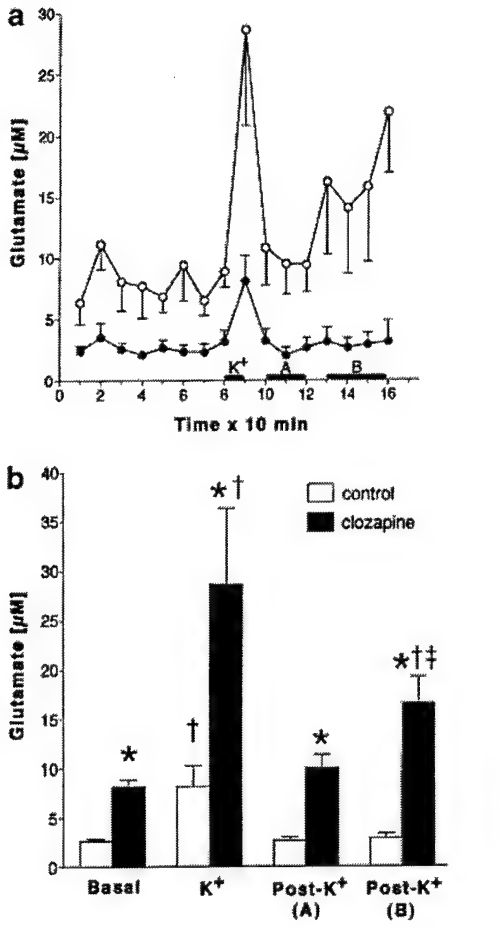

Figure 6 Extracellular glutamate concentrations are increased in clozapine-treated rats. (a) Time course of the changes in glutamate concentrations in frontal cortex dialysates of freely moving control (black circles) and clozapine-treated (white circles) rats. KCl (100 mM) was perfused for a 10-min period ('K^+' horizontal bar). The first three fractions following KCl stimulation were labeled 'A' and the last four fractions were labeled 'B'. Each point represents the mean ± SEM of five control or five clozapine-treated rats. All clozapine-treated fractions were statistically different ($P < 0.05$) *vs* the corresponding control time points. (b) Effects of chronic clozapine treatment on basal, K^+-evoked and post-K^+ glutamate output from rat frontal cortex. Bars represent the mean glutamate output ± SEM of the eight fractions collected before KCl stimulation (*basal*), the peak K^+-evoked value ± SEM (K^+), the mean glutamate output ± SEM of the first three fractions (labeled 'A' in (a)) collected following KCl stimulation [post-K^+ (A)], and the mean glutamate output ± SEM of the last four fractions (labeled 'B' in (a)) collected following KCl stimulation [post-K^+ (B)] in control and clozapine-treated rats. *, $P < 0.01$ *vs* control of each group; †, $P < 0.01$ *vs* corresponding (control or clozapine) basal; ‡, $P < 0.05$ *vs* post-K^+ (A) clozapine.

being observed in the cerebral neocortex. This is consistent with the results of previous studies of clozapine's effects on glutamatergic synapses: (i) clozapine-induced up-regulation of GluR1 and GluR2 expression has been demonstrated in the prefrontal cortex but not in the striatum;[13] (ii) GLT-1 mRNAs in the striatum are only modestly affected by clozapine treatment;[38] and (iii) clozapine administration increases extracellular Glu levels in the prefrontal cortex but not in the striatum.[39] Overall, these data indicate that clozapine's effects on glutamatergic transmission are much stronger in the cerebral cortex than in other brain regions. In addition, clozapine effects on dopamine[40,41] and GABA[42] levels and on c-*fos* induction[43–45] are significantly higher in the cerebral cortex than in subcortical regions; taken together these data support the hypothesis that the cerebral cortex is the preferential site for clozapine action.[46] Although we did not perform a systematic analysis of GLT-1 protein reduction in all cortical areas, the present results document that the effects of clozapine are strongest in cortical regions located rostral to the bregma. Since clozapine-induced changes in AMPA receptor subunits[13,47] and Glu levels[39] are also more pronounced in the frontal regions, it is conceivable that clozapine's action on glutamatergic, as on dopaminergic and GABAergic (see above), transmission is more intense in the frontal neocortex.

Given that a considerable amount of data indicate that some of the symptoms of schizophrenia may be subtended by a reduced efficacy of glutamatergic transmission[1–8] (see however Moghaddam and Adams[48]), our results suggest that clozapine exerts at least partly its therapeutic effect by reducing glutamate transport and raising extracellular glutamate levels. Although application of data from rodents to a complex human disease requires caution, the present data suggest for the first time that glutamatergic hypofunction in schizophrenia may partly result from changes in GLT-1 expression and/or activity.

Acknowledgements

This paper is dedicated to GianFranco Marchesi (1940–1998), Professor of Psychiatry at the University of Ancona, who stimulated this study. This work was supported by a Theodore and Vana Stanley Foundation Research Award (to FC) and by grants from Telethon (962/97 to FC) and University del Pais Vasco (CM). We are grateful to Marco Catalano, Aldo Rustioni, and Giulio Tononi for critical comments on an earlier version of this paper and Andrea Minelli for helpful discussions.

References

1 Olney JW, Farber NB. Glutamate receptor dysfunction and schizophrenia. *Arch Gen Psychiatry* 1995; **52**: 998–1007.
2 Tsai G, Passani L, Slusher BS, Carter R, Baer L, Kleinmann JE *et al.* Abnormal excitatory neurotransmitter metabolism in schizophrenic brains. *Arch Gen Psychiatry* 1995; **52**: 829–836.
3 Akbarian S, Sucher NJ, Bradley D, Tafazzoli A, Trinh D, Hetrick WP *et al.* Selective alterations in gene expression for NMDA receptor subunits in prefrontal cortex of schizophrenics. *J Neurosci* 1996; **16**: 19–30.
4 Benes FM. The role of glutamate in the pathophysiology of schizophrenia. In: Conti F, Hicks TP (eds). *Excitatory Amino Acids and the Cerebral Cortex.* Cambridge: MIT, 1996, pp 361–374.
5 Carlsson A, Hansson LO, Waters N, Carlsson ML. A glutamatergic

deficiency model of schizophrenia. *Br J Psychiatry* 1999; **174**(37S): 2–6.
6 Mohn AR, Gainetdinov RR, Caron MG, Koller BH. Mice with reduced NMDA receptor expression display behaviors related to schizophrenia. *Cell* 1999; **98**: 427–436.
7 Tamminga C. Glutamatergic aspects of schizophrenia. *Br J Psychiatry* 1999; **174**(37S): 12–15.
8 Meador-Woodruff JH, Healy DJ. Glutamate receptor expression in schizophrenic brain. *Brain Res Rev* 2000; **31**: 288–294.
9 Javitt DC, Zukin SR. Recent advances in the phencyclidine model of schizophrenia. *Am J Psychiatry* 1991; **148**: 1301–1308.
10 Conti F, Weinberg RJ. Shaping excitation at glutamatergic synapses. *Trends Neurosci* 1999; **22**: 451–458.
11 Rothstein JD, Dykes-Hoberg M, Pardo CA, Bristol LA, Jin L, Kuncl RW *et al*. Knockout of glutamate transporters reveals a major role for astroglial transport in excitotoxicity and clearance of glutamate. *Neuron* 1996; **16**: 675–686.
12 Tanaka K, Watase K, Manabe T, Yamada K, Watanabe M, Takahashi K *et al*. Epilepsy and exacerbation of brain injury in mice lacking the glutamate transporter GLT-1. *Science* 1997; **276**: 1699–1702.
13 Fitzgerald LW, Deutch AY, Gasic G, Heinemann SF, Nestler EJ. Regulation of cortical and subcortical glutamate receptor subunit expression by antipsychotic drugs. *J Neurosci* 1995; **15**: 2453–2461.
14 Duncan GE, Zorn S, Lieberman JA. Mechanisms of typical and atypical antipsychotic drug action in relation to dopamine and NMDA receptor hypofunction hypotheses of schizophrenia. *Mol Psychiatry* 1999; **4**: 418–428.
15 Wahlbeck K, Cheine M, Essali A, Adams C. Evidence of clozapine's effectiveness in schizophrenia: a systematic review and meta-analysis of randomized trials. *Am J Psychiatry* 1999; **156**: 990–999.
16 See RE, Ellison G. Comparison of chronic administration of haloperidol and the atypical neuroleptics, clozapine and raclopride, in an animal model of tardive dyskinesia. *Eur J Pharmacol* 1990; **181**: 175–186.
17 Rupniak NMJ, Mann S, Hall MD, Fleminger S, Kilpatrick G, Jenner P *et al*. Differential effects of continuous administration for 1 year of haloperidol or sulpiride on striatal dopamine function. *Psychopharmacology* 1984; **84**: 503–511.
18 Titeler M, Seeman P. Radioligand labeling of pre- and postsynaptic dopamine receptors. *Adv Biochem Psychopharmacol* 1980; **24**: 159–165.
19 Wilk S, Stanley M. Clozapine concentrations in brain regions: relationship to dopamine metabolite increase. *Eur J Pharmacol* 1978; **51**: 101–107.
20 Baldessarini RJ, Centorrino F, Flood JG, Volpicelli SA, Huston-Lyons D, Cohen BM. Tissue concentrations of clozapine and its metabolities in the rat. *Neuropsychopharmacology* 1993; **9**: 117–124.
21 Gao XM, Hashimoto T, Cooper TB, Tamminga CA. The dose-response characteristics of rat oral dyskinesias with chronic haloperidol or clozapine administration. *J Neural Transm* 1997; **104**: 97–104.
22 Fischer V, Schmitt U, Weigmann H, Von Keller B, Reuss S, Hiemke C *et al*. Chronical haloperidol and clozapine treatment in rats: differential RNA display analysis, behavioral and serum level determination. *Prog Neuropsychopharmacol Biol Psychiatry* 1998; **22**: 1129–1139.
23 Paxinos G, Watson C. *The Rat Brain in Stereotaxic Coordinates*. Academic Press: New York, 1982.
24 Conti F, De Biasi S, Minelli A, Rothstein JD, Melone M. EAAC1, a high-affinity glutamate transporter, is localized to neurons and astrocytes in the cerebral cortex. *Cereb Cortex* 1998; **8**: 108–116.
25 Rothstein JD, Martin L, Levey AI, Dykes-Hoberg M, Jin L, Wu D *et al*. Localization of neuronal and glial glutamate transporters. *Neuron* 1994; **13**: 713–725.
26 Minelli A, DeBiasi S, Brecha NC, Vitellaro Zuccarello L, Conti F. GAT-3, a high affinity GABA plasma membrane transporter, is localized exclusively to astrocytic processes in the cerebral cortex. *J Neurosci* 1996; **16**: 6255–6264.
27 Chomsczynski P, Sacchi N. Single-step method of RNA isolation by acid guanidinium thiocyanate-phenol-chloroform extraction. *Anal Biochem* 1987; **162**: 156–159.
28 Matute C, Miledi R. Neurotransmitter receptors and voltage-dependent Ca^{2+} channels encoded by mRNA from the adult corpus callosum. *Proc Natl Acad Sci USA* 1993; **90**: 3270–3274.
29 Domercq M, Sánchez-Gómez MV, Areso P, Matute C. Expression of glutamate transporters in rat optic nerve oligodendrocytes. *Eur J Neurosci* 1999; **11**: 2226–2236.
30 Pellegrini-Giampietro DE, Peruginelli F, Meli E, Cozzi A, Albani-Torregrossa S, Pellicciari R *et al*. Protection with metabotropic glutamate 1 receptor antagonists in models of ischemic neuronal death: time-course and mechanisms. *Neuropharmacology* 1999; **38**: 1607–1619.
31 Pines G, Danbolt NC, Bjoras M, Zhang Y, Bendaham A, Eide L *et al*. Cloning and expression of a rat brain L-glutamate transporter. *Nature* 1992; **360**: 464–467.
32 Meltzer HY. Pre-clinical pharmacology of atypical antipsychotic drugs: a selective review. *Br J Psychiatry* 1996; **168** (Suppl 29): 23–31.
33 Leveque J-C, Macias W, Rajadhyaksha A, Carlson RR, Barczak A, Kang S *et al*. Intracellular modulation of NMDA receptor function by antipsychotic drugs. *J Neurosci* 2000; **20**: 4011–4020.
34 Baldessarini RJ, Frankenburg FR. Clozapine. A novel antipsychotic agent. *New Engl J Med* 1991; **324**: 746–754.
35 Allison DB, Mentore JL, Heo M, Chandler LP, Cappelleri JC, Infante MC *et al*. Antipsychotic-induced weight gain: a comprehensive research synthesis. *Am J Psychiatry* 1999; **156**: 1686–1696.
36 Bustillo JR, Buchanan RW, Irish D, Breier A. Differential effect of clozapine on weight: a controlled study. *Am J Psychiatry* 1996; **153**: 817–819.
37 Bromel T, Blum WF, Ziegler A, Schulz E, Bender M, Fleischhaker C *et al*. Serum leptin levels increase rapidly after initiation of clozapine therapy. *Mol Psychiatry* 1998; **3**: 76–80.
38 Schneider JS, Wade T, Lidsky TI. Chronic neuroleptic treatment alters expression of glial glutamate transporter GLT-1 mRNA in the striatum. *NeuroReport* 1998; **9**: 133–136.
39 Daly DA, Moghaddam B. Actions of clozapine and haloperidol on the extracellular levels of excitatory amino acids in the prefrontal cortex and striatum of conscious rats. *Neurosci Lett* 1993; **152**: 61–64.
40 Kuroki T, Meltzer HY, Ichikawa J. Effects of antipsychotic drugs on extracellular dopamine levels in rate medial prefrontal cortex and nucleus accumbens. *J Pharmacol Exp Ther* 1999; **288**: 774–781.
41 Youngren KD, Inglis FM, Pivirotto PJ, Jedema HP, Bradberry CW, Goldman-Rakic PS *et al*. Clozapine preferentially increases dopamine release in the rhesus monkey prefrontal cortex compared with the caudate nucleus. *Neuropsychopharmacology* 1999; **20**: 403–412.
42 Bourdelais AJ, Deutch AY. The effects of clozapine on extracellular GABA levels in the prefrontal cortex of the rat: an *in vivo* microdialysis study. *Cereb Cortex* 1994; **4**: 69–77.
43 Robertson GS, Fibiger HC. Neuroleptics increase c-fos expression in the forebrain: contrasting effects of haloperidol and clozapine. *Neuroscience* 1992; **46**: 315–328.
44 Deutch AY, Duman RS. The effects of antipsychotic drugs on Fos protein expression in the prefrontal cortex: cellular localization and pharmacological characterization. *Neuroscience* 1996; **70**: 377–389.
45 Merchant KM, Figur LM, Evans DL. Induction of c-fos mRNA in rat medial prefrontal cortex by antipsychotic drugs: role of dopamine D2 and D3 receptors. *Cereb Cortex* 1996; **6**: 561–570.
46 Lidow MS, Williams GV, Goldman-Rakic PS. The cerebral cortex: a case for a common site of action on antipsychotics. *Trends Pharmacol Sci* 1998; **19**: 136–140.
47 Spurney CF, Baca SM, Murray AM, Jaskiw GE, Kleinman JE, Hyde TM. Differential effects of haloperidol and clozapine on ionotropic glutamate receptors in rats. *Synapse* 1999; **34**: 266–276.
48 Moghaddam B, Adams BW. Reversal of phencyclidine effects by a group II metabotropic glutamate receptor agonist in rats. *Science* 1998; **281**: 1349–1352.

THE JOURNAL OF BIOLOGICAL CHEMISTRY
Vol. 277, No. 2, Issue of January 11, pp. 1174–1181, 2002
Printed in U.S.A.

Mechanisms for Reversible Regulation between G_{13} and Rho Exchange Factors*

Received for publication, June 7, 2001, and in revised form, November 5, 2001
Published, JBC Papers in Press, November 6, 2001, DOI 10.1074/jbc.M105274200

Clark D. Wells‡, Mu-Ya Liu§, Mandy Jackson¶, Stephen Gutowski‡, Pamela M. Sternweis‡, Jeffrey D. Rothstein¶, Tohru Kozasa‖, and Paul C. Sternweis‡**

From the ‡Department of Pharmacology, University of Texas, Southwestern Medical Center at Dallas, Texas 75390-9041, §Hybrigen Inc., Dallas, Texas 75207-2307, the ¶Department of Neurology and Neuroscience, Johns Hopkins University, Baltimore, Maryland 21287, and the ‖Department of Pharmacology and the Department of Anatomy and Cell Biology, University of Illinois, Chicago, Illinois 60612

The heterotrimeric G proteins, G_{12} and G_{13}, mediate signaling between G protein-coupled receptors and the monomeric GTPase, RhoA. One pathway for this modulation is direct stimulation by $G\alpha_{13}$ of p115 RhoGEF, an exchange factor for RhoA. The GTPase activity of both $G\alpha_{12}$ and $G\alpha_{13}$ is increased by the N terminus of p115 Rho guanine nucleotide exchange factor (GEF). This region has weak homology to the RGS box sequence of the classic regulators of G protein signaling (RGS), which act as GTPase-activating proteins (GAP) for G_i and G_q. Here, the RGS region of p115 RhoGEF is shown to be distinctly different in that sequences flanking the predicted "RGS box" region are required for both stable expression and GAP activity. Deletions in the N terminus of the protein eliminate GAP activity but retain substantial binding to $G\alpha_{13}$ and activation of RhoA exchange activity by $G\alpha_{13}$. In contrast, GTRAP48, a homolog of p115 RhoGEF, bound to $G\alpha_{13}$ but was not stimulated by the α subunit and had very poor GAP activity. Besides binding to the N-terminal RGS region, $G\alpha_{13}$ also bound to a truncated protein consisting only of the Dbl homology (DH) and pleckstrin homology (PH) domains. However, $G\alpha_{13}$ did not stimulate the exchange activity of this truncated protein. A chimeric protein, which contained the RGS region of GTRAP48 in place of the endogenous N terminus of p115 RhoGEF, was activated by $G\alpha_{13}$. These results suggest a mechanism for activation of the nucleotide exchange activity of p115 RhoGEF that involves direct and coordinate interaction of $G\alpha_{13}$ to both its RGS and DH domains.

Heterotrimeric G proteins mediate signals from seven transmembrane receptors to a wide array of effectors, including adenylyl cyclase, ion channels, phospholipases, and the exchange factor p115 RhoGEF (1). Every G protein is composed of a heterotrimer made up of α, β, and γ subunits. The four G protein families, G_i, G_q, G_s, and G_{12}, have been categorized by their sequence identity and the functional similarity of their α subunits (2, 3). The G_{12} family contains two members, α_{12} and α_{13} (4), which have been implicated in cellular transformation (5), gastrulation of *Drosophila melanogaster* (6), vascular development in mice (7), and actin re-arrangement (8–10). The cytoskeletal changes mediated by G_{13} have been shown in several studies to require the monomeric Rho GTPases (10).

Both the heterotrimeric G proteins and monomeric Rho GTPases utilize the same basic cycle of regulation. The inactive proteins contain bound GDP. Activation is facilitated by guanine nucleotide exchange factors (GEFs)[1] that promote dissociation of GDP and subsequent binding of GTP to the G protein. GTPase-activating proteins (GAPs) return the GTPase to the inactive state by accelerating hydrolysis of the terminal phosphate of the bound GTP (2, 3, 11).

Members of the RGS (regulators of G protein signaling) family of proteins can act as GAPs for heterotrimeric G proteins (12–14). RGS proteins that have been characterized to date function by increasing the intrinsic rate of GTP hydrolysis of $G\alpha$ subunits through allosteric binding (15). This mechanism was first worked out for RGS4, which acts upon $G\alpha_i$ and $G\alpha_q$ (16, 17). The smallest region capable of accelerating GTPase activity is called the RGS box. This domain is characterized by strong primary sequence identity and structural similarity among the four RGS family members for which structures are known: RGS4 (18), GAIP (19), axin/conductin (20), and RGS9 (21).

LARG (22), PDZ RhoGEF (23), p115 RhoGEF (24), and GTRAP48 (25) are guanine nucleotide exchange factors for Rho; all share a highly conserved region that interacts specifically with $G\alpha_{12}$ and/or $G\alpha_{13}$ (22, 23, 25, 26). This region invariantly lies N-terminal to the tandem Dbl homology (DH) (27) and Pleckstrin homology (PH) (28) domains found in all four proteins. Even though these N-terminal regions contain only weak sequence identity to a stereotypical RGS box, the structure of this region in p115 RhoGEF (aa 42–252) is similar to the folding pattern of other RGS boxes (29). The high sequence identity among these regions in the four RhoGEFs suggests structural identity, and this clear subfamily of RGS domains is subsequently referred to as the rgRGS (RhoGEF RGS) domain.

The best-studied member of this group, p115 RhoGEF, was initially isolated as a protein that tightly bound the nucleotide free form of RhoA and increased the nucleotide exchange rate of RhoA (24). The rgRGS domain within the N terminus of p115 RhoGEF was subsequently established as a GAP for $G\alpha_{12}$ and

* This work was supported by National Institutes of Health Grants GM31954 (to P. C. S.), GM07062 (to C. D. W.), and GM61454 (to T. K.) and by the Robert A. Welch Foundation (to P. C. S.). The costs of publication of this article were defrayed in part by the payment of page charges. This article must therefore be hereby marked "*advertisement*" in accordance with 18 U.S.C. Section 1734 solely to indicate this fact.

** To whom correspondence should be addressed: Dept. of Pharmacology, University of Texas, Southwestern Medical Center at Dallas, 5323 Harry Hines Blvd., Dallas, TX 75390-9041. Tel.: 214-648-2835; Fax: 214-648-2971; E-mail: Paul.Sternweis@UTSouthwestern.edu.

[1] The abbreviations used are: GEF, guanine nucleotide exchange factor; LPA, lysophosphatidic acid; S1P, sphingosine 1-phosphate; DH, Dbl homology; PH, pleckstrin homology; GAP, GTPase-activating protein; GST, glutathione *S*-transferase; Rho, Ras homology; RGS, regulators of G protein signaling; GTPγS, guanosine 5′-3-*O*-(thio)triphosphate; CMV, cytomegalovirus; aa, amino acid(s).

$G\alpha_{13}$ (26). Most interestingly, p115 RhoGEF is also an effector of $G\alpha_{13}$, which increases the activity of p115 RhoGEF as a guanine nucleotide exchange factor (GEF) for RhoA (1). Recently, GTRAP48 was found to be a GEF for RhoA that also binds $G\alpha_{13}$, but the functional implications of this interaction are not known (25).

In this study, the interaction of p115 RhoGEF and GTRAP48 with the G_{12} family of heterotrimeric G proteins is more precisely defined. Deletion analysis of p115 RhoGEF provides evidence that regions outside of the apparent classic RGS box are required for accelerating the GTPase activity of $G\alpha_{13}$. A mechanism for stimulation of p115 RhoGEF by $G\alpha_{13}$ is suggested by the determination of a second binding site for $G\alpha_{13}$ in the tandem DH/PH domains of p115 RhoGEF. Finally, GTRAP48 was found to bind $G\alpha_{13}$ and act as a weak GAP on the α subunit, but its nucleotide exchange activity was not stimulated by $G\alpha_{13}$.

MATERIALS AND METHODS

Plasmids and Viruses for Expression of Protein—The cDNA encoding full-length p115 RhoGEF (24) was used for amplification of fragments of p115 RhoGEF by the polymerase chain reaction. All fragments were amplified with an N-terminal *Eco*RI site and a C-terminal *Hin*dIII site for cloning into pCMV5-myc (provided by Melanie Cobb), pGEX-KG (30), and a modified pTrc D expression vector as described previously (31). Briefly, the intervening sequence between the hexa-histidine tag (HIS) and the *Eco*RI restriction site of pTrc C (Invitrogen) was replaced with the amino acids Met-Gly-Ala. Fragments were transferred via *Eco*RI/*Xba*I sites from pCMV5 into pVL1392-EE (31), which contains an N-terminal EE tag (EYMPME) (24). Baculoviruses were produced through co-transfection of SF9 cells with pVL1392-EE vectors and BakPak6 that was digested with *Bsu*36I (CLONTECH). The N-terminal DNA fragments of p115 RhoGEF were amplified by PCR and cloned into pGEX-KG and pTrc D. The different pieces of p115 RhoGEF are named by the primers used for their amplification. All cDNA constructs were sequenced to confirm correct amplification and construction.

Expression and Purification of Proteins—All GTRAP48 and p115 RhoGEF proteins were expressed via baculovirus in cultured *Spodoptera frugiperda* (SF9) cells or in the transformed BL21(DE3) strain of *Escherichia coli*. Recombinant EE-tagged proteins were expressed in SF9 cells after infection with baculovirus. The expressed proteins were purified from lysates by affinity chromatography with anti-EE coupled Sepharose (BAbCO) as described elsewhere (32). N-terminal fragments of p115 RhoGEF and GTRAP48 were produced in *E. coli* as either HIS-tagged fusion proteins or as chimeras with GST (glutathione *S*-transferase). GST-tagged proteins were purified by chromatography using glutathione-Sepharose (Amersham Biosciences, Inc.) and solution A (25 mM NaHEPES, pH 7.5, 1 mM dithiothreitol, 50 mM NaCl) containing the protease inhibitors (2.5 μg/ml leupeptin, 1 μg/ml pepstatin A, 21 μg/ml phenylmethylsulfonyl fluoride, 21 μg/ml N^{α}-*p*-tosyl-L-lysine chloromethyl ketone, 21 μg/ml tosylphenylalanyl chloromethyl ketone, and 21 μg/ml N^{α}-*p*-tosyl-L-arginine methyl ester). HIS-tagged proteins were purified by isolation with Ni^{2+}-nitrilotriacetic acid resin (Qiagen) in 25 mM NaHEPES, pH 7.5, 2.5 mM β-mercaptoethanol, 50 mM NaCl, and the protease inhibitors.

$G\alpha_{13}$ was prepared as described by Singer *et al* (33). Prenyl RhoA was co-expressed with GST-tagged guanine nucleotide dissociation inhibitor via *Baculovirus* in SF9 cells (32). Lysates were prepared by freeze-thawing cell pellets three times in Solution A containing protease inhibitors. After removing particulate material by centrifugation at 100,000 $\times$ *g*, the cytosol was passed over a glutathione-Sepharose column and eluted with the same solution containing 1% cholate to separate RhoA from GST-guanine nucleotide dissociation inhibitor. Proteins were concentrated, and cholate was removed by dilution of samples with solution A containing protease inhibitors and final concentration via pressure filtration through an Amicon PM10 membrane.

Antisera—Three purified protein pieces of p115 RhoGEF were used to generate polyclonal antisera (31). Antisera specific for fragments consisting of aa 1–252, 288–637, and 760–912 are termed U2760, U2762, and U2764, respectively. B860, an antiserum specific for $G\alpha_{13}$ (33) and the antiserum specific for $G\alpha_{12}$ (34) were described previously. A polyclonal antibody that specifically recognizes the myc tag (catalog number Sc-789) was purchased from Santa Cruz Biotechnology.

Binding of Purified EE-tagged p115 RhoGEF and EE-tagged Pieces of p115 RhoGEF to $G\alpha_{13}$—$G\alpha_{13}$ was activated by incubation with solution B (25 mM NaHEPES, pH 7.5, 100 mM NaCl, 1 mM EDTA, 1 mM dithiothreitol) containing AMF (30 μM $AlCl_3$, 5 mM $MgCl_2$, and 10 mM NaF) and protease inhibitors for 10 min. Activated $G\alpha_{13}$ (5 pmol) was mixed with the indicated concentrations of exchange factor, which had been pre-bound to anti-EE-Sepharose, and the final volume was adjusted to 200 μl with solution B and AMF if indicated. Samples were incubated for 1 h on a rocking platform at 4 °C. The beads were then pelleted in a microcentrifuge for 1 min and washed twice with solution B. The p115 RhoGEF proteins and $G\alpha_{13}$ were eluted for 15 min at room temperature with 50 μl of solution B containing EE peptide (EYMPME) at a final concentration of 100 μg/ml. $G\alpha_{13}$ in the supernatant was visualized by SDS-PAGE and by immunoblot analysis using the B860 antibody.

Binding of GST-tagged rgRGS Domains of p115 RhoGEF and GTRAP48 to $G\alpha_{13}$—The purified GST-tagged domains were bound to 20 μl of glutathione-Sepharose (packed beads) and washed in solution B to remove unbound protein. Activated $G\alpha_{13}$ (5 pmol, activated as described above) was added to the indicated amount of immobilized rgRGS domain in 200 μl of solution B. After incubation on a rocking platform for 1 h at 4 °C, the samples were washed three times with solution B. The beads were then boiled in SDS sample buffer, and the eluted $G\alpha_{13}$ was visualized by SDS-PAGE and by immunoblot analysis using the B860 antibody.

Co-immunoprecipitations of $G\alpha_{12}$ or $G\alpha_{13}$ with myc-tagged p115 RhoGEF or GTRAP48 Pieces—COS cells were grown to 80% confluency in 60-mm dishes. The cells were then transfected using the FuGENE transfection reagent (Hoffman-LaRoche) with pCMV5-myc vectors that expressed the different exchange factors. Cells were also co-transfected with pCMV5 plasmids expressing either $G\alpha_{13}$ or $G\alpha_{12}$. Transfected cells were incubated at 37 °C in 5% CO_2 for 24 h. Cells were then lysed in solution B containing 0.1% Triton X-100. Non-extracted material was removed from the lysates by centrifugation at 13,600 $\times$ *g* for 5 min. The cleared lysates were then incubated with protein G-Sepharose in solution B for 30 min at 4 °C to remove proteins that bound nonspecifically to the Sepharose resin. After removal of the resin, the samples were added to protein G-Sepharose coupled to a monoclonal antibody directed against the myc tag and further incubated for 1 h at 4 °C on a rocking platform. The Sepharose beads were pelleted and washed three times with solution B. Proteins were eluted by boiling in SDS sample buffer and visualized by immunoblot analysis with specific antibodies against either the myc-tag, $G\alpha_{12}$, or $G\alpha_{13}$.

GAP Assays for $G\alpha_{13}$—$G\alpha_{13}$ (600 pmol) was loaded with [γ-^{32}P]GTP for 15 min in 300 μl of 20 mM NaHEPES, pH 8.0, 1 mM dithiothreitol, 5 mM EDTA, 0.05% polyoxyethylene 10-laurelether, 5 μM GTP, and 50 cpm /fmol [γ-^{32}P]GTP. Samples were then rapidly gel-filtered by centrifugation at 4 °C through 2 ml of Sephadex G50 resin that was previously equilibrated with buffer C (50 mM NaHEPES, pH 8.0, 1 mM dithiothreitol, 5 mM EDTA, and 0.05% polyoxyethylene 10-laurelether) to remove free [γ-^{32}P]GTP and [^{32}P]P_i. Hydrolysis of GTP was initiated by adding 60 pmol of the treated $G\alpha_{13}$ (about 2 pmol of loaded $G\alpha_{13}$) to buffer C containing 8 mM $MgSO_4$, 1 mM GTP, and the proteins to be tested for GAP activity. After incubation for the indicated times at 4 °C, aliquots (50 μl) were quenched with 750 μl of 5% (w/v) NoritA in 50 mM NaH_2PO_4. The mixtures were then centrifuged at 2000 rpm for 5 min, and 500 μl of supernatant containing [^{32}P]P_i was counted by liquid scintillation spectrometry.

Binding of GTPγS to RhoA—Binding of GTPγS to 2 μM RhoA was assayed at 30 °C in 20 μl of solution containing 20 μM GTPγS, [^{35}S]GTPγS (200,000 cpm), 50 mM NaHEPES, pH 7.5, 1 mM EDTA, 50 mM NaCl, 1 mM dithiothreitol, and 5 mM $MgCl_2$. $G\alpha_{13}$ was added to a final concentration of 100 nM after being activated for 10 min in binding buffer containing AMF. After mixing, assays were stopped at various times by the addition of 2 ml of filtration buffer (20 mM TrisCl, pH 8.0, 25 mM $MgCl_2$, 100 mM NaCl), and the proteins were immediately collected by filtration through BA-85 filters (Intermountain Scientific). The amount of [^{35}S]GTPγS bound to RhoA on each dried filter was determined by liquid scintillation spectrometry. The apparent rates of guanine nucleotide exchange for RhoA were examined at three to four concentrations to determine the average turnover rate for each p115 RhoGEF piece.

RESULTS

Mutants of p115 RhoGEF and GTRAP48 were used to identify the domains responsible for binding to $G\alpha_{13}$, stimulation of RhoA exchange activity by $G\alpha_{13}$, and acceleration of GTPase activity of $G\alpha_{12}$ and $G\alpha_{13}$. Schematic representations of these mutants are shown in Figs. 1*A* and 4*A*. Purified proteins de-

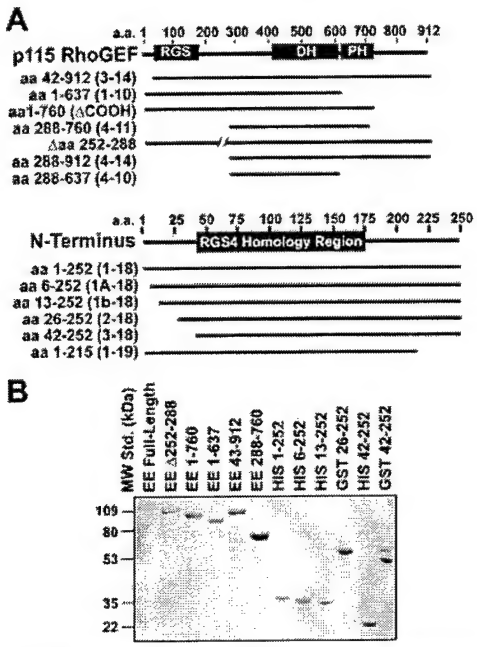

FIG. 1. **Constructs of p115 RhoGEF utilized in this study.** *A*, the domain structure of the full-length exchange factor and an expansion of the N terminus are shown at the *top* and *bottom* of the panel, respectively. The *lines* represent the composition of expressed constructs, and the specific amino acids encoded by each construct are listed at the *left*. The nomenclature in *parentheses* is derived from the oligomers used for amplification of the designated piece. *B*, different purified p115 RhoGEF pieces from representative preparations (see "Materials and Methods") used for this study were separated by SDS-PAGE and stained with Coomassie Blue R-250 dye.

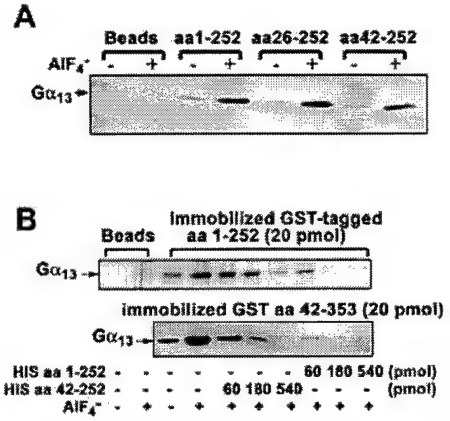

FIG. 2. **The region encompassing the rgRGS domain of p115 RhoGEF binds $G\alpha_{13}$.** *A*, 20 pmol of p115 rgRGS pieces, GST (aa 1–252), GST (aa 25–252), and GST (aa 42–252), were bound to glutathione-Sepharose and incubated with 5 pmol of $G\alpha_{13}$ either in the presence or absence of aluminum fluoride (AlF_4^-). The amount of $G\alpha_{13}$ bound to the immobilized pieces was visualized by immunoblot analysis using the B860 antibody (1:1000 dilution) as described under "Materials and Methods." *B*, relative binding of p115 rgRGS (aa 1–252) and p115 rgRGS (aa 42–252) to $G\alpha_{13}$. Either 20 pmol of p115 rgRGS GST (aa 1–252) or GST (aa 42–252) was bound to glutathione-Sepharose in the absence or presence of increasing amounts of HIS-tagged p115 rgRGS (aa 1–252) or HIS-tagged p115 rgRGS (aa 42–252) as indicated. The mixtures were then incubated with 5 pmol of $G\alpha_{13}$ as indicated under "Materials and Methods." After washing, the amount of $G\alpha_{13}$ bound to the immobilized GST-RGS chimeric proteins was visualized by immunoblot analysis using the B860 antibody.

rived from these constructs after expression via baculovirus infection of Sf9 cells or expression in *E. coli* are shown in Figs. 1*B* and 4*B*.

Expression of the p115 RhoGEF rgRGS Domains—Stable expression of the N terminus of p115 RhoGEF (aa 1–248) as a fusion protein with GST has been shown previously, and aa 45–161 were predicted to form an RGS box (26). However, subsequent deletion mutants of this N terminus identified two areas outside of the predicted RGS box that were necessary for stable expression of protein. Because p115 RhoGEF was successively deleted from the N terminus by 7 or 13 amino acids, the level of expression remained stable. Further deletion up to aa 17 or 21 resulted in fragments that did not express intact protein. This N-terminal region, which apparently interferes with protein stability, ends at or before amino acid 25, because a fragment of p115 RhoGEF encoded by aa 25–252 can be expressed at 100–200 μg/gram of *E. coli* (wet weight). The deletion of the first 41 amino acids resulted in a domain, p115 RhoGEF (aa 42–252), which was expressed at levels comparable to domains with intact N termini.

Disruption of the region lying C-terminal to the predicted RGS box that lies between amino acids 161 and 252 also affected expression of protein. Protein fragments starting with aa 1 and ending at aa 248 or 252 express extremely well in *E. coli* (3–4 mg/g of packed wet cells). However, p115 RhoGEF (aa 1–215) could only be expressed poorly at 30–40 μg/g (wet weight), and this was only possible in SF9 cells. Fragments of p115 RhoGEF with shorter C termini, which encoded either aa 25–190 or aa 42–170, showed little to no detectable expression in either bacteria or SF9 cells (data not shown).

Binding of p115 RhoGEF rgRGS Mutants to $G\alpha_{13}$—The p115 rgRGS fragments consisting of aa 1–252, 25–252, and 42–252 were expressed and purified as fusion proteins with an N-terminal GST domain (Fig. 1*A*). All three bound preferentially to the activated form of $G\alpha_{13}$ (Fig. 2*A*). The relative binding affinity of p115 rgRGS (aa 1–252) and (aa 42–252) for $G\alpha_{13}$ was then assessed by competitive binding (Fig. 2*B*). HIS-tagged p115 rgRGS (aa 1–252) and (aa 42–252) proteins were added at increasing concentrations to compete with a fixed amount of the immobilized GST-tagged constructs for binding of $G\alpha_{13}$. 60 pmol of HIS-tagged p115 rgRGS (aa 1–252) effectively reduced binding of 20 pmol of immobilized GST-tagged p115 rgRGS (aa 1–252) to $G\alpha_{13}$. In contrast, 60 pmol of p115 rgRGS (aa 42–252) had little effect, and higher concentrations (180 and 540 pmol) were needed to substantially reduce binding of the $G\alpha_{13}$ to 20 pmol of immobilized GST-tagged p115 rgRGS (aa 1–252). Similarly, HIS-tagged p115 rgRGS (aa 1–252) was a much more effective inhibitor of binding of $G\alpha_{13}$ to immobilized GST-tagged p115 rgRGS (aa 42–252) than the HIS-tagged p115 rgRGS (aa 42–252). Both comparisons demonstrate that p115 rgRGS (aa 1–252) bound to $G\alpha_{13}$ with 5- to 10-fold greater avidity than the truncated rgRGS of p115 RhoGEF (aa 42–252). Thus, the N-terminal residues of p115 rgRGS are not necessary for binding to $G\alpha_{13}$ but do contribute significantly to the affinity of this interaction.

Definition of the Minimal p115 RhoGEF rgRGS Domain Required for Acceleration of $G\alpha_{13}$ GTPase—Several N-terminal fragments of p115 RhoGEF, which included aa 1–252, 6–252, 13–252, 25–252, 42–252, and 1–215 (described in Figs. 1*A* and 3*A*), were tested for their ability to stimulate the GTPase activity of $G\alpha_{13}$. Single-turnover assays were utilized, which measure the release of $[^{32}P]P_i$ upon hydrolysis of $[\gamma\text{-}^{32}P]GTP$ that had been pre-bound to $G\alpha_{13}$. Assays were performed as described by Singer *et al* (33), with the modifications outlined under "Materials and Methods." As shown previously for a GST fusion protein containing the first 246 amino acids of p115 RhoGEF (26), the p115 rgRGS (aa 1–252) stimulated the GTPase activity of $G\alpha_{13}$ as well as the full-length exchange factor (Fig. 3*B*). However, a protein with further truncation at its C terminus, p115 rgRGS (aa 1–215), was a less effective

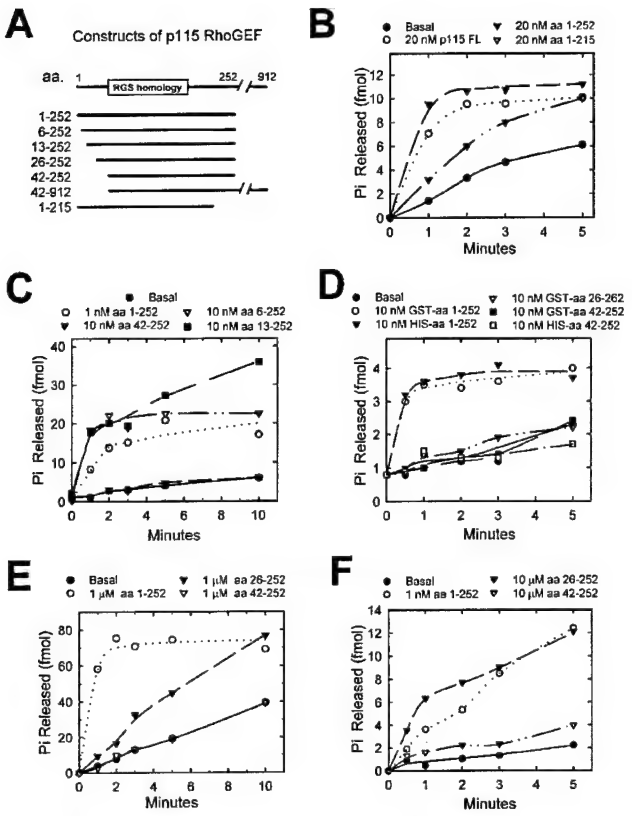

FIG. 3. **Definition of the regions within p115 RhoGEF required for acceleration of the GTPase activity of $G\alpha_{13}$.** $G\alpha_{13}$ was loaded with [γ-^{32}P]GTP and incubated at 4 °C with the indicated p115 rgRGS domains as described under "Materials and Methods." The amount of [^{32}P]P_i released from GTP was assessed at the times indicated. The variability in extent of P_i release reflects differential loading of $G\alpha_{13}$ and the actual amount of $G\alpha_{13}$-GTP added in the experiment. *A*, schematic representation of the p115 rgRGS constructs used; see also Fig. 1*A*. *B*, release of [^{32}P]P_i due to the intrinsic hydrolysis of GTP bound to $G\alpha_{13}$ (basal, *closed circles*) was compared with rates of release in the presence of 20 nM p115 RhoGEF full-length (*open circles*), 20 nM p115 rgRGS (aa 1–252) (*closed triangles*), or 20 nM p115 rgRGS (aa 1–215) (*open triangles*). *C*, hydrolysis of GTP bound to $G\alpha_{13}$ either in the absence (basal, *closed circles*) or presence of the indicated p115 rgRGS domains: 1 nM HIS p115 rgRGS (aa 1–252) (*open circles*), 10 nM HIS p115 rgRGS (aa 42–252) (*closed triangles*), 10 nM HIS p115 rgRGS (aa 6–252) (*open triangles*), or 10 nM HIS p115 rgRGS (aa 13–252) (*closed squares*). *D*, hydrolysis of GTP bound to $G\alpha_{13}$ either in the absence (basal, *closed circles*) or presence of 10 nM p115 rgRGS domains: GST p115 rgRGS (aa 1–252) (*open circles*), HIS p115 rgRGS (aa 1–252) (*closed triangles*), GST p115 rgRGS (aa 25–252) (*open triangles*), GST p115 rgRGS (aa 42–252) (*closed squares*), or HIS p115 rgRGS (aa 42–252) (*open squares*). *E*, hydrolysis of GTP bound to $G\alpha_{13}$ either in the absence (basal, *closed circles*) or presence of 1 μM p115 rgRGS domains: GST aa 25–252 (*closed triangles*), HIS aa 1–252 (*open circles*), or HIS 42–252 (*open triangles*). *F*, the GTPase activity of $G\alpha_{13}$ was measured alone (basal, *closed circles*) or in the presence of the indicated concentrations of p115 rgRGS domains: 1 nM HIS aa 1–252 (*open circles*), 10 μM HIS aa 42–252 (*open triangles*), or 10 μM GST aa 25–252 (*closed triangles*).

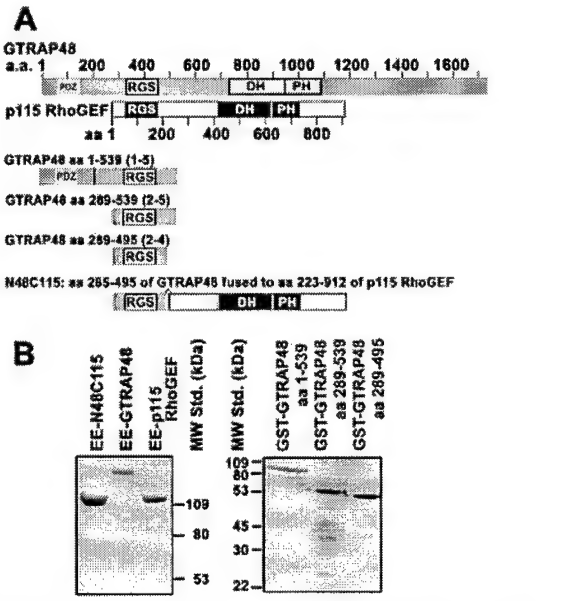

FIG. 4. **Constructs and expression of GTRAP48 and p115 RhoGEF.** *A*, constructs derived from GTRAP48 and p115 RhoGEF are shown. The amino acids encoded in each construct are also listed. Nomenclature in *parentheses* is based on the oligomers used in their construction. *B*, representative preparations of purified proteins that were derived from GTRAP48 and p115 RhoGEF (see "Materials and Methods") and used in this study were separated by SDS-PAGE and stained with Coomassie Blue R-250 dye.

stimulator of the GTPase activity of $G\alpha_{13}$. Removal of additional C-terminal residues resulted in unstable proteins that had no detectable stimulation of the GTPase activity of $G\alpha_{13}$ (data not shown).

The effects of N-terminal deletion are shown in Fig. 3 (*C–F*). Removal of the first 5 or 12 N-terminal amino acids, p115 rgRGS (aa 6–252) or p115 rgRGS (aa 13–252), respectively, did not alter GAP activities toward $G\alpha_{13}$ (Fig. 3*C*). Removal of the first 17 or 21 N-terminal amino acids did not allow expression of protein domains as discussed previously. P115 rgRGS (aa 25–252) was expressed modestly as a viable domain. Although an active GAP, the potency of this construct was only about 0.1% that of the full-length rgRGS domain encoded within aa 1–252 (Fig. 3, *D–F*). Finally, deletion of the N terminus up to the predicted RGS box, p115 RhoGEF (aa 42–252), produced a fragment that expressed well (see above). Despite binding strongly to $G\alpha_{13}$ (about 10–20% as well as p115 rgRGS (aa 1–252), see Fig. 2*B*), this fragment had essentially no GAP activity toward $G\alpha_{13}$ (Fig. 3, *C–E*). The hint of activity observed at 10 μM (Fig. 3*E*) is similar to nonspecific effects of adding other control proteins and is not increased at higher concentrations of p115 rgRGS (aa 42–252).

Binding of GTRAP48 to $G\alpha_{13}$ and $G\alpha_{12}$—GTRAP48 has been shown to bind to $G\alpha_{13}$ (25), but the functional consequences and potential interaction with $G\alpha_{12}$ are unknown. The domain arrangements of GTRAP48 and p115 RhoGEF are compared in Fig. 4*A*, and schematic descriptions of various constructs are shown. In a chimeric protein, N48C115, the N-terminal rgRGS region of p115 RhoGEF is replaced with the homologous region from GTRAP48. Examples of purified proteins that were expressed via these constructs with EE or GST tags are shown in Fig. 4*B*.

The ability of GTRAP48 to bind to $G\alpha_{12}$ as well as $G\alpha_{13}$ was assessed by immunoprecipitation after transient expression in COS cells. COS cells were transfected with either myc-tagged GTRAP48 or myc-tagged p115 RhoGEF and either constitutively active $G\alpha_{13}$ (Q226L) or constitutively active $G\alpha_{12}$ (Q229L). Both p115 RhoGEF and GTRAP48 bound to $G\alpha_{13}$ in the presence of AlF_4^-. Although p115 RhoGEF also bound well to $G\alpha_{12}$, the interaction of this α subunit with GTRAP48 is apparently weaker and was hard to detect (Fig. 5*A*, see "Discussion"). The dependence of association of these GTPase-deficient forms of $G\alpha_{12}$ and $G\alpha_{13}$ on AlF_4^- may seem surprising. However, this reflects both the multiple states of the α subunits upon lysis of cells in GDP and slow conversion of Gα·GTP to Gα·GDP through slow hydrolysis or nucleotide exchange over

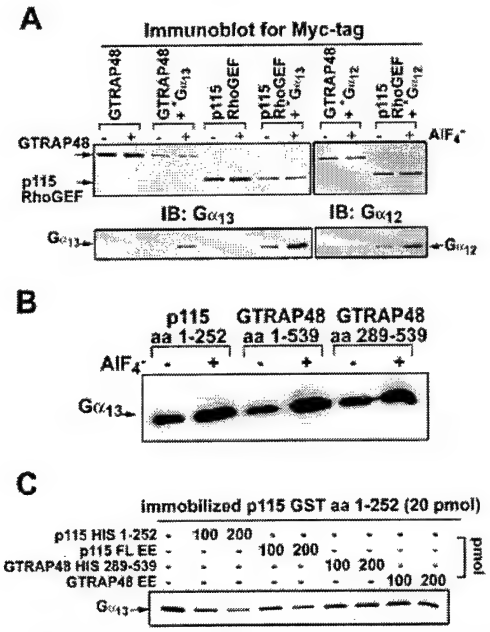

FIG. 5. **Binding of GTRAP48 to $G\alpha_{13}$ and $G\alpha_{12}$.** *A*, myc-tagged GTRAP48 or p115 RhoGEF were co-transfected into COS cells with either constitutively active $G\alpha_{13}$ (Q226L) or $G\alpha_{12}$ (Q229L). After expression and lysis of cells, the exchange factors were immunoprecipitated with antibodies specific for the myc tag in the presence or absence of aluminum fluoride as described under "Materials and Methods." Immunoprecipitates were separated by SDS-PAGE, and the relative amount of exchange factor was visualized by immunoblot (*IB*) analysis using an anti-myc antibody (*top panel*). The amount of $G\alpha_{12}$ or $G\alpha_{13}$ that co-immunoprecipitated with exchange factor was visualized with their respective specific polyclonal antibodies (*bottom panel*). *B*, binding of constructs encoding the rgRGS domain of GTRAP48 to $G\alpha_{13}$. 70 pmol of GST-tagged GTRAP48 (aa 289–539), GTRAP48 rgRGS (aa 289–495), or p115 rgRGS (aa 1–252) were immobilized on glutathione-Sepharose and incubated with 50 pmol of purified $G\alpha_{13}$ in the presence or absence of aluminum fluoride. The relative amount of $G\alpha_{13}$ bound to the rgRGS constructs after washing the Sepharose beads is shown by immunoblot analysis using B860 antisera. *C*, the relative binding affinities of p115 RhoGEF, p115 rgRGS (aa 1–252), GTRAP48, and GTRAP48 (aa 289–539) for $G\alpha_{13}$ were compared by incubating increasing concentrations of each piece with 20 pmol of immobilized GST-tagged p115 rgRGS (aa 1–252) and 10 pmol of $G\alpha_{13}$. The relative amounts of $G\alpha_{13}$ bound to GST p115 RhoGEF (aa 1–252) after washing were detected by immunoblot analysis using B860 antisera.

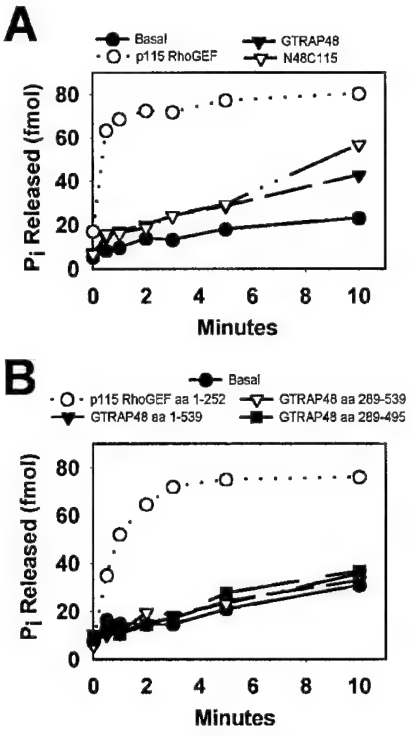

FIG. 6. **Stimulation of $G\alpha_{13}$ GTPase by GTRAP48 and its subdomains.** $G\alpha_{13}$ was loaded with [γ-^{32}P]GTP, and the acceleration of its intrinsic GTPase activity by p115 RhoGEF or GTRAP48 was measured as described under "Materials and Methods." *A*, the GTPase activity of $G\alpha_{13}$ was measured alone (basal, *closed circles*) or in the presence of 30 nM GTRAP48 (*closed triangles*), 30 nM N48C115 (*open triangles*), or 30 nM p115 RhoGEF (*open circles*). *B*, the GTPase activity of $G\alpha_{13}$ was measured without activators (*closed circles*), or in the presence of 30 nM p115 RhoGEF (aa 1–252) (*open circles*), 30 nM GTRAP48 (aa 1–539) (*closed triangles*), 30 nM GTRAP48 (aa 289–539) (*open triangles*), or 30 nM GTRAP48 (aa 289–495) (*closed squares*).

the extensive timeframe required for the immunoprecipitation.

To define the regions in GTRAP48 responsible for binding $G\alpha_{13}$, two segments, which included sequences homologous to the rgRGS domain of p115 RhoGEF, were expressed and examined. The first segment encodes aa 1–539, which includes the PDZ-and proline-rich domains that precede the rgRGS domain (Fig. 4). The second construct encodes aa 285–495, which contains amino acids homologous to the N-terminal region of p115 RhoGEF (Fig. 4). Both constructs of GTRAP48 were found to preferentially bind the activated form of $G\alpha_{13}$ (Fig. 5*B*).

The relative affinities of GTRAP48, a fragment of GTRAP48 (aa 289–539), and p115 RhoGEF for $G\alpha_{13}$ were assessed by competitive binding with immobilized GST-tagged p115 rgRGS aa (1–252) (Fig. 5*C*). Purified full-length p115 RhoGEF and HIS-tagged p115 rgRGS (aa 1–252) effectively attenuated binding of activated $G\alpha_{13}$ to the immobilized p115 rgRGS at stoichiometries of 5- to 10-fold over the immobilized domain. In contrast, EE-tagged GTRAP48 or its HIS-tagged rgRGS domain, GTRAP48 (aa 289–539), at concentrations of 5- to 10-fold over the GST-tagged p115 rgRGS (aa 1–252) showed little competition for binding to $G\alpha_{13}$. Thus, although the GTRAP48 rgRGS domain bound $G\alpha_{13}$, it did so with a definitively lower affinity than the p115 rgRGS domain.

GTRAP48 Is a Poor GAP for $G\alpha_{13}$—The ability of GTRAP48 to stimulate the GTPase activity of $G\alpha_{13}$ in a single-turnover assay is shown in Fig. 6*A*. Both GTRAP48 and N48C115 (a chimera derived from GTRAP48 and p115 RhoGEF; Fig. 4*A*) displayed low but significant stimulation of the GTPase activity of $G\alpha_{13}$. However, their activities were substantially less than the stimulation obtained with an equivalent amount of p115 RhoGEF. The N-terminal fragments of GTRAP48, which contain its rgRGS domain, failed to stimulate the GTPase activity of $G\alpha_{13}$ at the concentrations tested (Fig. 6*B*). Thus, by this *in vitro* measure, the rgRGS domain is only a poor GAP for $G\alpha_{13}$ at best. This contrasts with the robust GAP activity of p115 rgRGS.

Identification of a Second Binding Site for $G\alpha_{13}$ within p115 RhoGEF—The N-terminal 248 amino acids in p115 RhoGEF are known to interact with $G\alpha_{12}$ and $G\alpha_{13}$ and assumed to be important for stimulation of exchange activity by $G\alpha_{13}$ (1, 26). Interestingly, fragments of p115 RhoGEF that did not contain the rgRGS region, but did contain the DH and PH domains, also bound $G\alpha_{12}$ and $G\alpha_{13}$ (Fig. 7*A*). As expected, all pieces of p115 RhoGEF that contained the rgRGS domain, p115 wild type, p115 RhoGEF (aa 1–760), and p115 RhoGEF (aa 1–637) bound the activated form of $G\alpha_{13}$ in these pull-down assays. Fragments representing the C-terminal tail (aa 760–912) and the DH domain (aa 288–637) did not bind $G\alpha_{13}$. A fragment encoding the PH domain of p115 RhoGEF (aa 637–760) also did not bind $G\alpha_{13}$ (data not shown). However, a fragment of p115

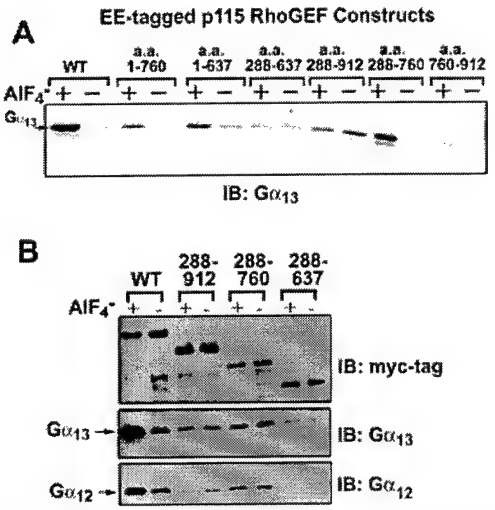

FIG. 7. **The DH/PH domain of p115 RhoGEF contains a second binding site for $G\alpha_{13}$.** *A*, purified EE-tagged p115 RhoGEF and truncated pieces of p115 RhoGEF were bound to Sepharose beads that had been conjugated to anti-EE antibodies. After incubation with purified $G\alpha_{13}$ (5 pmol), either in the presence or absence of aluminum fluoride (as indicated), the beads were washed and the relative amount of $G\alpha_{13}$ that remained bound to immobilized p115 RhoGEF constructs was determined by immunoblot (*IB*) with B860 antisera after separation by SDS-PAGE. *B*, COS cells were transfected with myc-tagged p115 RhoGEF pieces and $G\alpha_{13}$ or $G\alpha_{12}$. The exchange factors were then immunoprecipitated using an antibody directed against the myc tag. The amount of exchange factor and any associated $G\alpha_{12}$ or $G\alpha_{13}$ pulled down were visualized by immunoblot with the respective anti-myc (*top panel*), B860 (*middle panel*), and anti-$G\alpha_{12}$ (*bottom panel*) antibodies.

RhoGEF that consists essentially of the DH and PH domains (aa 288–760), bound $G\alpha_{13}$ almost as well as the full-length protein, and this binding showed a marked dependence on the activated state (AlF_4^-) of $G\alpha_{13}$. In contrast, p115 RhoGEF (aa 288–912), which contains the C terminus of p115 RhoGEF as well as the DH and PH domains, bound $G\alpha_{13}$ with low avidity, and this association was not dependent on AlF_4^-. This could explain the failure to see binding of the p115 RhoGEF (aa 246–912) protein to $G\alpha_{13}$ in the previous study by Hart *et al* (1).

Binding of p115 RhoGEF pieces to $G\alpha_{12}$ or $G\alpha_{13}$ was also tested by transient co-expression in COS cells of the G protein and myc-tagged p115 RhoGEF wild type, p115 RhoGEF (aa 288–912), p115 RhoGEF (aa 288–760), or p115 RhoGEF (aa 288–637) as indicated (Fig. 7*B*). Co-immunoprecipitations of the α subunits with specific myc-tagged proteins support the *in vitro* data with purified proteins. $G\alpha_{13}$ bound to proteins that contained the DH and PH domains, but lacked the rgRGS region. The same pattern was observed with binding of $G\alpha_{12}$. A weaker interaction with the $G\alpha$ subunits was also observed when the C terminus was present. In contrast to the *in vitro* measurement, there was little dependence on activation of the G proteins with AlF_4^- (Fig. 7*B*).

Functional Mapping of the Domains in p115 RhoGEF Required for Stimulation of Exchange Activity by $G\alpha_{13}$—The ability of different truncated p115 RhoGEF proteins to effect exchange of guanine nucleotide on RhoA was determined either in the presence or absence of $G\alpha_{13}$ that had been activated with AlF_4^- (Table I). Average rates of turnover for stimulation of RhoA were determined at a fixed concentration of RhoA and at various concentrations of exchange factor as described under "Materials and Methods." All of the constructs that contained the rgRGS region could be stimulated by $G\alpha_{13}$. Thus, removal of the first 41 N-terminal amino acids of p115 RhoGEF in p115 RhoGEF (aa 42–912) (described in Fig. 1*A*) or of the C terminus in p115 RhoGEF (aa 1–760) did not affect activation of RhoA

TABLE I
Stimulation of truncated p115 RhoGEF constructs by $G\alpha_{13}$

The apparent turnover rate for each p115 RhoGEF construct is based on the measured number of moles of GTPγS bound to RhoA. This was determined by measuring the amount of RhoA that bound [^{35}S]GTPγS over time and at multiple concentrations of exchange factor as described under "Materials and Methods." The rates calculated from each time course were plotted against the amount of exchange factor used, and an average apparent turnover rate was determined by linear regression analysis. The rate measurements were made either in the presence or absence of 200 nM $G\alpha_{13}$, which was activated with aluminum fluoride. The last column indicates the -fold activation over basal activity affected by $G\alpha_{13}$. The basal rates of turnover for these proteins were reported previously (31). A coefficient of determination, R^2, that measured the degree to which the derivatives of the apparent rates fit a linear regression model was 0.99 or greater except for the α_{13}-stimulated rate of p115 RhoGEF (aa 288–760), which was 0.98.

p115 RhoGEF constructs	Basal rate	Rate in the presence of $G\alpha_{13}$	Activation
		min^{-1}	*-fold*
p115 RhoGEF full-length	140	400	2.9
p115 RhoGEF Δ252–288	30	150	5.0
p115 RhoGEF (aa 1–760)	14	50	3.6
p115 RhoGEF (aa 1–637)	3	11	3.7
p115 RhoGEF (aa 42–912)	70	180	2.6
p115 RhoGEF (aa 288–760)	7	7	1.0

exchange activity by $G\alpha_{13}$. P115 RhoGEF (aa 1–637), which encodes the rgRGS domain and the DH domain but lacks the PH domain and C terminus, has greatly reduced basal activity, but this activity was still stimulated by $G\alpha_{13}$. Removal of 32 amino acids (aa 252–288) that lie between the rgRGS domain and the DH domain and have a marked effect on basal activity (31) also did not reduce stimulation by $G\alpha_{13}$. In contrast, removal of the entire rgRGS domain in p115 RhoGEF (aa 288–760) eliminated sensitivity to $G\alpha_{13}$ (Table I).

GTRAP48 is also an exchange factor with specificity for RhoA (25). However, $G\alpha_{13}$ did not stimulate RhoA exchange mediated by GTRAP48 (Fig. 8*A*). To test whether the rgRGS domain of GTRAP48 was capable of mediating stimulation by $G\alpha_{13}$, it was used to replace the native rgRGS domain of p115 RhoGEF (see N48C115 in Fig. 4*A* for details). Interestingly, the RhoA nucleotide exchange activity of the N48C115 chimera was activated 3- to 4-fold by $G\alpha_{13}$ (Fig. 8*B*). This indicates that the GTRAP48 rgRGS domain can mimic this function of the p115 rgRGS domain in the context of the rest of the p115 RhoGEF molecule.

DISCUSSION

The rgRGS Domain of p115 RhoGEF Is Unique from the Classic RGS Proteins—RGS proteins were originally identified in genetic screens as negative regulators of G protein signaling (35–37). The majority of RGS proteins were subsequently cloned by degenerate PCR using primers based on the RGS boxes of these founder members (15). The lack of sequence identity between the RGS and rgRGS domains would explain why the latter proteins were not identified by strategies using PCR or homology searching of data bases. The elucidation of the N terminus of p115 RhoGEF as a GAP for $G\alpha_{12}$ and $G\alpha_{13}$ (26) led to the suggestion of potential structural relationships with the RGS family and initiated identification of the subfamily of highly homologous rgRGS domains in PDZ RhoGEF (KIAA0380) (23), LARG (KIAA0382) (22), and GTRAP48 (25).

A region, designated the RGS box (about 110 amino acids), has been shown to be sufficient for the GAP activity (38) of several members of the RGS family, including RGS4, GAIP, and RGS10. The studies reported here demonstrate that this is not the case with the p115 rgRGS domain. Secondary structure analysis of p115 RhoGEF suggested that amino acids 45–161 would likely comprise an RGS box (26). Initial observations

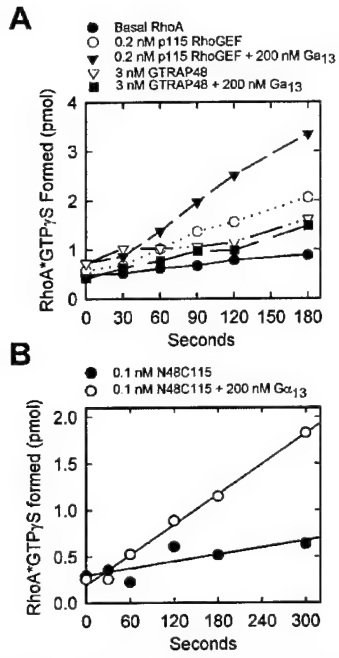

FIG. 8. **Regions outside the rgRGS domain of GTRAP48 and p115 RhoGEF determine specificity for activation by $G\alpha_{13}$.** *A*, the rate of exchange of GTRAP48 is not stimulated by $G\alpha_{13}$. Binding of [^{35}S]GTPγS to RhoA was measured along a 3-min time course without exchange factor (*closed circles*), with 0.2 nM p115 RhoGEF in the absence (*open circles*) or presence (*closed triangles*) of 200 nM $G\alpha_{13}$ and AlF_4^-, or with 10 nM GTRAP48 in either the absence (*open triangles*) or presence (*closed squares*) of 200 nM $G\alpha_{13}$ and AlF_4^-. *B*, the nucleotide exchange rate of N48C115 is stimulated by $G\alpha_{13}$. Binding of [^{35}S]GTPγS to RhoA was measured along a 5-min time course in the presence of 0.1 nM N48C115 and either the absence (*closed circles*) or presence (*open circles*) of $G\alpha_{13}$ and AlF_4^-.

showed that aa 1–246 of p115 RhoGEF possessed GAP activity equivalent to the full-length enzyme (26). Reduction of the C-terminal end of this piece by 31 amino acids, p115 RhoGEF (aa 1–215), results in poor expression and reduced GAP activity. Further truncation of C-terminal residues results in proteins that express very poorly and have no measurable GAP activity (data not shown). Deletion of the N-terminal 25 amino acids of p115 RhoGEF reduced GAP activity over 99%. Removal of the N-terminal 41 amino acids still allowed expression of this domain but reduced binding to $G\alpha_{13}$ by 80–90% (Fig. 2*B*) and completely eliminated GAP activity (Fig. 3, *C–F*). Thus, an RGS region of p115 RhoGEF that retains some catalytic function requires ~200 residues (aa 26–216); full function requires more.

These data indicate significant differences between this rgRGS domain and the classic RGS domains. First, the rgRGS domain requires an extended C terminus for stability and, perhaps, function. This is supported by the recent elucidation of crystallographic structures for the rgRGS domain of p115 RhoGEF (29) and the rgRGS domain of PDZ RhoGEF (39). Both of these rgRGS domains show similarity to the RGS box structure (15, 19–21) in their core regions (aa 45–161 of p115 RhoGEF) but also show close association of their core regions with C-terminal residues that form three α-helices and fold back onto the core. The capability of p115 RhoGEF (aa 42–252) to bind, but not act as a GAP on $G\alpha_{13}$, offers a clear dissociation of these two activities. In contrast, mutational analysis of classic RGS proteins indicates that reductions in GAP activity correlate much more strongly with decreases in binding avidity between the RGS and the targeted G protein α subunit (40). Because RGS4 binds and allosterically stabilizes the transition state of the switch 1 and switch 2 domains of $G\alpha_i$, it is hypothesized that any reduction in binding energy would also reduce the degree of stabilization of the transitions state (15, 40, 41). The clear dissociation of binding and GAP activity in the p115 rgRGS indicates that it has a novel mechanism of accelerating the GTPase activity of $G\alpha_{12}$ and $G\alpha_{13}$.

Comparison of the rgRGS Domains of GTRAP48 and p115 RhoGEF—GTRAP48, a recently characterized protein with an apparent rgRGS domain, was previously shown to bind $G\alpha_{13}$ (25). Binding of GTRAP48 to $G\alpha_{13}$ was confirmed in the current studies, but binding to $G\alpha_{12}$ was not readily detected (Fig. 5). GTRAP48 could act as a very poor GAP for $G\alpha_{12}$ (data not shown). Thus, GTRAP48 can interact with $G\alpha_{12}$, albeit weakly. The GAP activity of GTRAP48 for $G\alpha_{13}$ was also poor and truncated proteins that contained its rgRGS region and could also bind $G\alpha_{13}$ had little to no GAP activity (Fig. 6). Similar to GTRAP48, the rgRGS domain of PDZ RhoGEF also interacted with $G\alpha_{12}$ and $G\alpha_{13}$ and was a very poor GAP for $G\alpha_{13}$.[2] This latter phenotype contrasts with the rgRGS region of p115 RhoGEF encoded within aa 1–252, which is as good as the full-length p115 RhoGEF at activating the GTPase activity of $G\alpha_{13}$. The lack of identity between the highly negatively charged N-terminal region of p115 rgRGS (aa 26–41) and the matching region of GTRAP48 (aa 314–326) may provide one explanation for the observed low activity of GTRAP48. Removal of these amino acids eradicates the GAP activity in p115 RhoGEF. These findings then suggest that GTRAP48 is not a major GAP for the G_{12} family. Alternatively, it is possible that another factor, yet to be identified, provides the functional equivalent of the N-terminal residues (aa 26–41) in the p115 rgRGS to effect stimulation of GAP activity by GTRAP48.

The Mechanisms of p115 RhoGEF for GAP Activity on $G\alpha_{13}$ and Mediation of Rho Exchange Activity by $G\alpha_{13}$ Are Different—Initial experiments indicated that the N-terminal region of p115 RhoGEF, which encompasses the rgRGS domain, was sufficient for GAP activity (26). The inability of p115 RhoGEF (aa 288–760) but not of p115 RhoGEF (aa 1–760) to be stimulated by $G\alpha_{13}$ indicates that the first N-terminal 288 amino acids of p115 RhoGEF (which contains the rgRGS domain) are important for this process. What is the role of the GAP activity in this regulation? The observation that removal of the N-terminal 41 amino acids in p115 RhoGEF eradicates GAP activity, but has no effect on the ability of activated $G\alpha_{13}$ to stimulate exchange activity, indicates both structural and functional divergence in these activities. Thus, the stimulation of GTPase activity has no impact on the mechanism for stimulation of exchange activity and should only impact rates of inactivation.

Interactions between $G\alpha_{13}$ and Regions Outside the rgRGS Domain of p115 RhoGEF Play a Role in Activation of Exchange Activity by $G\alpha_{12}$—The abrogation of regulation upon removal of its rgRGS domain suggests three mechanisms by which the exchange activity of p115 RhoGEF is stimulated by $G\alpha_{13}$. One mechanism would utilize the interaction of $G\alpha_{13}$ with the rgRGS region to alleviate an autoinhibitory action of the domain on exchange activity. This is most unlikely, because truncation of this rgRGS actually caused a reduction in basal exchange activity (31) rather than an increase that would be expected from removing an autoinhibitory constraint. The more rigorous characterization reported here contrasts with an initial observation that the activity of a p115 RhoGEF fragment lacking the N terminus (aa 246–912) was greater than that of the full-length protein. One reason for this discrepancy is the use of prenylated RhoA in the current studies. Preny-

[2] T. Kozasa and P. Sternweis, unpublished data.

lated RhoA is a much more potent substrate for p115 RhoGEF (32) than the non-prenylated GTPase used previously. P115 RhoGEF (aa 246–912) exhibits less of an increase in activity toward the prenylated form of RhoA than wild type p115 RhoGEF and, therefore, is less active than p115 RhoGEF in this context (data not shown).

A second mechanism would use binding of $G\alpha_{13}$ to the rgRGS domain to induce an allosteric mechanism for activation by which the rgRGS region causes higher nucleotide exchange activity of the DH domain on RhoA. In a third scenario, binding of the rgRGS domain to $G\alpha_{13}$ helps stabilize interaction of $G\alpha_{13}$ with another part of p115 RhoGEF to promote a higher activity state of the DH domain.

The discovery that $G\alpha_{13}$ binds to a second region of p115 RhoGEF outside of the rgRGS domain suggests that the third mechanism is most likely. Because the rgRGS domain alone provides the same GAP activity as the full-length protein (Fig. 3), this second site of interaction is clearly not needed for this function and is more likely to play a key role in the stimulation of exchange activity. The location of this second site appears to be in the area of the DH domain. A construct composed essentially of the DH and PH domains, p115 RhoGEF (aa 288–760), binds $G\alpha_{13}$ better than to a comparable construct missing the PH domain, p115 RhoGEF (aa 288–637) (Fig. 7, *A* and *B*), or to the PH domain alone (data no shown). However, the ability of $G\alpha_{13}$ to effectively stimulate a truncated protein that contained the rgRGS and DH domains but lacked the PH domain, p115 RhoGEF (aa 1–637), suggests that this second site of interaction is still present. The higher affinity observed when the PH domain is present may be due to stabilization of the DH domain and preservation of higher affinity for $G\alpha_{13}$. The drastically reduced basal exchange activity of p115 RhoGEF (aa 1–637) shown previously (31) (and in Fig. 8*A*) and the apparent low affinity of constructs lacking the PH domain for RhoA (31) are consistent with this interpretation.

Although GTRAP48 has rgRGS and DH domains that are similar in sequence and arrangement to the corresponding domains in p115 RhoGEF, $G\alpha_{13}$ does not stimulate the exchange activity of GTRAP48, *in vitro*. The physiological implication of this difference is not known. It is possible that the interaction of $G\alpha_{13}$ with GTRAP48 could be stimulatory *in vivo* by mediating localization of the exchange factor or that another factor may be required to mediate a regulatory effect of $G\alpha_{13}$ on GTRAP48. Alternatively, it is possible that G_{13} does not regulate the activity of GTRAP48 in the cellular milieu. Attempts to directly answer this question by overexpression of the exchange factor and $G\alpha_{13}$ have not yet yielded definitive results for two major reasons. Expression of GTRAP48 has been highly variable, especially when co-expressed with $G\alpha_{13}$ (*e.g.* Fig. 5*A*, compare *lanes 1* and *2* with *lanes 3* and *4*). Furthermore, the expression of $G\alpha_{13}$ alone gives robust activation of Rho and downstream events. The use of alternative and better controlled expression systems may eventually allow better analysis of this putative regulation.

The differential response of GTRAP48 and p115 RhoGEF to $G\alpha_{13}$ may be explained by dissimilarities between the rgRGS or DH domains of these two exchange factors, because these domains in p115 RhoGEF are sufficient for activation of exchange activity by $G\alpha_{13}$. To address this question, the rgRGS domain of p115 RhoGEF was replaced with the rgRGS domain of GTRAP48 to make the N48C115 chimera. The ability of this chimera to be stimulated by $G\alpha_{13}$ just like wild type p115 RhoGEF strongly argues that the rgRGS domains of these two proteins are functionally equivalent when mediating activation of exchange activity by $G\alpha_{13}$. Thus, differences within GTRAP48 and p115 RhoGEF that lie outside the rgRGS domain must explain their disparate responses to $G\alpha_{13}$. The rgRGS domain of p115 RhoGEF may, therefore, function to tether and/or position $G\alpha_{13}$ so that it can directly interact with the DH domain of p115 RhoGEF. Alternatively, interaction with the rgRGS may induce conformational changes in $G\alpha_{13}$ that yield an ability to stimulate exchange.

Acknowledgements—We thank Jana Hadas for superb technical support, Bill Singer for comments on the manuscript, and James Chen for advice on sequence analysis. We also thank Melanie Cobb for various cDNA constructs used in this study.

REFERENCES

1. Hart, M. J., Jiang, X., Kozasa, T., Roscoe, W., Singer, W. D., Gilman, A. G., Sternweis, P. C., and Bollag, G. (1998) *Science* **280,** 2112–2114
2. Gilman, A. G. (1987) *Annu. Rev. Biochem.* **56,** 615–649
3. Hepler, J. R., and Gilman, A. G. (1992) *Trends Biochem. Sci.* **17,** 383–387
4. Strathmann, M. P., and Simon, M. I. (1991) *Proc. Natl. Acad. Sci. U. S. A.* **88,** 5582–5586
5. Jiang, H., Wu, D., and Simon, M. I. (1993) *FEBS Lett.* **330,** 319–322
6. Parks, S., and Wieschaus, E. (1991) *Cell* **64,** 447–458
7. Offermanns, S., Mancino, V., Revel, J. P., and Simon, M. I. (1997) *Science* **275,** 533–536
8. Buhl, A. M., Johnson, N. L., Dhanasekaran, N., and Johnson, G. L. (1995) *J. Biol. Chem.* **270,** 24631–24634
9. Gohla, A., Harhammer, R., and Schultz, G. (1998) *J. Biol. Chem.* **273,** 4653–4659
10. Sah, V. P., Seasholtz, T. M., Sagi, S. A., and Brown, J. H. (2000) *Annu. Rev. Pharmacol. Toxicol.* **40,** 459–489
11. Nobes, C., and Hall, A. (1994) *Curr. Opin. Genet. Dev.* **4,** 77–81
12. Berman, D. M., and Gilman, A. G. (1998) *J. Biol. Chem.* **273,** 1269–1272
13. Watson, N., Linder, M. E., Druey, K. M., Kehrl, J. H., and Blumer, K. J. (1996) *Nature* **383,** 172–175
14. Hunt, T. W., Fields, T. A., Casey, P. J., and Peralta, E. G. (1996) *Nature* **383,** 175–177
15. Wilkie, T. M. (2000) *Annu. Rev. Biochem.* **69,** 795–827
16. Berman, D. M., Wilkie, T. M., and Gilman, A. G. (1996) *Cell* **86,** 445–452
17. Hepler, J. R., Berman, D. M., Gilman, A. G., and Kozasa, T. (1997) *Proc. Natl. Acad. Sci. U. S. A.* **94,** 428–432
18. Tesmer, J. J., Berman, D. M., Gilman, A. G., and Sprang, S. R. (1997) *Cell* **89,** 251–261
19. de Alba, E., De Vries, L., Farquhar, M. G., and Tjandra, N. (1999) *J. Mol. Biol.* **291,** 927–939
20. Spink, K. E., Polakis, P., and Weis, W. I. (2000) *EMBO J.* **19,** 2270–2279
21. Slep, K. C., Kercher, M. A., He, W., Cowan, C. W., Wensel, T. G., and Sigler, P. B. (2001) *Nature* **409,** 1071–1077
22. Fukuhara, S., Chikumi, H., and Gutkind, J. S. (2000) *FEBS Lett.* **485,** 183–188
23. Fukuhara, S., Murga, C., Zohar, M., Igishi, T., and Gutkind, J. S. (1999) *J. Biol. Chem.* **274,** 5868–5879
24. Hart, M. J., Sharma, S., elMasry, N., Qiu, R. G., McCabe, P., Polakis, P., and Bollag, G. (1996) *J. Biol. Chem.* **271,** 25452–25458
25. Jackson, M., Song, W., Liu, M. Y., Jin, L., Dykes-Hoberg, M., Lin, C. I., Bowers, W. J., Federoff, H. J., Sternweis, P. C., and Rothstein, J. D. (2001) *Nature* **410,** 89–93
26. Kozasa, T., Jiang, X., Hart, M. J., Sternweis, P. M., Singer, W. D., Gilman, A. G., Bollag, G., and Sternweis, P. C. (1998) *Science* **280,** 2109–2111
27. Cerione, R. A., and Zheng, Y. (1996) *Curr. Opin. Cell Biol.* **8,** 216–222
28. Lemmon, M. A., and Ferguson, K. M. (1998) *Curr. Top. Microbiol. Immunol.* **228,** 39–74
29. Chen, Z., Wells, C. D., Sternweis, P. C., and Sprang, S. R. (2001) *Nat. Struct. Biol.* **8,** 805–809
30. Guan, K. L., and Dixon, J. E. (1991) *Anal. Biochem.* **192,** 262–267
31. Wells, C. D., Gutowski, S., Bollag, G., and Sternweis, P. C. (2001) *J. Biol. Chem.* **276,** 28897–28905
32. Wells, C., Jiang, X., Gutowski, S., and Sternweis, P. C. (2002) *Methods Enzymol.* **345,** 371–372
33. Singer, W. D., Miller, R. T., and Sternweis, P. C. (1994) *J. Biol. Chem.* **269,** 19796–19802
34. Kozasa, T., and Gilman, A. G. (1995) *J. Biol. Chem.* **270,** 1734–1741
35. Koelle, M. R., and Horvitz, H. R. (1996) *Cell* **84,** 115–125
36. Lee, B. N., and Adams, T. H. (1994) *Mol. Microbiol.* **14,** 323–334
37. Dohlman, H. G., Apaniesk, D., Chen, Y., Song, J., and Nusskern, D. (1995) *Mol. Cell. Biol.* **15,** 3635–3643
38. Popov, S., Yu, K., Kozasa, T., and Wilkie, T. M. (1997) *Proc. Natl. Acad. Sci. U. S. A.* **94,** 7216–7220
39. Longenecker, K. L., Lewis, M. E., Chikumi, H., Gutkind, J. S., and Derewenda, Z. S. (2001) *Structure (Camb.)* **9,** 559–569
40. Srinivasa, S. P., Watson, N., Overton, M. C., and Blumer, K. J. (1998) *J. Biol. Chem.* **273,** 1529–1533
41. Berman, D. M., Kozasa, T., and Gilman, A. G. (1996) *J. Biol. Chem.* **271,** 27209–27212

Inhibition of Cyclooxygenase-2 Protects Motor Neurons in an Organotypic Model of Amyotrophic Lateral Sclerosis

Daniel B. Drachman, MD,
and Jeffrey D. Rothstein, MD, PhD

The pathogenesis of motor neuron loss in amyotrophic lateral sclerosis (ALS) is thought to involve both glutamate-mediated excitotoxicity and oxidative damage due to the accumulation of free radicals and other toxic molecules. Cyclooxygenase-2 (COX-2) may play a key role in these processes by producing prostaglandins, which trigger astrocytic glutamate release, and by inducing free radical formation. We tested the effects of COX-2 inhibition in an organotypic spinal cord culture model of ALS. The COX-2 inhibitor (SC236) provided significant protection against loss of spinal motor neurons in this system, suggesting that it may be useful in the treatment of ALS.

Drachman DB, Rothstein JD. Inhibition of cyclooxygenase-2 protects motor neurons in an organotypic model of amyotrophic lateral sclerosis. Ann Neurol 2000;48:792–795

There is increasing evidence that glutamate-mediated excitotoxicity plays an important role in the pathogenesis of amyotrophic lateral sclerosis (ALS).[1,2] Glutamate released by presynaptic neurons normally stimulates motor neurons, and its synaptic actions are rapidly terminated by specific glutamate transporters on astrocytic and neuronal membranes surrounding the synapse. Accumulation of glutamate in the synaptic space can exert neurotoxic effects mediated by the entry of Ca^{2+} in motor neurons and the production of various toxic molecules.[2] Impairment of glutamate uptake by the astrocytic transporters is thought to play an important role in the pathogenesis of ALS.[1,2] It is now clear that astrocytes not only take up glutamate but that they also synthesize and release substantial amounts of glutamate. Astrocytic glutamate release may be stimulated by prostaglandins via a calcium-dependent pathway,[3,4] and this triggers additional glutamate release from the astrocytes by a positive feedback mechanism. Prostaglandins are produced within the central nervous system by the enzymatic action of cyclooxygenase-2 (COX-2), which catalyzes the synthesis of prostaglandins from arachidonic acid. Inhibitors of COX can powerfully inhibit astrocytic glutamate release.[3] Thus, COX-2 inhibitors might have a therapeutic effect in ALS by inhibiting astrocytic release of glutamate. Furthermore, the fact that COX-2 plays a pivotal role in inflammatory processes in the central nervous system[5] has led us to anticipate that its inhibition could have additional therapeutic benefit in ALS.

To evaluate the therapeutic effect of COX-2 inhibition, we used an in vitro model of glutamate excitotoxicity.[6] Mammalian spinal cord slices are maintained in an organotypic culture system in which the motor neurons normally remain intact for more than 3 months. When astroglial transport of glutamate is inhibited by threo-hydroxyaspartate (THA), however, the spinal cord sections exhibit persistent elevation of glutamate levels and undergo gradual loss of motor neurons. This model system has been used in the preclinical evaluation of agents of potential interest for the treatment of ALS.[7] In the present study, we used a selective COX-2 inhibitor (SC236; Monsanto/Searle, St Louis, MO), which is homologous to celecoxib, a drug currently in use for the treatment of arthritis. Our findings show that the addition of SC236 to THA-treated spinal cord cultures resulted in highly significant protection against loss of motor neurons.

Material and Methods

Organotypic spinal cord cultures were prepared from lumbar spinal cords of 8-day-old rat pups sectioned transversely into 350-μm slices and cultured on Millicell CM (Millipore Corp, Bedford, MA) semipermeable culture inserts at 37°C with 5% CO_2 and 95% humidity. Under these conditions, more than 95% of cultures retain cellular organization, with survival of motor neurons in excess of 3 months. Culture media consisted of HEPES-buffered minimum essential medium (50%) with 25% heat-inactivated horse serum and 25% Hanks' balanced salt solution supplemented with D-glucose (25.6 mg/ml) and glutamine (0.2 M). Seven days after culture preparation, THA was added to experimental cultures at 150 μM, which produces excitotoxic damage to motor neurons within 3 to 4 weeks. SC236 was added as indicated to achieve final concentrations from 0 to 100 μM. Parallel spinal cord cultures with no drugs added, THA alone, SC236 alone, and SC236 plus THA were run simultaneously. Experiments at each concentration of SC236 were repeated three to five times. A total of 25 to 47 cultures were used for each treatment. The medium, with THA and SC236 at indicated concentrations, was changed twice a week. The cultures were maintained for 4 weeks and pre-

From the Department of Neurology, The Johns Hopkins School of Medicine, Baltimore, MD.

Received May 1, 2000, and in revised form Jun 14. Accepted for publication Jun 15, 2000.

Address correspondence to Dr Drachman, Department of Neurology, Johns Hopkins School of Medicine, Meyer Building 5-119, 600 North Wolfe Street, Baltimore, MD 21287–7519.

pared as described below for quantification of motor neurons.

Motor neurons were identified by two immunocytochemical markers: SMI-32 stains nonphosphorylated neurofilaments, which are abundant in motor neuron cell bodies, and Islet-1 is a motor neuron–specific marker. Cultures were fixed with 4% paraformaldehyde in 0.1 M phosphate buffer for 30 minutes and then permeabilized with cold methanol or 0.1% Triton X-100 for SMI-32 and Islet-1 staining, respectively. Incubation with SMI-32 antibodies (1:8,000) or Islet-1 antibodies (1:100) was performed overnight at 4°C. After incubation with biotinylated horse anti-mouse antibodies and avidin-biotin complex reagents (Vector Labs, Burlingame, CA), color was developed with diaminobenzidine.

To quantify surviving motor neurons, whole-mount cultures immunostained by SMI-32 were used. The microscopist was unaware of the treatments used. Motor neurons were identified by three criteria: immunostaining with SMI-32, size greater than 25 μm, and localization to the ventral gray region of spinal cord (Fig 1). The motor neuron count using SMI-32 was verified by Islet-1 staining in some cases.

Results

Treatment with THA produces gradual motor neuron toxicity attributable to excessive extracellular glutamate. This mimics, in part, the loss of glutamate transport that occurs in sporadic ALS patients. We used a concentration of THA (150 μM) that produces motor neuron damage in 3 to 5 weeks.

Fig 1. Administration of cyclooxygenase-2 (COX-2) inhibitor SC236 significantly protected against glutamate-mediated toxicity. Spinal cord organotypic cultures were incubated with the glutamate transporter inhibitor threo-hydroxyaspartate (THA) for 4 weeks in vitro along with the COX-2 inhibitor SC236 as indicated. THA alone produced a large loss of motor neurons. SC236 protected against THA-mediated toxicity over a wide concentration range. $^{**}p < 0.01$ *when compared with THA-treated cultures.* $^{*}p < 0.05$ *when compared with THA-treated cultures.*

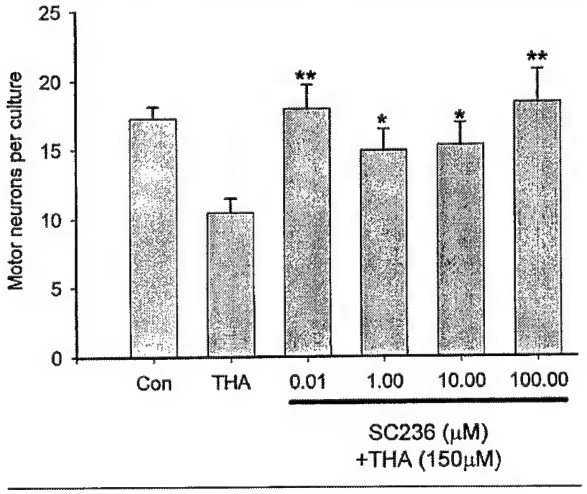

Addition of THA alone resulted in a highly significant loss of motor neurons compared with control untreated cultures (see Figs 1 and 2). SC236 added to the THA-treated cultures potently and significantly protected motor neurons against excitotoxic damage at all concentrations tested (see Figs 1 and 2). The apparent lack of dose response is unexplained but could reflect a plateau effect. Nevertheless, this COX-2 inhibitor prevented the excitotoxic loss of motor neurons. We also noted a moderate decrease of motor neurons in cultures treated with SC236 alone.

Discussion

These experiments were undertaken to test the hypothesis that inhibition of COX-2 activity could prevent excitotoxic motor neuron loss in an ALS-like organotypic spinal cord culture model. This hypothesis was based on the key role of COX-2 in the production of prostaglandins and the demonstrated effects of prostaglandins in stimulating astroglial glutamate release and producing inflammatory changes as well as a variety of toxic molecules. Our findings show that COX-2 inhibition had a highly significant protective effect on motor neurons in this model system.

Different forms of COX exist in two isoforms: COX-1, which is constitutively expressed at extremely low levels in the nervous system but is not inducible, and COX-2, which is present throughout the central nervous system[8,9] and is highly inducible. The different forms of COX catalyze the rate-limiting steps in the synthesis of prostaglandins.[8,10] COX-2 is present in neurons and astrocytes[11,12] as well as in macrophages and microglia.[13] COX-2 has been demonstrated in the anterior horns of the spinal cord[14–17] and specifically in motor neurons of rat spinal cord by immunocytochemistry.[14,16] COX-2 is an inducible enzyme[8,11] that increases in the brain after synaptic activity, seizures, or ischemia[9] and in the spinal cord after trauma to the cord[16] or peripheral noxious stimuli such as inflammatory arthritis.[15] Proinflammatory cytokines, including interleukin-1β, upregulate the expression of COX-2 in astrocytes as well as in other cells.[8,11] Of particular interest, interleukin-1β is markedly elevated in spinal cords of a mutant superoxidase dismutase 1^{G93A} mouse model of ALS and plays a role in apoptotic neuronal cell death in that model.[18]

It is likely that the effectiveness of COX-2 inhibition in preventing excitotoxic motor neuron death in our model system is due to the interruption of multiple processes, which can interact in a vicious cycle to produce progressive damage to motor neurons and astrocytes. One such mechanism is the prostaglandin-induced release of glutamate from astrocytes and secondarily from neurons, which induces excitotoxic damage. Excitotoxicity of the released glutamate is further enhanced because of the decreased buffering ca-

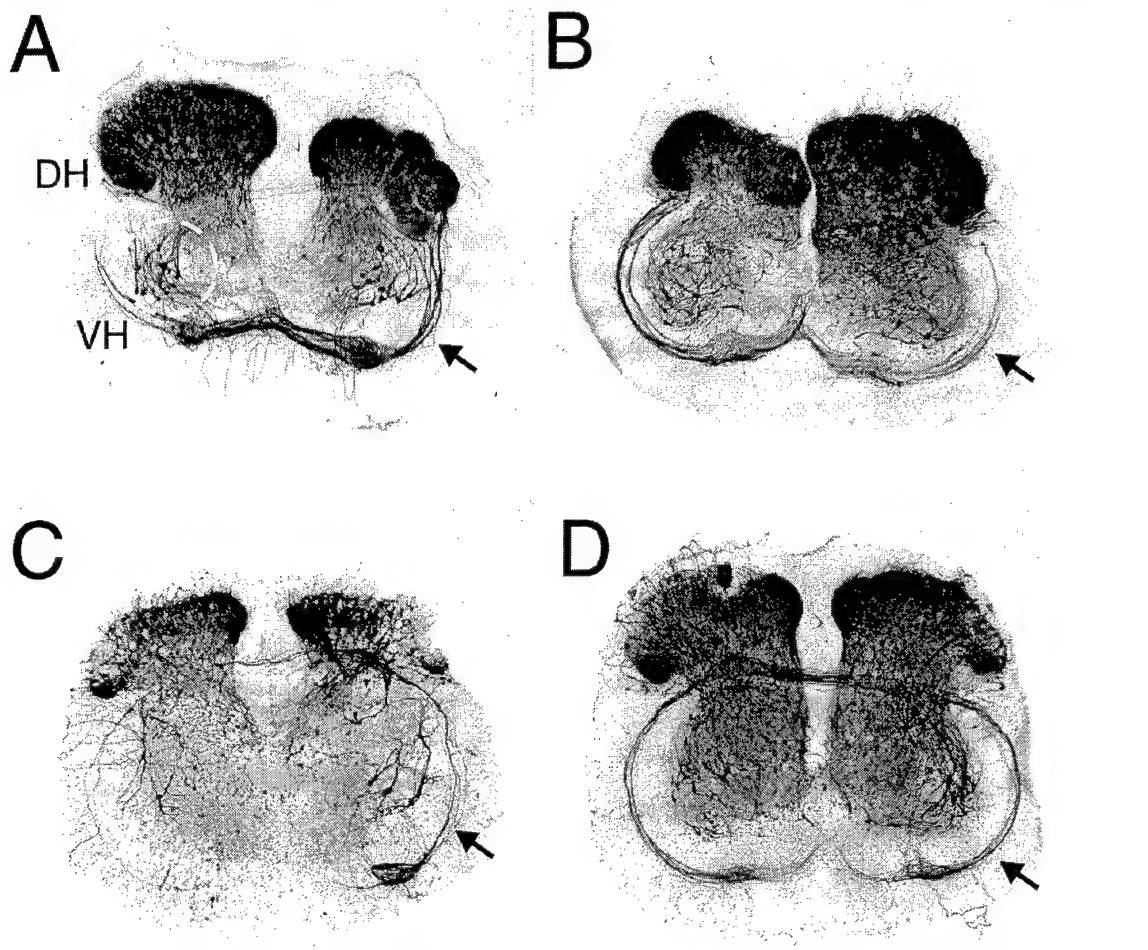

Fig 2. Cyclooxygenase-2 (COX-2) inhibitor SC236 protected against threo-hydroxyaspartate (THA)–induced chronic glutamate toxicity. Organotypic spinal cord cultures were maintained for 4 weeks, and motor neurons were identified by staining neurofilaments with SMI-32. (A) Control culture with no THA or SC236. Labeled motor neuron cell bodies in the ventral horn are within the dotted circle labeled VH. (B) SC236-treated cultures (without THA). (C) THA-treated culture showing loss of motor neurons bilaterally in the ventral horns and loss of motor axons. (D) Culture treated with SC236 (10 μM) and THA showing protection of motor neurons. DH = dorsal horn; VH = ventral horn; arrow = *motor axons.*

pacity of astrocytes due to impairment of astrocytic glutamate transport, actual loss of astrocytes,[1] and potentiation of excitotoxic effects of glutamate by overexpression of COX-2 in neurons.[10] In ALS, any of the stimuli or inflammatory molecules noted above could initiate upregulation of COX-2. The process may be self-perpetuating, with damage and dysfunction of neurons and astrocytes spreading contiguously in widening areas as is commonly observed clinically in ALS.

COX-2 inhibitors also interrupt inflammatory processes that result in the production of free radicals and other toxic molecules. Inhibition of COX-2 has been shown to protect against the effects of global ischemia or reperfusion injury in the brain and trauma to the spinal cord.[16,19] There is a recent report that a soluble aspirin analog may delay the onset of motor deficits in mutant superoxidase dismutase 1 mice.[20]

The present results suggest that COX-2 inhibition could have therapeutic effects in ALS by altering the cascade of pathogenic processes that otherwise cause relentless progression of motor neuron damage. Inhibition of COX-2 could break the pathogenetic cycle by (1) preventing prostaglandin-mediated release of glutamate from astrocytes and (2) interrupting an important pathway that otherwise leads to the production of free radicals, toxic and proinflammatory molecules which damage neurons and glia and upregulate the activity of COX-2. The availability of COX-2 inhibitors that readily penetrate the central nervous system and are relatively nontoxic facilitates therapeutic trials in animal models of ALS.

The SC236 was supplied by Monsanto Searle, which also provided partial support for these studies.

We thank Dr K. Andreasson for helpful discussions throughout these studies and Carol Coccia for carrying out highly skilled technical work.

References

1. Rothstein JD, Martin LJ, Kuncl RW. Decreased glutamate transport by the brain and spinal cord in amyotrophic lateral sclerosis. N Engl J Med 1992;326:1464–1468 (Comments)
2. Shaw PJ, Ince PG. Glutamate, excitotoxicity and amyotrophic lateral sclerosis. J Neurol 1997;244(Suppl 2):S3–14
3. Bezzi P, Carmignoto G, Pasti L, et al. Prostaglandins stimulate calcium-dependent glutamate release in astrocytes. Nature 1998;391:281–285
4. Sanzgiri RP, Araque A, Haydon PG. Prostaglandin E(2) stimulates glutamate receptor-dependent astrocyte neuromodulation in cultured hippocampal cells. J Neurobiol 1999;41:221–229
5. Boldyrev AA, Carpenter DO, Huentelman MJ, et al. Sources of reactive oxygen species production in excitotoxin-stimulated cerebellar granule cells. Biochem Biophys Res Commun 1999; 256:320–324
6. Rothstein JD, Jin L, Dykes-Hoberg M, Kuncl RW. Chronic inhibition of glutamate uptake produces a model of slow neurotoxicity. Proc Natl Acad Sci USA 1993;90:6591–6595
7. Corse AM, Bilak MM, Bilak SR, et al. Preclinical testing of neuroprotective neurotrophic factors in a model of chronic motor neuron degeneration. Neurobiol Dis 1999;6:335–346
8. Williams CS, DuBois RN. Prostaglandin endoperoxide synthase: why two isoforms? Am J Physiol 1996;270:G393–400
9. Kaufmann W, Andreasson K, Isakson P, Worley P. Cyclooxygenases and the central nervous system. Prostaglandins 1997;54: 601–624
10. Kelley KA, Ho L, Winger D, et al. Potentiation of excitotoxicity in transgenic mice overexpressing neuronal cyclooxygenase-2. Am J Pathol 1999;155:995–1004
11. O'Banion MK, Miller JC, Chang JW, et al. Interleukin-1 beta induces prostaglandin G/H synthase-2 (cyclooxygenase-2) in primary murine astrocyte cultures. J Neurochem 1996;66:2532–2540
12. Hirst WD, Young KA, Newton R, et al. Expression of COX-2by normal and reactive astrocytes in the adult rat central nervous system. Mol Cell Neurosci 1999;13:57–68
13. Tomimoto H, Akiguchi I, Wakita H, et al. Cyclooxygenase-2 is induced in microglia during chronic cerebral ischemia in humans. Acta Neuropathol (Berl) 2000;99:26–30
14. Goppelt-Struebe M, Beiche F. Cyclooxygenase-2 in the spinal cord: localization and regulation after a peripheral inflammatory stimulus. Adv Exp Med Biol 1997;433:213–216
15. Ebersberger A, Grubb BD, Willingale HL, et al. The intraspinal release of prostaglandin E2 in a model of acute arthritis is accompanied by an up-regulation of cyclooxygenase-2 in the spinal cord. Neuroscience 1999;93:775–781
16. Resnick DK, Graham SH, Dixon CE, Marion DW. Role of cyclooxygenase 2 in acute spinal cord injury. J Neurotrauma 1998;15:1005–1013
17. Willingale HL, Gardiner NJ, McLymont N, et al. Prostanoids synthesized by cyclo-oxygenase isoforms in rat spinal cord and their contribution to the development of neuronal hyperexcitability. Br J Pharmacol 1997;122:1593–1604
18. Li M, Ona VO, Guegan C, et al. Functional role of caspase-1 and caspase-3 in an ALS transgenic mouse model. Science 2000;288:335–339
19. Nakayama M, Uchimura K, Zhu RL, et al. Cyclooxygenase-2 inhibition prevents delayed death of CA1 hippocampal neurons following global ischemia. Proc Natl Acad Sci USA 1998;95: 10954–10959
20. Barneoud P, Curet O. Beneficial effects of lysine acetylsalicylate, a soluble salt of aspirin, on motor performance in a transgenic model of amyotrophic lateral sclerosis. Exp Neurol 1999; 155:243–251

Down's Syndrome Is Associated with Increased 8,12-*iso*-iPF$_{2\alpha}$-VI Levels: Evidence for Enhanced Lipid Peroxidation In Vivo

Domenico Praticò, MD,* Luigi Iuliano, MD,† Giulia Amerio, MD,‡ Lina X. Tang, BSc,* Joshua Rokach, MD,§ Giuseppe Sabatino, MD,‡ and Francesco Violi MD†

Postmortem and in vitro studies have shown that oxidative stress plays a role in the pathogenesis of many of the clinical features of Down's syndrome. The isoprostane 8,12-*iso*-iPF$_{2\alpha}$-VI is a specific marker of lipid peroxidation. We found elevated levels of this isoprostane in urine samples of subjects with Down's syndrome compared with those of matched controls, which correlated with the duration of the disease. These results suggest that increased in vivo lipid peroxidation is a prominent component early in the course of Down's syndrome.

Praticò D, Iuliano L, Amerio G, Tang LX, Rokach J, Sabatino G, Violi F. Down's syndrome is associated with increased 8,12-*iso*-iPF$_{2\alpha}$-VI levels: evidence for enhanced lipid peroxidation in vivo. Ann Neurol 2000;48:795–798

Caused by the triplication of chromosome 21, Down's syndrome (DS) is one of the most common human cytogenetic abnormalities.[1] Those with DS suffer from a wide range of symptoms that are considered to occur through damage caused by overexpression of normal gene products encoded by extra gene copies present on this chromosome.[2] Human copper/zinc-superoxide dismutase (SOD1) is one of these genes, and increased levels of this enzyme as a result of gene dosage have been shown in DS subjects.[3] The increased gene dosage for SOD1 has been proposed to contribute to the precocious dementia of Alzheimer's type and mental retardation that occurs as part of the syndrome.[4] High

From *The Center for Experimental Therapeutics, University of Pennsylvania, Philadelphia, PA; †Institute of Clinica Medica I, University "La Sapienza," Rome, and ‡Children's Hospital of the University of Chieti, Chieti, Italy; and §Claude Pepper Institute and Department of Chemistry, Florida Institute of Technology, Melbourne, FL.

Received Apr 3, 2000, and in revised form Jun 28. Accepted for publication Jun 28, 2000.

Address correspondence to Dr Praticò, Center for Experimental Therapeutics, University of Pennsylvania, BRB II/III, Room 812, 421 Curie Boulevard, Philadelphia, PA 19104.

Cellular/Molecular Neuroscience: Senior Editor Gary Westbrook

A neuronal glutamate transporter contributes to neurotransmitter GABA synthesis and epilepsy.

(Running Title: EAAC1, GABA synthesis and epilepsy)

Jehuda P. Sepkuty[1], Akiva S. Cohen[2], Christine Eccles[1], Azhar Rafiq[3], Kevin Behar[4], Raquelli Ganel[1], Douglas A. Coulter[2], Jeffrey D. Rothstein[1]

[1]Departments of Neurology and Neuroscience, Johns Hopkins University, Johns Hopkins Hospital, Baltimore; [2]Departments of Pediatrics and Neuroscience, University of Pennsylvania School of Medicine and the Stokes Research Institute of Children's Hospital of Philadelphia; [3]Medical College of Virginia of Virginia Commonwealth University; [4]Department of Psychiatry, Yale University

Address all correspondence to:

Jeffrey D. Rothstein, Johns Hopkins University, Department of Neurology, Meyer 6-109

600 N. Wolfe Street, Baltimore, MD. 21287-7247.

Tel. (410) 614-3846, Fax (410) 955-0672, email: jrothste@JHMI.edu

Number of: Pages 25; Figures 5; Tables 0.

Words in: Abstract 170; Introduction 313; Discussion 890

Acknowledgements. This work was supported by funding from NIH (NS 40151, NS36465 and NS33958 to JDR, and NS 32403 and NS 38572 to DAC).

ABSTRACT:

The predominant neuronal glutamate transporter, EAAC1, is localized to the dendrites and somata of many neurons. Rare pre-synaptic localization is restricted to GABA terminals. Because glutamate is a precursor for GABA synthesis, we hypothesized that EAAC1 may play a role in regulating GABA synthesis and thus, could cause epilepsy in rats when inactivated. Reduced expression of EAAC1, by antisense treatment, led to behavioral abnormalities including staring/freezing episodes and electrographic (EEG) seizures. Extracellular hippocampal and thalamocortical slice recordings showed excessive excitability in antisense treated rats. Patch clamp recordings of miniature inhibitory postsynaptic currents (mIPSCs) conducted in CA1 pyramidal neurons in slices from EAAC1 antisense treated animals demonstrated a significant decrease in mIPSC amplitude, indicating decreased tonic inhibition. There was a 50% loss of hippocampal GABA levels associated with knockdown of EAAC1, and newly synthesized GABA from extracellular glutamate was significantly impaired by reduction of EAAC1 expression. EAAC1 may participate in normal GABA neurosynthesis and limbic hyperexcitability, while epilepsy can result from a disruption of the interaction between EAAC1 and GABA metabolism.

Key words: EAAC1, transport, antisense, GABA, metabolism, Epilepsy

Glutamate transport is the major mechanism controlling extracellular glutamate levels, preventing excitotoxicity, and averting neural damage associated with epilepsy. (McBean, Roberts, 1985; Rothstein et al., 1992; Rothstein et al., 1993; Robinson et al., 1993b; Robinson et al., 1993a; Rothstein et al., 1994; Rothstein et al., 1996; Tanaka et al., 1997) Glutamate transporters are localized to the membranes of synaptic terminals and astroglial processes that ensheath synaptic complexes. (Rothstein et al., 1994;

Rothstein et al., 1996; Conti et al., 1998; Danbolt et al., 1992; He et al., 2000; Hertz, 1979; Kanai et al., 1993; Kanner, Schuldiner, 1987) GLAST (EAAT-1) (Storck et al., 1992; Arriza et al., 1994) and GLT-1 (EAAT-2) (Arriza et al., 1994; Pines et al., 1992) are astroglial glutamate transporters, EAAC1 (EAAT-3) (Arriza et al., 1994; Kanai, Hediger, 1992; Shashidharan et al., 1994; Kanai et al., 1995; Bjoras et al., 1996; Nakayama et al., 1996; Velaz-Faircloth et al., 1996; Eskandari et al., 2000) EAAT-4 (Fairman et al., 1995) and EAAT-5 (Arriza et al., 1997) are neuronal proteins. Astroglial glutamate transporters are responsible for up at least 80% of the high affinity glutamate transport and the majority of synaptic inactivation.

EAAC1 is highly concentrated in the somata and dendrites of many neurons, especially those in the hippocampus, striatum, cerebellum, and olfactory bulb. There is little evidence for glutamate transporter proteins in the pre-synaptic terminal - with one exception. EAAC1 has been localized to inhibitory GABAergic neurons, including cerebellar Purkinje cells (Rothstein et al., 1994),(Conti et al., 1998; He et al., 2000; Levy et al., 1993) highly concentrated in presynaptic GABAergic terminals. Because of its unusual localization to GABA terminals we hypothesized that the loss of EAAC1 could alter pre-synaptic GABA metabolism, perhaps by altering a precursor supply of glutamate. In this study we now show that EAAC1 contributes to new synthesis of inhibitory neurotransmitter GABA, and that loss of EAAC1 produces "staring" epilepsy.

MATERIALS AND METHODS

Intraventricular Antisense Administration

All animal experiments were performed with approval by the Johns Hopkins Animal Care and Use Committee. Male Sprague-Dawley rats (250-350 g) were anesthetized with chloral hydrate 4% (1 ml/100 g). Antisense oligonucleotides (ODN) were infused intraventricularly by mini-osmotic pumps as described

previously, including oligonucleotides to EAAC1, GLAST and GLT-1 (Rothstein et al., 1996). Lyophilized oligonucleotides were reconstituted in artificial cerebrospinal fluid (Rothstein et al., 1996; Wagner, 1994; Wahlestedt, 1994) at a concentration of 2.5 mg/ml and dialyzed (Rothstein et al., 1996) and then filtered (0.22 μm) prior to use. Four EEG screw electrodes were placed on the skull during the same procedure (1 frontal and 1 parietal on each side). Antisense and sense oligodeoxynucleotides were delivered at a rate of 1-10 μg/hr over a 9-12 day period.

Video-EEG recording

Four EEG electrodes (Plastics One, Inc. VA.) were mounted on the skull with cranioplastic cement during the stereotaxic placement of the cannula (one frontal and one parietal on each side, 2 and 3 mm from the midline skull suture, respectively). Rats underwent daily EEG recording in a chamber that allowed unrestrained movement while recording. Signals were recorded using Grass EEG machine model 8-16 with amplifiers with a band pass filter set between 1 and 70 Hz. Sensitivity was set to 7 μV/mm and paper speed to 30 cm/sec. Two channels were recorded. Bipolar and referential recordings were performed while the rat was awake and mobile in the chamber. EEG was sampled for twenty minutes or until seizure activity occurred. If seizure activity occurred, observation was continued until five minutes of non-epileptiform EEG activity had been recorded. Clinical behavior was monitored by video camera during the EEG recording. EEG recording and interpretation was done with the recorder/interpreter blinded to the treatment.

Extracellular thalamocortical and hippocampal entorhinal cortical field potential slice recording

Four antisense EAAC1 experimental and four sense EAAC1 control rats were decapitated 10 days after infusion. Thirteen antisense and ten sense thalamocortical slices were recorded. Rat thalamocortical slices were prepared using the slice angle developed by Agmon and Connors (Agmon, Connors, 1991; Coulter, Lee, 1993). Connections were verified by microscopic examination of slices. Once cut and

visualized, slices were transferred to an incubator, where they were kept submerged in warmed (35^0C) oxygenated medium until use. The slice medium was composed of (in mM): NaCl 130; Kcl 3; NaH_2PO_4 1.25; $MgCl_2$ 0; $NaHCO_3$ 26; and Dextrose 10. A separate incubator allowed pre-exposure of individual slices to low Mg^{2+} medium prior to recording. Slices were incubated for at least 1 h after dissection, and for 1 h or more in low Mg^{2+} medium before recording. Prior to recording, slices were transferred to an interface type recording chamber, where they were maintained at 35^0C. Differential Ac-coupled extracellular recordings were conducted using 2 MΩ insulated tungsten electrodes (band pass filtered at 10-3,000 Hz). Recording was conducted from cortex in one channel and thalamus in the second channel.

Five antisense EAAC1 experimental and three sense EAAC1 control rats were decapitated 10 days after infusion for hippocampal enthorinal cortex (HEC) slice experiments, and eight antisense and five sense slices were recorded. In brief, brain slices were prepared using previously reported methods (Rafiq et al., 1993). Rats were anesthetized with halothane, decapitated, and the brain quickly removed and chilled for 1-2 min in a modified sucrose-based artificial cerebrospinal fluid (SACSF) composed of (in mM): sucrose 200; KCl 3; NA_2PO_4 1.25; $MgCl_2$ 0.9; $CaCl_2$ 2; $NaHCO_3$ 26; and glucose 10 (equilibrated with 95% O_2 / 5% CO_2). After a 1 minute wash in cold SACSF, the two hemispheres were dissected by midsagittal dissection. Hemispheres were immediately returned to oxygenated, cold SACSF until needed for slicing. Each hemisphere was individually blocked and sectioned in an inclined 12^0 transverse plane, modified from Jones and Heinemann (1988), with the use of a vibratome (Lancer 1000, St. Louis, MO). Brain slices were subsequently transferred to a holding chamber where they were kept submerged in artificial cerebrospinal fluid (ACSF) containing in mM: NaCl 130; KCl 3; NA_2PO_4 1.25; $MgCl_2$ 0.9; $CaCl_2$ 2; $NaHCO_3$ 26; and glucose 10, warmed to 32^0 C and vigorously bubbled with 95% O_2 / 5% CO_2 for a period of 1-2 h. Prior to recording, slices were transferred to an interface-type recording chamber, where they were perfused with 35^0C ACSF at 1-1.5 ml/min. for extracellular recording experiments.

Extracellular field potential recordings were made with the use of insulated tungsten electrodes, placed in the pyramidal cell body layers of area CA1, Ca3 and the dentate gyrus of each slice. (Coulter, Lee, 1993; Rafiq et al., 1993; Jones, Heinemann, 1988). All slice recordings and interpretation was done with the recorder/interpreter blinded to the treatment.

Quantification of excitability

EEG and hippocampal slice recordings were analyzed by manually counting spikes (Daly and Pedley 1990) during the whole record for each rat and slice on the 10^{th} treatment day. Spike count in the EEG recordings of all EAAC1 antisense-treated rats were compared to spike count in the EEG recordings of three controls: sense-EAAC1, GLT-1 antisense and GLAST antisense treated rats. The average number of spikes per minute in each group was compared [ANOVA followed by Fisher's Projected Least Significant Difference (PLSD) for spikes/min.]. All the spontaneous interictal spikes (SISs) in the hippocampal slice recordings were counted and compared between the EAAC1 antisense and sense EAAC1 treated rats (Student's *t* test). The thalamocortical slice recordings were analyzed by manual measurement of the duration of discharges in seconds and calculating the average duration of discharges (seconds discharge per minute recording) in each slice, then comparing the averages of EAAC1 antisense and sense EAAC1 treated rats (Student's *t* test).

Patch recording in brain slices

Male Sprague-Dawley rats were used in all experiments. Recordings were obtained from visually identified pyramidal neurons in stratum pyramidale of area CA1 of the rat hippocampus. For the purpose of this study animals were divided into four groups: EAAC1 antisense treated rats, controls (sense treated rats and naive rat controls), and GLAST antisense treated rats. Brain slices were prepared using previously reported methods (Rafiq et al., 1993). In brief, rats were anesthetized with halothane, decapitated, and the brain quickly removed and chilled for 1-2 min in a modified sucrose-based artificial

cerebrospinal fluid (aCSF) composed of (in mM): sucrose, 201; KCl, 3.2; $NaHPO_4$, 1.25; $MgCl_2$, 2; $CaCl_2$, 2; $NaHCO_3$, 26; and glucose, 10 (equilibrated with 95% O_2 / 5% CO_2 at 32.5°C). The brain was glued, frontal side down, to a glass platform with cyanoacrylate cement, and coronal whole brain slices, (225 μM) were sectioned using a Vibratome (Lancer 1000, St. Louis, MO). Brain slices were subsequently hemisected, transferred to a holding chamber, and incubated in warm (35°C) normal aCSF containing 126 mM NaCl substituted for sucrose, and allowed to equilibrate for at least 2 hours before being transferred to the recording chamber.

Whole-cell voltage-clamp recordings were conducted at room temperature from visually identified CA1 pyramidal neurons using infrared differential interference contrast or Hoffman modulation contrast video microscopy (Stuart et al., 1993; Cohen et al., 2000). Cells were voltage clamped at -60 mV and signals were recorded and amplified with an Axopatch 1D (Axon Instruments, Foster City, CA), filtered at 2kHz , digitized and sampled at 44 kHz with a PCM digitizer (Neuro-Corder DR-890, Neurodata instruments, NY, NY) and stored on videotape for off-line analysis. Electrodes were fabricated from thick wall borosilicate glass (World Precision Instruments, Sarasota, FL) and pulled to a resistance between 2-6 MΩ when filled with an internal solution composed of (in mM): CsCl, 135; HEPES, 10; $MgCl_2$, 2; MgATP 4; pH 7.25 (CsOH) on a two stage puller (Narishige PP-83, East Meadow, NY). To isolate $GABA_A$-mediated events TTX (400 nM) and the excitatory amino acid antagonists D-AP5 (50 μM) and CNQX (6 μM) were added to the the superfusing aCSF.

Recorded mIPSCs were reacquired using Dempster software (Strathclyde, Glasgow, UK), which collects events using a manually controlled threshold detector, and is capable of detecting events as small as 2-3X the baseline noise. To attempt to minimize cases of inadequate space clamp, neurons were used for analysis only when series resistance (Rs) was less than 20 MΩ, and at least 80% series resistance compensation was achieved. Rs was checked frequently throughout experiments, and neurons in which

Rs increased > 20% were discarded. The kinetics of mIPSCs i.e., amplitude, rise and decay times were analyzed using cumulative probability histograms. mIPSC frequency was determined using Mini Analysis software (Synaptosoft Inc., Leonia, NJ). Reagents were purchased from the following vendors: all salts and diazepam from Sigma (St Louis, MO); D-2-amino-5-phosphonopentanoic acid (AP5), 6-cyano-7-nitroquinoxaline-2,3-dione (CNQX) from Research Biochemicals International (Natick, MA); tetrodotoxin (TTX) from Calbiochem (La Jolla, CA). All drugs were made as stock solutions, and then diluted to their final concentration in the bathing medium. Statistical significance between cumulative probability distributions in control and drug conditions in individual neurons was assessed at the $p < 0.05$ confidence level using the Kolmogorov-Smirnov non-parametric statistical test. Two-tailed unpaired Student's t-tests were performed to determine statistical significance at the $p < 0.05$ confidence level when comparing different treatment groups. All mIPSCs recordings and interpretation was done with the recorder/interpreter blinded to the treatment.

GABA Levels

Dissected brain regions were homogenized in 0.1 N perchloric acid. After thiol derivatization, levels of GABA were determined using high performance liquid chromatography (HPLC) (0.18 M sodium acetate/ 41% acetonitrile buffer (pH 5.0) mobile phase at a flow rate of 2.5 ml/min) employing a 5 nm reverse phase column (ODS Biocal, BioRad) coupled with electrochemical detection (BioAnalytical Systems). Retention time for GABA was approximately 6.5 minutes as confirmed with [^{14}C] GABA standard. Tissue protein levels were determined by a Coomassie blue assay. Levels of total GABA are expressed as nmol/mg protein.

GABA Metabolism

Supernatants (30μL) from [^{14}C] glutamate uptake experiments were mixed with 0.1N perchloric acid (165 μL), 5 μL 5-aminovaleric acid (45 μM solution in 0.1N perchloric acid) and 800 μL of "working

reagent" (opthaldialdehyde-OPA solution) and the solution was incubated at room temperature for 6 minutes. The working reagent was prepared by dissolving 67.1 mg of opthaldialdehyde (OPA) in 50 ml methanol, 56 μL of t-butylthiol (TBT), 15 ml of 1 M carbonate buffer (pH 9.6) and the mixture was brought to a final volume of 100 ml with about 30 ml water. Exactly 6 min after the addition of the OPA solution to the sample, 50 μL of the derivatized sample was analyzed by HPLC. Authentic GABA standards allowed quantification of total GABA levels in the samples. Fractions of each sample were collected (30 sec/fraction) and 300 μL aliquots were mixed with 3 ml of scintillation cocktail and [^{14}C] activity was analyzed by liquid scintillation spectroscopy (Wallac). Specific activity of [^{14}C]GABA was calculated for each sample. Protein was measured according to the method of Lowry et al with bovine serum albumin as standard. [^{14}C] GABA specific activities were compared in antisense and sense treated samples, in experiments of naive rats with and without DL-threo-β-hydroxy-aspartic acid (THA) and in experiments of naive rats treated with 6-Diazo-5-oxo-L-norleucine (DON), dihydrokainate (DHK) at times T=0 and T=30min.

Tissue preparation and C^{14} glutamate uptake

Antisense and sense treated rats were decapitated 10 days after antisense infusion and brains were rapidly removed, placed into chilled, oxygenated (95% O_2/5% CO_2) Krebs-Ringer bicarbonate (KRB) Buffer (119 mM NaCl, 4.8 mM KCl, 1.7 mM $CaCl_2$, 1.2 mM $MgCl_2$, 1.2 mM KH_2PO_4, 23.8 mM $NaHCO_3$, 5.5 mM glucose, pH 7.4)[50]. After 30 seconds the brain was placed on a chilled aluminum block (4°C) and hippocampus and thalamus were dissected from 1 mm coronal sections, followed by slicing into 0.25 mm prisms (McIlwain tissue chopper, Brinkman Instr.). Prisms were suspended in chilled fresh KRB buffer in microvials (Eppendorf) on ice. DON, an inhibitor of phosphate-activated glutaminase (Sigma) was added to the microvial to a final concentration of 10 mM. The microvials containing antisense and sense (control) treated hippocampi and thalami were incubated with shaking at 37°C for 15 minutes. The

vials were then centrifuged (500 RPM, 5 minutes) and DON was washed out using the chilled KRB buffer. In some experiments, after washing out DON, THA was added to hippocampal prisms in the microvials to a final concentration of 1 mM. The vials were incubated for 15 minutes in 37°C and the reaction was stopped on ice. While on ice in chilled fresh KRB oxygenated buffer, glutamate (20 μM final), [^{14}C]glutamate (~1 μCi) and DL-gabaculline (20 μM final) were added and incubated at 37°C for 30 minutes (Behar, Boehm, 1994; Sibson et al., 1998). The reaction was terminated by chilling on ice and adding 0.4 N perchloric acid. Some tissue was reserved for the HPLC assay of GABA. The tissue was homogenized, frozen and thawed at 37°C twice to break the cell membranes and the homogenate was centrifuged at 14,000 RPM for 20 minutes at 4°C. The remaining pellet was dissolved in 200 μL of 1 N NaOH for protein assay. The supernatant fraction was filtered through 0.45 μm pore syringe filter and stored in –70°C until GABA analysis.

Immunoblots

Antisense and sense treated rats were decapitated after 10 days of intraventricular treatment and the brains were rapidly removed and placed on a chilled aluminum block (4°C). Coronal sections of brain were sliced at 1-2 mm intervals from the occipital pole to the olfactory bulbs. Immunoblots of the tissue homogenates were prepared with affinity- purified polyclonal oligopeptide antibodies to EAAC1 as described previously (Rothstein et al., 1994; Rothstein et al., 1996)

RESULTS

Antisense Knockdown of EAAC1

Previous studies had demonstrated reliable and specific knockdown of EAAC1 expression following chronic intraventricular administration of antisense (AS) oligonucleotides (Rothstein et al., 1996). By 8-10 days after administration of EAAC1 antisense oligonucleotides, expression of EAAC1

was reduced by more than 60% (Fig. 1a). Sense oligonucleotides (Fig.1a) had no effect on EAAC1 expression, neither did random oligonucleotides, or antisense to other glutamate transporters - GLT-1 or GLAST (Rothstein et al., 1996). Loss of EAAC1 leads to a small loss in total tissue glutamate transporter activity. (Rothstein et al., 1996)

Subacute Loss of EAAC1 Leads to Epilepsy: Video-EEG recording:

To evaluate the epileptogenicity of EAAC1 antisense (AS) treatment, EEG and video were recorded in awake and ambulating rats (n=32). Up to four days after oligonucleotide treatment, no differences in behavior or the EEG patterns were noted between the study group and the control treatments (EAAC1 sense, GLAST antisense-treated and GLT-1 antisense-treated). The EEG consisted of a normal mixture of frequencies without spikes (Fig. 1 b, e; GLT and GLAST antisense controls were not different from untreated or sense treated animals, not shown). Beginning on the fourth day following EAAC1 antisense infusion, brief staring episodes and "freezing" like postures were observed, that were not seen in EAAC1 sense controls, or in GLAST antisense-treated and GLT-1 antisense-treated animals. The GLT-1 and GLAST antisense-treated animals showed some motor slowing, but no staring/freezing episodes. The behavioral episodes of the EAAC1 antisense treated rats correlated with EEG changes, marked by brief runs of rhythmic spikes, again not seen in the controls (Fig.1c,f: GLT-1 and GLAST antisense controls were not different, not shown). These behavioral manifestations deteriorated daily, coupled with worsening EEG. The tenth day of infusion (a time point corresponding to a maximal 70%-90% loss of EAAC1 protein) (Rothstein et al., 1996), the behavioral changes consisted of prolonged freezing and staring episodes with occasional tonic posturing of the forepaws. The EAAC1 sense control rats did not show behavioral changes and the GLT-1 and GLAST antisense controls manifested severe motor weakness without posturing, freezing, or staring episodes. Corresponding to the long staring and freezing episodes (as recorded by simultaneous video EEG recording), the EEG recording showed

prolonged runs of 4-6 per second spikes and spike and wave complexes, along with slowing and reduced fast activity of the background. No epileptiform EEG changes were recorded in the controls. In two out of seven GLT-1 antisense controls there were a few spikes, but no runs of spikes, rhythmic spikes, or spike and wave complexes were seen. (Fig.1d,g: GLT-1 and GLAST antisense controls were not different, not shown). The mean number of spikes per minute in the EAAC1 antisense-treated group (12.03, n=6) was significantly higher then the mean number of spikes per minute in the three other control group: sense- EAAC1 (0.98, n=5) antisense GLT-1 (2.99, n=6) and antisense GLAST (0.57, n=4). (Fig. 1h, ANOVA p=0.034). Fisher's PLSD for spikes/min. showed a significant difference between the study group antisense EAAC1 and each of the control groups: sense EAAC1 (p=0.0016), antisense GLT-1 (p=0.0051) and antisense GLAST (p=0.0020) without a difference among the different control groups. This finding implies significant and specific epileptiform activity associated with EAAC1 antisense treatment.

Extracellular thalamocortical field potential slice recording:

To explore the physiological basis of EAAC1 antisense oligonucleotide epileptogenesis, extracellular slice recording and intracellular recording were used to test the hypothesis that hyperexcitation associated with the EAAC1 antisense treatment was due to decreased inhibition. Extracellular field potentials from thalamocortical and hippocampal slices of rat brains, relevant to both absence and partial complex seizures respectively, were recorded in study animals and controls.

Extracellular thalamocortical slice recordings showed excessive excitability from the EAAC1 antisense rats as compared to sense-treated controls. Recordings from thalamocortical slices, in the study group showed prolonged runs of spontaneous bursts of spike discharges (as displayed from the thalamic channel) (Fig. 2a), which at close scrutiny showed 6-7/second spike and slow wave complexes (not shown). Because of the use of magnesium free-medium, these runs were occasionally present in sense

control slices, but were much less frequent and very short in duration. Typical control thalamocortical slices showed occasional brief spontaneous bursting spike discharges (Fig. 2b). Quantitative analysis comparing the mean duration of these spike discharges (seconds discharges per minute recording) in the thalamocortical slices of antisense-treated rats (8.1, n=13) to slices of sense controls (2.8, n=10) showed significant hyperexcitability of the study group ($p= 0.013$, Fig. 2c).

Extracellular hippocampal-entorhinal cortical (HEC) slice recording

Extracellular hippocampal slice recordings showed increased excitability from EAAC1 antisense rats as compared to sense controls. The typical recording of HEC slices in the EAAC1 antisense group showed very frequent spontaneous interictal spikes (Fig. 2d), whereas in recordings of EAAC1 sense-treated rats such spikes were found much less frequently (Fig. 2e). The mean number of spikes per minute in all the HEC slices recorded in antisense-treated rats (14.6, n=5) was increased compared to sense-treated controls, (1.66, n=3) but the difference was not statistically significant ($p= 0.16$, Fig. 2f). There was a strong correlation between the mean number of spikes per minute in hippocampal slices and the mean number of spikes per minute on EEG ($r= 0.97$, $p<0.0001$ data not shown).

Whole-cell visualized slice patch recording

The limbic hyperexcitability observed in extracellular recording in HEC slices from EAAC1 antisense treated animals (see above) suggests that the reduction of functional levels of EAAC1 transporter protein may promote seizure generation by a decrease of releasable GABA. In order to test this hypothesis directly, miniature inhibitory postsynaptic currents (mIPSCs), which are mediated by the spontaneous release of single GABA quanta, in hippocampal area CA1 in EAAC1 antisense-treated, EAAC1 sense-treated, GLAST antisense-treated, and naive animals, were recorded. GLT-1 antisense oligonucleotide treated animals were not utilized in this analysis because the hippocampus was severely damaged by this treatment (Rothstein et al, 1996). The median mIPSC amplitude recorded in CA1

pyramidal neurons from EAAC1 antisense oligonucleotide-treated animals (n=10; number of events = 2486) was significantly smaller (-29.8±3 pA, $p<0.05$ unpaired t-test) than that recorded in EAAC1 sense oligonucleotide-treated (-39.4±2 pA, n=5; number of events = 1023), GLAST antisense oligonucleotide-treated (-38.5±2 pA, n=6; number of events = 1140) and naive (-37.1±1, n=3; number of events = 879) controls (Fig. 3a1-a3, b1 and c1). The 90% decay time (T90) was significantly faster in the EAAC1 antisense-treated group compared to both GLAST antisense and EAAC1 sense groups (Fig 3b2 and c2). However, caution should be used in interpretation of this result because the 50% decay times (T50) were not significant between the three groups (T50 = 8.97±2; 10.13±2; 10.5±1 for EAAC1 antisense, EAAC1 sense- and GLAST antisense-treated respectively). The current measured corresponding to the T90 decay time is very close to our limit of detection. Due to our lack of confidence in the T90 decay time measurement, we calculated the weighted decay taus for EAAC1 antisense, sense and GLAST antisense-treated groups. The weighted decay taus were calculated by dividing the area of the events by their peak amplitudes, and the median values were compared. In similar fashion to the T90 decay time data, we found that the EAAC1 antisense-treated group decayed significantly faster ($p < 0.05$) than both EAAC1 sense- and GLAST antisense-treated groups. The median weighted taus were 12.75 ± 1.9 (n=10); 15.25 ± 1.0 (n=5), and 16.83 ± 3.1 (n=6) for EAAC1 antisense, EAAC1 sense- and GLAST antisense-treated groups respectively. Miniature IPSC mean frequency was similar in all three groups recorded (3.2 +/- 2.1 Hz for GLAST antisense, 3.44 +/- 1.7 Hz for EAAC1 sense and 3.8 +/- 1.1 Hz for EAAC1 antisense).

Regional brain GABA

Because of the decreased inhibition demonstrated by the voltage-clamp recording studies described above, total GABA was measured in the hippocampus and thalamus of antisense-treated animals compared to sense controls, and also in other brain regions, close and far from the intraventricular oligonucleotide infusion.(Rothstein et al., 1994) HPLC analysis of selected brain regions indicated that

GABA levels were decreased 50% ($p < 0.05$) in the hippocampus and mildly decreased (non-significantly) in the thalamus of EAAC1 antisense but not in controls (sense n=4 and AS n=7, Fig. 4a).

New [^{14}C] GABA metabolism in normal rats

To determine if changes in GABA reflect a coupling of EAAC1-mediated glutamate transport and GABA metabolism, new synthesis of GABA in EAAC1 antisense treated rats was measured using [U-^{14}C] glutamate in the presence of selective enzyme inhibitors to block glutamate repletion from astrocytic glutamine and GABA catabolism. New glutamate synthesis from astrocytic glutamine was blocked with the glutaminase inhibitor, DON and GABA catabolism was prevented by Gabaculine, a potent and irreversible inhibitor of GABA transaminase. Application of the GABA-transaminase inhibitor permitted the experiments to be conducted under conditions of net GABA synthesis. In order to test whether any potential GABA labeling from ^{14}C-glutamate was transporter-dependent in the control hippocampal tissue, and because no specific pharmacological inhibitor of EAAC1 currently exists, it was necessary to use the non-specific glutamate transport inhibitor, THA.

Newly synthesized [^{14}C] GABA from [U-^{14}C] glutamate in hippocampal tissue from normal rats incubated in the presence of DON and gabaculine was significantly lower (specific activity 2.225, n=3 vs. 6.072, n=6, $p = 0.003$) in the presence of THA (Fig. 4b), suggesting that GABA synthesis is dependent on glutamate transport. To test the effect of DON alone on GABA synthesis, DON was added to hippocampal tissue acquired from normal rats at time 0 (without adding glutamate) and this was compared to DON which was added to other hippocampal tissue from control rats at time 0 and was followed by addition and incubation with cold and ^{14}C-glutamate and gabaculine for 30 minutes. Newly synthesized ^{14}C-GABA is reflected by the difference in ^{14}C-GABA specific activity between the tissue with added glutamate compared to the tissue with no added glutamate and there was a nonsignificant difference (increment from specific activity 0.2733, n=6 to 0.3967, n=6, $p = 0.19$, Fig. 4c). This difference could be

explained by new GABA synthesis from glutamate taken up into synaptic terminals by EAAC1. Alternatively, the enzymatic inhibition of glutaminase, by DON, may have been incomplete and the difference could be explained by astroglial glutamine supply. That is, ^{14}C-glutamate may have been transported into astrocytes, by the astroglial transporter GLT-1, then converted to ^{14}C-glutamine, and shuttled to the GABA neuron. However, when DHK, a specific and potent blocker of GLT-1 in addition to DON were added to hippocampal tissue from control rats at time 0 (without adding glutamate) and this was compared to DHK and DON which were added to other hippocampal tissue from normal rats at time 0 and was followed by addition and incubation with cold and ^{14}C-glutamate and gabaculine for 30 minutes, there was a significant difference (increment from specific activity 0.172, n=11 to 0.338, n=11, p= 0.01). Newly synthesized ^{14}C-GABA is reflected by the difference in ^{14}C-GABA specific activity between the tissue with added glutamate compared to the tissue with no added glutamate and there was a significant difference, i.e increased GABA labeling this time (Fig. 4d).

The opposite result, i.e., decreased GABA labeling, would be expected if GABA was labeled from glutamine synthesized from [^{14}C]glutamate uptake by astroglia, due to DHK blockade of this uptake. Thus, increased GABA labeling following application of DHK suggests that inhibition of the astroglial transporter led to an increase in extracellular glutamate with more now available for transport through EAAC1 and GABA synthesis. This suggests that EAAC1 is important for GABA synthesis in normal rats.

New [^{14}C] GABA metabolism in antisense treated rats and sense controls:

To more fully evaluate the role of EAAC1-mediated transport in GABA metabolism, new GABA synthesis was measured in hippocampal slices prepared from EAAC1 sense and antisense treated rats in the presence of DON and Gabaculine. [^{14}C] GABA specific activity in hippocampal tissue of antisense-treated rats was significantly lower (1.65, n=7) compared to sense controls (4.03, n=6, p=0.017, Fig. 5a).

The newly formed [^{14}C] GABA over the 30 min incubation period was increased non significantly in the antisense-treated {from 1.85 to 2.66 nmol/mg protein (x 10^{-5}), n=6, Fig. 5c}, compared to significant increase {from 1.51 to 5.4 nmol/mg protein (x 10^{-5}), n=6, p=0.02, Fig. 5b} in the sense-treated tissue. Furthermore, the rate of [^{14}C] GABA synthesis was about five times slower {0.027 nmol/mg protein (x 10^{-5})/minute, n=6}in the antisense compared with the rate of synthesis in the EAAC1 sense treated tissue {0.13 nmol/mg protein(x 10^{-5})/minute, n=6, Fig. 5d}.

DISCUSSION

Together, these in vivo and in vitro studies demonstrate that EAAC1 antisense treated rats develop epilepsy and limbic hyperexcitability, and that this hyperexcitability may be due, in part, to a reduction in new GABA synthesis in the hippocampus. These studies also suggest that glutamate transporters in general, and EAAC1 specifically, have a role in synthesis of new GABA in the hippocampus of normal naive rats.

The EEG and behavioral monitoring have shown that EAAC1 antisense treated rats develop behavioral changes manifested as staring/freezing episodes, which occur simultaneously with EEG epileptiform changes. These changes are specific and maximal at the time of maximal EAAC1 knockdown. The phenotype of the rats in this study differs from the EAAC1 deficient mice reported by Peghini et al.(Peghini et al., 1997) EAAC1 null mice have a deficit of the transporter protein during ontological development allowing for compensatory responses, whereas antisense knockdown results in the loss of this transporter during adulthood. Noteworthy in EAAC1 null mice was the decrease in locomotor activity with episodes of locomotor arrest (Peghini et al., 1997); however, simultaneous EEG recording to rule out seizures were not reported in their study. In the present study, extracellular field potential recordings from both thalamocortical and hippocampal slices of antisense treated rats showed hyperexcitability. The hippocampal hyperexcitability was correlated with the EEG hyperexcitability.

Based on this finding, and because of the large decrease in GABA synthesis, whole-cell patch clamp recordings of CA1 pyramidal neurons were performed. The data suggest that EAAC1 antisense-induced hyperexcitability may be attributed to a decrease in mIPSC amplitude, but not mIPSC frequency, in CA1 pyramidal neurons.

A balance of excitation and inhibition is essential for the maintenance of normal function in the brain. Golan et al showed that GABA concentration determines the efficacy of inhibition (Golan et al., 1996). In the present study a decrease in total GABA was observed in the hippocampus of antisense-treated rats, but not in sense controls. This decrease was not significant in other regions, although present in the thalamus also. Inhibiting GABA synthesis causes seizures and some of the effects of anticonvulsants occur through interference with enzymes associated with GABA metabolism(Petroff et al., 1996a; Petroff et al., 1996b).

High affinity glutamate transporter subtypes have been found to be specifically localized to both neuronal and astroglial membranes. Under normal conditions, these proteins maintain low extracellular levels of glutamate. A series of studies suggest that the astroglial transporters, GLT1 in particular, are primarily responsible for the synaptic inactivation of glutamate, and from preventing excitotoxic injury (Bergles, Jahr, 1997; Otis, Kavanaugh, 2000; Otis, Jahr, 1998). Nevertheless, EAAC1 is the predominant neuronal transporter present widely throughout the CNS dendrites and somata of large and small pyramidal neurons. But its function in normal synaptic biology has eluded investigators. Molecular anatomic studies suggested that this protein was unexpectedly localized to presynaptic GABA terminals (Rothstein et al., 1994; Conti et al., 1998; He et al., 2000). Subsequently, preliminary antisense knock-down studies suggested a relationship between this protein and tissue GABA levels (Rothstein et al., 1996).

GABA is synthesized primarily from the α-decarboxylation of glutamate by glutamate decarboxylase (Martin, Rimvall, 1993). An alternate pathway for GABA synthesis via putrescine has been described (Seiler, Al-Therib, 1974). Although the contribution of this pathway to GABA synthesis appears to be small in the mature rat brain (~1% of total GABA synthesis, (Noto et al., 1986), putrescine has been shown to be a GABA precursor in the developmentally immature retina (Yamasaki et al., 1999). GABA carbon, which is lost from GABAergic neurons, must be replenished from other cells because mature neurons do not possess the necessary enzymes for de novo synthesis. Glutamine produced in astrocytes is a major precursor of GABA, although few quantitative studies of the precursors of GABA in vivo have been reported. Neostriatal microinjections of methionine sulfoximine, an inhibitor of glutamine synthetase, resulted in only a ~50% reduction of GABA synthesis (Paulsen et al., 1988), suggesting that a pathway(s) other than glutamine may also supply glutamate precursors for GABA synthesis in this brain region. The large decrease in GABA levels and GABA synthesis from extracellular ^{14}C-glutamate in the hippocampus following knockdown of EAAC1 indicate that direct transport of glutamate into GABAergic neurons can provide precursors for GABA synthesis. Furthermore, the electrophysiologic studies suggest that the loss of EAAC1 leads to decreased miniature inhibitory postsynaptic currents consistent with decreased presynaptic release of GABA.

Taken together, these metabolic and electrophysiologic studies clearly document a relationship between the presynaptic glutamate transporter and the inhibitory transmitter GABA. In turn, these metabolic studies strongly suggest that the mechanism of epilepsy in the EAAC1 anti-sense knock-down rats is mediated by decreased GABA synthesis, and therefore, decreased CNS inhibition. The data suggest that in normal rat brain EAAC1 may have an important role in GABA synthesis. Recently, GTRAP3-18, an EAAC1 inhibitory modulator was described (Lin & Orlov et al., 2001), suggesting that under normal conditions EAAC1 may be modulated, perhaps to regulate presynaptic GABA synthesis. Preliminary

studies also show that increased GTRAP3-18, through inhibition of EAAC1 (like antisense) produces epilepsy (Sepkuty et al., 2001). Overall, these studies suggest a novel interaction between excitatory amino acid transporters and an inhibitory amino acid neurotransmitter system. Furthermore, they raise new possibilities of manipulating GABA metabolism through direct or indirect modulation of EAAC1 (e.g. GTRAP3-18) and may provide novel therapeutic modalities for the treatment of epilepsy.

REFERENCES

Agmon A, Connors BW (1991) Thalamocortical responses of mouse somatosensory (barrel) cortex in vitro. Neuroscience 41:365-379.

Arriza JL, Eliasof S, Kavanaugh MP, Amara SG (1997) Excitatory amino acid transporter 5, a retinal glutamate transporter coupled to a chloride conductance. Proc.Natl.Acad.Sci.U.S.A 94:4155-4160.

Arriza JL, Fairman WA, Wadiche JI, Murdoch GH, Kavanaugh MP, Amara SG (1994) Functional comparisons of three glutamate transporter subtypes cloned from human motor cortex. J Neurosci 14:5559-69.

Behar KL, Boehm D (1994) Measurement of GABA following GABA-transaminase inhibition by gabaculine: a 1H and 31P NMR spectroscopic study of rat brain in vivo. Magn Reson Med 31:660-667.

Bergles DE, Jahr CE (1997) Synaptic activation of glutamate transporters in hippocampal astrocytes. Neuron 19:1297-1308.

Bjoras M, Gjesdal O, Erickson JD, Torp R, Levy LM, Ottersen OP, Degree M, StormMathisen J, Seeberg E, Danbolt NC (1996) Cloning and Expression Of a Neuronal Rat Brain Glutamate Transporter. Molecular Brain Research 36:163-168.

Cohen AS, Lin DD, Coulter DA (2000) Protracted postnatal development of inhibitory synaptic transmission in rat hippocampal area CA1 neurons. J Neurophysiol 84:2465-2476.

Conti F, DeBiasi S, Minelli A, Rothstein JD, Melone M (1998) EAAC1, a high-affinity glutamate transporter, is localized to astrocytes and gabaergic neurons besides pyramidal cells in the rat cerebral cortex. Cereb.Cortex. 8:108-116.

Coulter DA, Lee CJ (1993) Thalamocortical rhythm generation in vitro: extra- and intracellular recordings in mouse thalamocortical slices perfused with low Mg2+ medium. Brain Res 631:137-142.

Danbolt NC, Storm-Mathisen J, Kanner BI (1992) An [Na+ + K+]coupled L-glutamate transporter purified from rat brain is located in glial cell processes. Neuroscience 51:295-310.

Daly DD, Pedley TA (1990) Current practice of clinical electroencephalography (2nd edition): 275-276. Raven Press New York.

Eskandari S, Kreman M, Kavanaugh MP, Wright EM, Zampighi GA (2000) Pentameric assembly of a neuronal glutamate transporter. Proc Natl Acad Sci U S A 97:8641-8646.

Fairman WA, Vandenberg RJ, Arriza JL, Kavanaugh MP, Amara SG (1995) An excitatory amino-acid transporter with properties of a ligand-gated chloride channel. Nature 375:599-603.

Golan H, Talpalar AE, Schleifstein-Attias D, Grossman Y (1996) GABA metabolism controls inhibition efficacy in the mammalian CNS. Neurosci Lett 217:25-28.

He Y, Janssen WG, Rothstein JD, Morrison JH (2000) Differential synaptic localization of the glutamate transporter EAAC1 and glutamate receptor subunit GluR2 in the rat hippocampus. J Comp Neurol 418:255-269.

Hertz L (1979) Functional interactions between neurons and astrocytes I. Turnover and metabolism of putative amino acid transmitters. Prog Neurobiol 13:277-323.

Jones RS, Heinemann U (1988) Synaptic and intrinsic responses of medical entorhinal cortical cells in normal and magnesium-free medium in vitro. J Neurophysiol 59:1476-1496.

Kanai Y, Bhide PG, DiFiglia M, Hediger MA (1995) Neuronal high-affinity glutamate transport in the rat central nervous system. Neuroreport 6:2357-2362.

Kanai Y, Hediger MA (1992) Primary structure and functional characterization of a high- affinity glutamate transporter [see comments]. Nature 360:467-471.

Kanai Y, Smith CP, Hediger MA (1993) A new family of neurotransmitter transporters: the high-affinity glutamate transporters. FASEB J 7:1450-1459.

Kanner BI, Schuldiner S (1987) Mechanism of transport and storage of neurotransmitters. CRC Crit.Rev.Biochem. 22:1-38.

Levy LM, Lehre KP, Rolstad B, Danbolt NC (1993) A monoclonal antibody raised against an [Na(+)+K+]coupled L-glutamate transporter purified from rat brain confirms glial cell localization. FEBS Lett 317:79-84.

Lin CG, Orlov I, Ruggiero AM, Dykes-Hoberg M, Lee A, Jackson M, Rothstein JD (2001) Modulation of the neuronal glutamate transporter EAAC1 by the interacting protein GTRAP3-18. Nature 410:84-88.

Martin DL, Rimvall K (1993) Regulation of gamma-aminobutyric acid synthesis in the brain. J Neurochem 60:395-407.

McBean GJ, Roberts PJ (1985) Neurotoxicity of glutamate and dl-threo-hydroxyaspartate in the rat striatum. J.Neurochem. 44:247-254.

Nakayama T, Kawakami H, Tanaka K, Nakamura S (1996) Expression of three glutamate transporter subtype mRNAs in human brain regions and peripheral tissues. Brain Res Mol Brain Res 36:189-192.

Noto T, Hashimoto H, Nakao J, Kamimura H, Nakajima T (1986) Spontaneous release of gamma-aminobutyric acid formed from putrescine and its enhanced Ca2+-dependent release by high K+ stimulation in the brains of freely moving rats. J Neurochem 46:1877-1880.

Otis TS, Jahr CE (1998) Anion currents and predicted glutamate flux through a neuronal glutamate transporter. J.Neurosci. 18:7099-7110.

Otis TS, Kavanaugh MP (2000) Isolation of current components and partial reaction cycles in the glial glutamate transporter EAAT2. J Neurosci 20:2749-2757.

Paulsen RE, Odden E, Fonnum F (1988) Importance of glutamine for gamma-aminobutyric acid synthesis in rat neostriatum in vivo. J Neurochem 51:1294-1299.

Peghini P, Janzen J, Stoffel W (1997) Glutamate transporter EAAC-1-deficient mice develop dicarboxylic aminoaciduria and behavioral abnormalities but no neurodegeneration. EMBO J. 16:3822-3832.

Petroff OA, Behar KL, Mattson RH, Rothman DL (1996b) Human brain gamma-aminobutyric acid levels and seizure control following initiation of vigabatrin therapy. J Neurochem 67:2399-2404.

Petroff OA, Rothman DL, Behar KL, Mattson RH (1996a) Low brain GABA level is associated with poor seizure control. Ann Neurol 40:908-911.

Pines G, Danbolt NC, Bjoras M, Zhang Y, Bendahan A, Eide L, Koepsell H, Storm-Mathisen J, Seeberg E, Kanner BI (1992) Cloning and expression of a rat brain L-glutamate transporter [published erratum appears in Nature 1992 Dec 24-31;360(6406):768] [see comments]. Nature 360:464-7.

Rafiq A, DeLorenzo RJ, Coulter DA (1993) Generation and propagation of epileptiform discharges in a combined entorhinal cortex/hippocampal slice. J Neurophysiol 70:1962-1974.

Robinson MB, Djali S, Buchhalter JR (1993a) Inhibition of glutamate uptake with L-trans-pyrrolidine-2,4-dicarboxylate potentiates glutamate toxicity in primary hippocampal cultures. J Neurochem 61:2099-103.

Robinson MB, Sinor JD, Dowd LA, Kerwin JF, Jr. (1993b) Subtypes of sodium-dependent high-affinity L-[3H]glutamate transport activity: pharmacologic specificity and regulation by sodium and potassium. J.Neurochem. 60:167-179.

Rothstein JD, Dykes-Hoberg M, Pardo CA, Bristol LA, Jin L, Kuncl RW, Kanai Y, Hediger MA, Wang Y, Schielke J, Welty DF (1996) Knockout of glutamate transporters reveals a major role for astroglial transport in excitotoxicity and clearance of glutamate. Neuron 16:675-686.

Rothstein JD, Jin L, Dykes-Hoberg M, Kuncl RW (1993) Chronic inhibition of glutamate uptake produces a model of slow neurotoxicity. Proc.Natl.Acad.Sci.U.S.A. 90:6591-6595.

Rothstein JD, Martin L, Levey AI, Dykes-Hoberg M, Jin L, Wu D, Nash N, Kuncl RW (1994) Localization of neuronal and glial glutamate transporters. Neuron 13:713-725.

Rothstein JD, Martin LJ, Kuncl RW (1992) Decreased glutamate transport by the brain and spinal cord in amyotrophic lateral sclerosis. N.Engl.J.Med. 326:1464-1468.

Seiler N, Al-Therib MJ (1974) Putrescine catabolism in mammalian brain. Biochem J 144:29-35.

Sepkuty, JS, Orlov, I, Ruggerio, A, Rothstein JD; Increased expression of endogenous GTRAP3-18 causes epilepsy, possibly through its inhibitory effect on EAAC1 mediated glutamate transport. Soc. Neursocience Abstracts, 710.8, 2001

Shashidharan P, Huntley GW, Meyer T, Morrison JH, Plaitakis A (1994) Neuron-specific human glutamate transporter: molecular cloning, characterization and expression in human brain. Brain Res 662:245-50.

Sibson NR, Dhankhar A, Mason GF, Rothman DL, Behar KL, Shulman RG (1998) Stoichiometric coupling of brain glucose metabolism and glutamatergic neuronal activity. Proc Natl Acad Sci U S A 95:316-321.

Storck T, Schulte S, Hofmann K, Stoffel W (1992) Structure, expression, and functional analysis of a Na(+)-dependent glutamate/aspartate transporter from rat brain. Proc Natl Acad Sci U S A 89:10955-10959.

Stuart GJ, Dodt HU, Sakmann B (1993) Patch-clamp recordings from the soma and dendrites of neurons in brain slices using infrared video microscopy. Pflugers Arch 423:511-518.

Tanaka K, Watase K, Manabe T, Yamada K, Watanabe M, Takahashi K, Iwama H, Nishikawa T, Ichihara N, Hori S, Takimoto M, Wada K (1997) Epilepsy and exacerbation of brain injury in mice lacking the glutamate transporter GLT-1. Science 276:1699-1702.

Velaz-Faircloth M, McGraw TS, alandro MS, Fremeau RTJ, Kilberg MS, Anderson KJ (1996) Characterization and distribution of the neuronal glutamate transporter EAAC1 in rat brain. Am J Physiol 270:C67-C75

Wagner RW (1994) Gene inhibition using antisense oligodeoxynucleotides. Nature 372:333-335.

Wahlestedt C (1994) Antisense oligonucleotide strategies in neuropharmacology. Trends Pharmacol Sci 15:42-46.

Yamasaki EN, Barbosa VD, De Mello FG, Hokoc JN (1999) GABAergic system in the developing mammalian retina: dual sources of GABA at early stages of postnatal development. Int J Dev Neurosci 17:201-213.

FIGURE LEGENDS

Figure 1. Antisense EAAC1 treatment leads to loss of hippocampal EAAC1 expression and epilepsy. a. Immunoblots from hippocampal tissue of 3 antisense treated rats (4,5,6) have reduced expression of EAAC1 by 60-70% as compared to the hippocampus of 3 sense controls (1, 2, 3). (b,e) EEG of an awake ambulating adult rat 1 or 2 days after infusion of antisense (b) or sense (e). A normal mixture of frequencies without spikes was seen in both animals. (c,f) Recordings of the same rats (as in b and e respectively), on day 4 or 5. Runs of high voltage polyspike discharges for about 2.5 seconds, with return to baseline background EEG can be seen in the antisense-treated rat (c) but not in the sense-treated rat (f). (d,g) On days 9 or 10 the maximal antisense effect was seen, as prolonged continuous high voltage spikes, spike and wave complexes, background slowing, and decreased mixture of frequencies in the antisense treated rat (d) but not in the sense (g). (h) The mean number of spikes per minute on days 9 or 10 in antisense EAAC1 compared to three controls: antisense GLT-1, antisense GLAST and sense EAAC1 treated animals is significantly increased. * ANOVA with Fisher's PLSD for mean spikes/min $P < 0.005$ between the study group and each of the control groups, but not between the different controls.

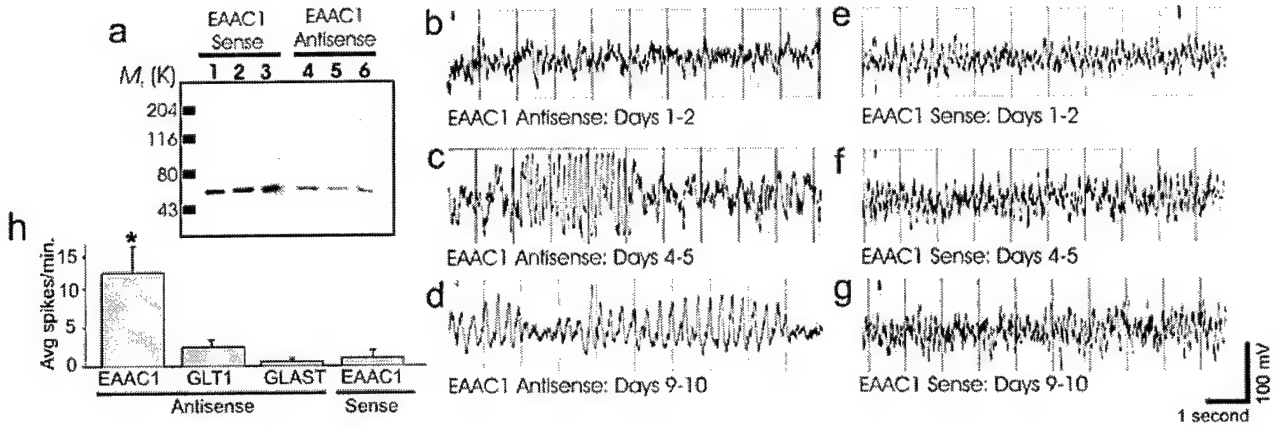

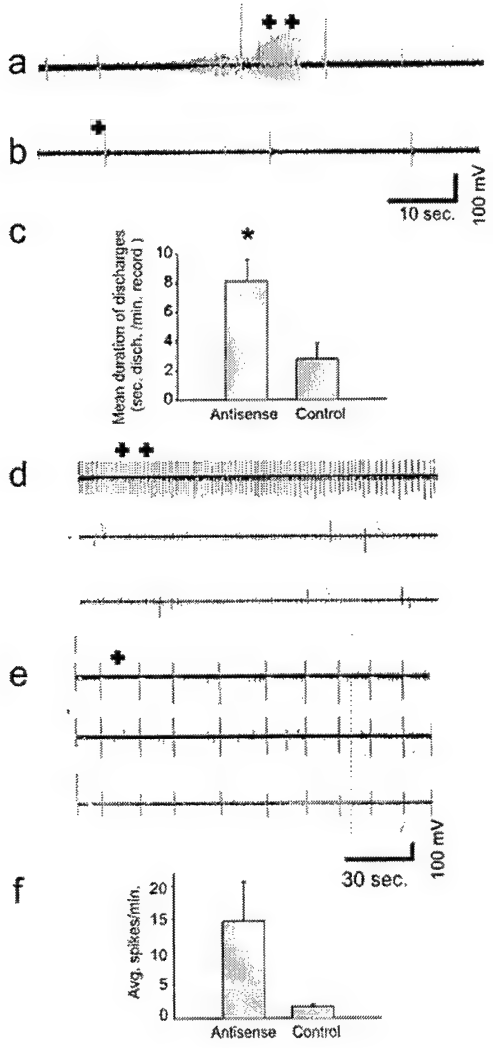

Figure 2. Thalamocortical and hippocampal-entorhinal cortical (HEC) slices of EAAC1 antisense treated rats are hyperexcitable. (a,b) Thalamocortical slice field potential recordings showing a 10 second run of spontaneous bursting rhythmic spike discharges (a, + +) in antisense treated tissue, but not in the controls (b) where occasional spontaneous spike discharges were seen (b, +) (a and b are recorded at 5mm/second paper speed). (c) The mean duration of spike discharges (seconds per minute) in the antisense treated thalamocortical slices was significantly increased compared to control. (d,e) HEC slice field potential recordings showing the occurrence of very frequent spontaneous interictal spikes (SISs) in the antisense treated rat slice (d, + +) and much less frequent SISs (e, +) in the sense treated rat slice (d and e recorded at 1mm/second). (f) Mean number of spikes per

minute in the HEC slices of antisense treated rats was increased.

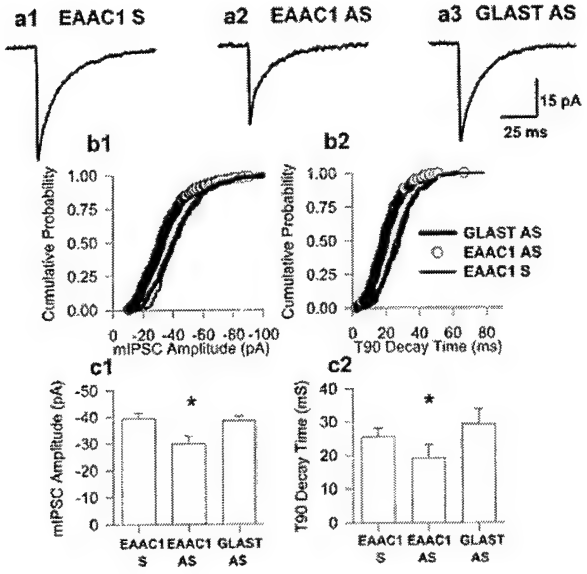

Figure 3. The hyperexcitability of hippocampal slices of EAAC1 antisense treated rats may be secondary to decreased inhibition in CA1 pyramidal neurons. (a) Representative mIPSCs (average of 50) from EAAC1 sense (a1), EAAC1 antisense (a2) and GLAST antisense (a3) CA1 pyramidal neurons. (b) Cumulative frequency amplitude (b1) and T90 decay time (b2) histograms for neurons in (a). (c) Histogram of mean mIPSC amplitudes (c1) and T90 decay times (c2) for the three populations. Asterisks denote significant differences ($p < 0.05$) between EAAC1 antisense-treated and both EAAC1 sense- and GLAST antisense-treated groups.

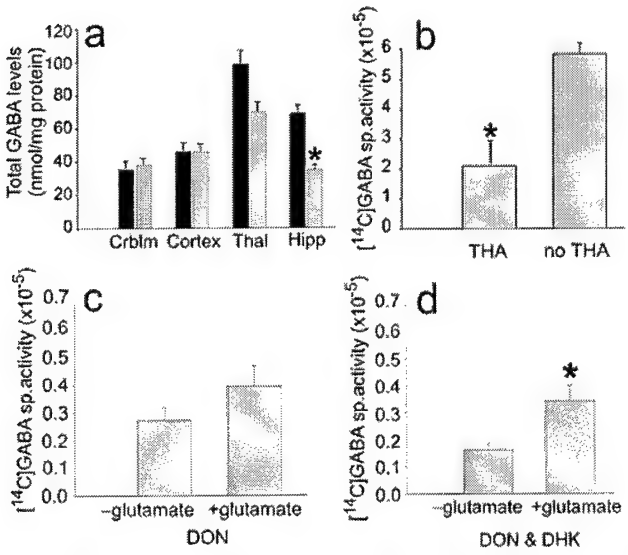

Figure 4. Total GABA is decreased significantly in the hippocampus (Hipp = Hippocampus), and nonsignificantly in the thalamus (Thal = Thalamus) of EAAC1 antisense treated rats, suggesting a role for EAAC1 in GABA synthesis in normal rats hippocampi. (a) Histograms of mean total GABA levels in different brain regions (Crblm = cerebellum) comparing antisense treated rats (grey) to sense controls (black). Antisense EAAC1 treatment leads to a loss of hippocampal GABA significantly and thalamic GABA nonsignificantly. (b)

THA significantly decreases the [^{14}C] GABA specific activity measured in hippocampal tissue of normal rats. (c) The addition of glutaminase inhibitor DON with glutamate to hippocampal tissue produces a non-significant increase in [^{14}C] GABA specific activity. (d) Addition of DON and DHK with glutamate to hippocampal tissue produces a significant increase in [^{14}C] GABA specific activity.

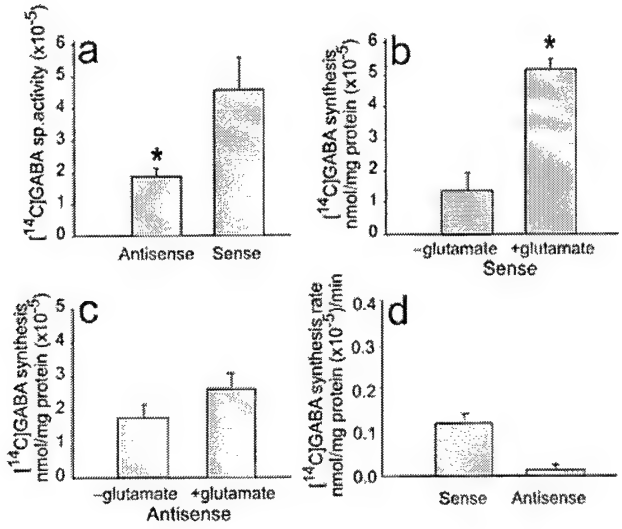

Figure 5. [^{14}C] GABA specific activity and synthesis rate are reduced in EAAC1 antisense treated rats.

(a) [^{14}C] GABA specific activity after incubation of hippocampal tissue with [^{14}C] glutamate is significantly decreased in EAAC1 antisense treated rats. (b) [^{14}C] GABA is significantly increased with addition of [^{14}C] glutamate in EAAC1 sense treated animals. (c) [^{14}C] GABA is not increased significantly with added [^{14}C] labeled glutamate in EAAC1 antisense treated animals. (d) The rate of [^{14}C] GABA synthesis with added [^{14}C] glutamate is five times faster in tissue of EAAC1 sense treated rats as compared to tissue of EAAC1 antisense treated rats.

10. Goujet, D. *Les Poissons Placoderms du Spitsberg. Arthrodires Dolichothoraci de la Formation de Wood Bay (Dévonien Inférieur)* (Cahiers de Paléontologie, Section Vertébrés, Paris, 1984).
11. Maisey, J. G. in *Major Events in Early Vertebrate Evolution* (ed. Ahlberg, P. E.) Ch. 16 (Taylor & Francis, London, in press).
12. Ahlberg, P. E. A re-examination of sarcopterygian interrelationships, with special reference to the Porolepiformes. *Zool. J. Linn. Soc.* **103**, 241–287 (1991).
13. Rosen, D. E., Forey, P. L., Gardiner, B. G. & Patterson, C. Lungfishes, tetrapods, paleontology and plesiomorphy. *Bull. Am. Mus. Nat. Hist.* **167**, 159–276 (1981).
14. Schultze, H.-P. & Cumbaa, S. L. in *Major Events in Early Vertebrate Evolution* (ed. Ahlberg, P. E.) Ch. 18 (Taylor & Francis, London, in press).
15. Cloutier, R. in *Devonian Fishes and Plants of Miguasha, Quebec, Canada* (eds Schultze, H.-P. & Cloutier, R.) 227–247 (Dr Friedrich Pfeil, Munich, 1996).
16. Forey, P. L. *et al.* A new coelacanth from the Middle Devonian of Latvia. *J. Vert. Paleont.* **20**, 243–252 (2000).
17. Jessen, H. L. Lower Devonian Porolepiformes from the Canadian Arctic with special reference to *Powichthys thorsteinssoni* Jessen. *Palaeontographica A* **167**, 180–214 (1980).
18. Chang, M. M. *The braincase of* Youngolepis, *a Lower Devonian Crossopterygian from Yunnan, southwestern China.* Thesis, Stockholm Univ. (1982).
19. Chang, M. M. *Diabolepis* and its bearing on the relationships between porolepiforms and dipnoans. *Bull. Mus. Natl Hist. Nat.* **17**, 235–268 (1995).
20. Zardoya, R. & Meyer, A. Evolutionary relationships of the coelacanth, lungfishes, and tetrapods based on the 28S ribosomal RNA gene. *Proc. Natl Acad. Sci. USA* **93**, 5449–5454 (1996).
21. Zardoya, R. *et al.* Searching for the closest living relative(s) of tetrapods through evolutionary analyses of mitochondrial and nuclear data. *Mol. Biol. Evol.* **15**, 506–517 (1998).
22. Janvier, P. & Phuong, T. H. Les vertébrés (Placodermi, Galeaspida) du Dévonien inférieur de la coupe de Lung Cô—Mia Lé, Province de Hà Giang, Viêt Nam, avec des données complémentaires sur les gisements à vertébrés du Dévonien inférieur du Bac Bo oriental. *Geodiversitas* **21**, 33–67 (1999).
23. Long, J. A. (ed.) *Palaeozoic Vertebrate Biostratigraphy and Biogeography* (Belhaven, London, 1993).
24. Swofford, D. L. *PAUP: phylogenetic analysis using parsimony, ver.3.1.1* (Illinois Natural History Survey, Campaigne, Illinois, 1993).

Supplementary information is available on *Nature*'s World-Wide Web site (http://www.nature.com) or as paper copy from the London editorial office of *Nature*.

Acknowledgements

We thank M. M. Chang, P. Janvier and M. I. Coates for useful discussions, U. Samuelson and Zhang Jie for photographic work, Lu Xiufen for specimen preparation and Hu Huiqing for artwork. M.Z. & X.Y. acknowledge the support from the Chinese Foundation of Natural Sciences, Ministry of Science & Technology (China), and National Geographic Society (US). X.Y. thanks Kean University for faculty research and development support.

Correspondence and requests for materials should be addressed to M.Z.

Modulation of the neuronal glutamate transporter EAAC1 by the interacting protein GTRAP3-18

Chien-Liang Glenn Lin*, Irina Orlov*, Alicia M. Rugglero, Margaret Dykes-Hoberg, Andy Lee, Mandy Jackson & Jeffrey D. Rothstein

Johns Hopkins University, Department of Neurology and Neuroscience, Meyer 6-109, 600 North Wolfe Street, Baltimore, Maryland 21287, USA
* *These authors contributed equally to this work*

Excitatory amino-acid carrier 1 (EAAC1) is a high-affinity Na^+-dependent L-glutamate/D, L-aspartate cell-membrane transport protein[1]. It is expressed in brain as well as several non-nervous tissues. In brain, EAAC1 is the primary neuronal glutamate transporter[2,3]. It has a polarized distribution in cells and mainly functions perisynaptically to transport glutamate from the extracellular environment[2–4]. In the kidney it is involved in renal acidic amino-acid re-absorption and amino-acid metabolism[5–7]. Here we describe the identification and characterization of an EAAC1-associated protein, GTRAP3-18. Like EAAC1, GTRAP3-18 is expressed in numerous tissues[8,9]. It localizes to the cell membrane and cytoplasm, and specifically interacts with carboxy-terminal intracellular domain of EAAC1. Increasing the expression of GTRAP3-18 in cells reduces EAAC1-mediated glutamate transport by lowering substrate affinity. The expression of GTRAP3-18 can be upregulated by retinoic acid, which results in a specific reduction of EAAC1-mediated glutamate transport. These studies show that glutamate transport proteins can be regulated potently and that GTRAP can modulate the transport functions ascribed to EAAC1. GTRAP3-18 may be important in regulating the metabolic function of EAAC1.

Using the C-terminal intracellular domain of EAAC1 (the last 87 amino acids) as bait in a yeast two-hybrid screen of an adult rat brain complementary DNA library, we isolated 78 clones displaying β-galactosidase activity. Restriction and sequencing analyses revealed that 10 of the clones with the strongest β-galactosidase activity were identical. This clone, designated E18, was completely sequenced and was found to be unique after GenBank analysis. JWA protein, (GenBank NP006398) a human, differentially displayed, vitamin-A-responsive gene, is 95% identical to E18, suggesting that E18 is a JWA protein homologue of rat.

E18 is a full-length complementary DNA containing an initiation methionine and a poly(A) tail. We named the protein glutamate transporter EAAC1-associated protein (GTRAP3-18). GTRAP3-18 encodes a protein of 188 amino acids (see Supplementary Information), with a calculated relative molecular mass of 22,500 (M_r 22.5K). Protein analysis indicated that it is a very hydrophobic protein with four possible transmembrane domains. Both the C-terminal and amino-terminal domains contain protein kinase C motifs and may be intracellular.

To confirm the yeast two-hybrid results, we examined the interaction of GTRAP3-18 with EAAC1 using *in vitro* and *in vivo* methods. For *in vitro* cell-free binding, EAAC1 was expressed as a fusion protein with glutathione *S*-transferase (GST), and GTRAP3-18 was produced and labelled with [^{35}S]methionine by *in vitro* transcription and translation. Purified GST or GST–EAAC1 fusion proteins immobilized on glutathione–sepharose were incubated with [^{35}S]labelled GTRAP3-18 protein. GTRAP3-18 bound specifically to immobilized GST–EAAC1 (lane 2) but not to GST alone (lane 3), indicating that they interact *in vitro* (Fig. 1a).

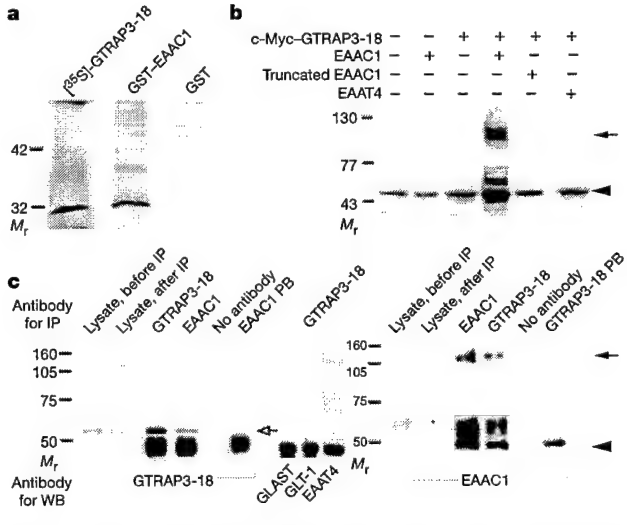

Figure 1 GTRAP3-18 interacts with EAAC1 *in vitro* and *in vivo*. **a**, SDS–PAGE analysis of cell-free *in vitro* binding. *In vitro* synthesized [^{35}S]-labelled GTRAP3-18 bound specifically to immobilized GST–EAAC1 and not to the negative control GST. **b**, Western blot analyses of immunoprecipitations from transfected HEK293 cells extracts, using anti-c-Myc antibodies for immunoprecipitation and anti-EAAC1 or EAAT4 antibodies for western blot. EAAC1 (monomer, arrowhead; dimer, arrow) was specifically co-immunoprecipitated with c-Myc–GTRAP3-18. An immunoprecipitation artifact is present in each lane at about 50–60K. **c**, Western blot (WB) analyses of immunoprecipitations (IP) from rat brain extracts. GTRAP3-18 (open arrowhead) was specifically co-immunoprecipitated with EAAC1. EAAC1 (monomer, arrowhead; dimer, arrow) was co-immunoprecipitated with GTRAP3-18. PB, peptide block.

We carried out immunoprecipitation experiments to test whether EAAC1 and GTRAP3-18 interact *in vivo*. Initial experiments were performed in transfected HEK293 cells using N-terminal c-Myc-tagged GTRAP3-18. As shown in Fig. 1b, EAAC1 co-immunoprecipitated with c-Myc–GTRAP3-18 in the cell extract prepared from co-expression cells (lane 4), but not from EAAC1 (lane 2) or c-Myc–GTRAP3-18 (lane 3) single-expression cells, which eliminated the possibility of artefacts arising from nonspecific immunobead binding or an antibody cross-reaction, respectively. A truncated EAAC1 lacking the interacting C-terminal domain (see below) did not co-immunoprecipitate with c-Myc–GTRAP3-18 (lane 5), further indicating an interaction between EAAC1 and GTRAP3-18. This interaction was specific, as EAAT4, another neuronal glutamate transporter subtype, was not immunoprecipitated with c-Myc–GTRAP3-18 (lane 6). Identical results were obtained using other cell lines (COS-7 and C6 glioma; data not shown).

To study the protein interaction *in vivo*, we used anti-EAAC1 or GTRAP3-18 polyclonal antibodies to immunoprecipitate EAAC1 or GTRAP3-18 from rat brain extract. EAAC1 co-immunoprecipitated specifically with GTRAP3-18, but not GLAST, GLT-1 or EAAT4 (Fig. 1c). Similarly, GTRAP3-18 co-immunoprecipitated with EAAC1. These studies suggest that EAAC1 and GTRAP3-18 can interact *in vivo*.

GTRAP3-18 messenger RNA was widely expressed in brain regions and body organs, consistent with the distribution of EAAC1 (Fig. 2a)[8,9]. Similarly, GTRAP3-18 protein was expressed in many neural and non-neural tissues, when examined using a polyclonal oligopeptide antibody to the N terminus of GTRAP3-18 (Fig. 2b). GTRAP3-18 protein seemed to aggregate as multimers.

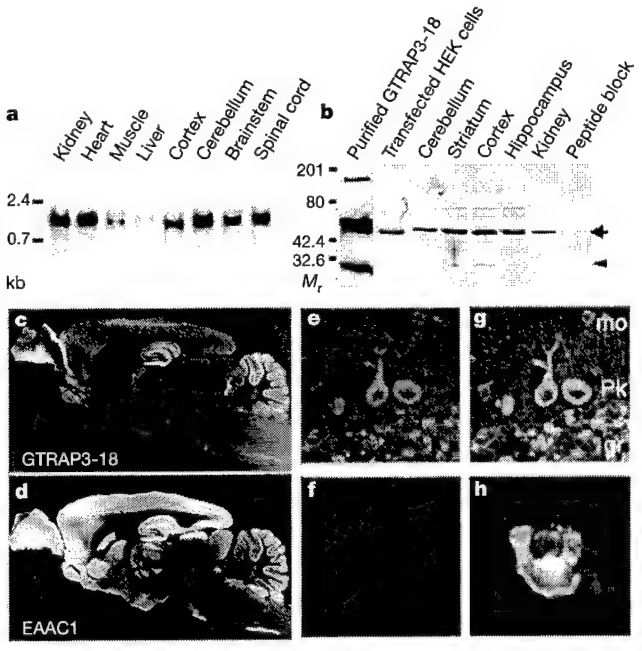

Figure 2 Tissue and cellular distribution of GTRAP3-18 protein and mRNA. **a**, Northern blot analysis of GTRAP3-18 mRNA. **b**, Western blot analyses of GTRAP3-18 protein. Pure GTRAP3-18 (~30K, arrowhead) monomer tended to form multimers including the dimer (arrow). Dimeric GTRAP3-18 was found in HEK293 cells transfected with GTRAP3-18 cDNA and tissue homogenates. **c**, **d**, Immunostaining of GTRAP3-18 and EAAC1 proteins in rat brain. **e–h**, Confocal microscopy of cellular colocalization of GTRAP3-18 and EAAC1. In the cerebellum, GTRAP3-18 (**e**, green), EAAC1 (**f**, red) reveals prominent cytosolic colocalization (**g**, yellow). mo, molecular layer; pk, Purkinje cell layer; gr, granular layer. In transfected HEK293 cells (**h**), EAAC1 (red) tends to localize to the cell surface whereas GTRAP3-18 was found typically cytosolic and co-localized with EAAC1 (yellow) at the cell membrane.

The dimeric form of GTRAP3-18 was the predominant species in tissue homogenates, and it was also observed when purified GTRAP3-18 protein was detected using the N-terminal GTRAP3-18 antibody (Fig. 2b, lane 1), and when c-Myc–GTRAP3-18 protein was detected using anti-c-Myc antibodies (Fig. 2b, lane 2).

Immunohistological analysis of rat brain revealed that GTRAP3-18 protein was expressed widely (Fig. 2c) and primarily localized to neurons such as cerebellar Purkinje cells (Fig. 2e, g), identical to the expression and localization[4] of EAAC1 (Fig. 2f, g)[2]. In transfected HEK293 cells, EAAC1 protein (red) seemed to be aggregated at the cell membrane (Fig. 2h), whereas GTRAP3-18 protein (green) was typically localized to the cell membrane and cytosol, and co-associated with EAAC1 protein (yellow) at the cell membrane.

We tested whether GTRAP3-18 modulates EAAC1 function by studying, 72 h after transfection, sodium-dependent [^{3}H]glutamate transport[3,10] in HEK293 cells co-expressing both proteins. Total glutamate transport decreased progressively with increasing expression of GTRAP3-18 protein (Fig. 3a). This effect was specific for EAAC1; co-expression of GTRAP3-18 with EAAT4 had no effect on transport activity. The inhibition of transport was not caused by a decrease of EAAC1 protein level by the co-expression of GTRAP3-18, as quantitated by western blot (Fig. 3b). Similarly, the loss of EAAC1 activity was not due to altered protein trafficking. Even at high levels of GTRAP3-18 expression—when little EAAC1-mediated transport was observed—surface biotinylation and confocal microscopy showed that EAAC1 surface expression was unaltered (Fig. 3b).

To evaluate the biochemical nature of altered transport, we carried out kinetic analyses with HEK293 cells co-expressing EAAC1 and GTRAP3-18. EAAC1 and GTRAP3-18 co-expressing cells showed a decrease in affinity (Michaelis constant, $K_m = 40\,\mu M$, $n = 4$, $P < 0.01$) without a shift in maximal velocity ($V_{max} = 0.99\,nmol\,min^{-1}$ per mg protein), when compared with cells only expressing EAAC1 ($K_m = 9\mu M$; $V_{max} = 1.02\,nmol\,min^{-1}$ per mg protein; Fig. 3c). Similar results were observed with other cell lines (COS7 and C6 glioma; data not shown).

These studies indicate that GTRAP3-18 modulates EAAC1 transport activity by decreasing its affinity for glutamate. On the basis of these results, we thought that GTRAP3-18 might tonically modulate EAAC1 activity. To test this, we used antisense oligomers to lower GTRAP3-18 expression in HEK293 cells. Notably, western blot analyses and glutamate uptake assays revealed that HEK293 cells endogenously express some EAAC1 and GTRAP3-18 protein, but do not express the transporter subtypes GLAST, GLT-1 or EAAT4. We transfected antisense oligomers, targeted to the 5′ GTRAP3-18 transcript, into HEK293 cells. Antisense oligomers specifically reduced endogenous GTRAP3-18 protein level (Fig. 3d, grey bars); EAAC1 protein level was not affected. Significantly, glutamate transport activity was elevated concomitantly with the reduction of GTRAP3-18 protein level (black bars).

We determined whether the *in vitro* modulation of EAAC1 by GTRAP3-18 is physiologically relevant, by administering GTRAP3-18 antisense oligomers intraventricularly. Eleven days of antisense treatment resulted in a reduction of GTRAP3-18 protein level and a significant increase in cortical glutamate uptake, whereas glutamate uptake was not altered in animals treated with the sense oligomer (Fig. 3e). The effect was due to increased EAAC1-mediated transport because it was not altered by dihydrokainic acid (DHK), an inhibitor of GLT-1-mediated glutamate transport[11]. In kinetic studies of DHK-insensitive, cortical glutamate uptake from antisense-treated animals, the apparent affinity for glutamate was increased (antisense $K_m = 10\,\mu M$; $V_{max} = 1.08\,nmol\,min^{-1}$ per mg protein) compared with artifical cerebrospinal-fluid (CSF)-treated or sense-treated control animals (control $K_m = 19.7\,\mu M$; $V_{max} = 1.08\,nmol\,min^{-1}$ per mg protein; Fig. 3f). These results suggest that GTRAP3-18 negatively modulates EAAC1 glutamate transport activity *in vivo*.

Human GTRAP3-18 (JWA protein), as described above, was originally identified as a retinoic-acid-responsive gene. We therefore tested whether retinoic acid could upregulate GTRAP3-18 expression and consequently inhibit EAAC1-mediated glutamate transport in HEK293 cells. Retinoic acid induced a large increase in GTRAP3-18 expression, over a non-toxic dose range from 1 to 10 μM (Fig. 4a). A significant decrease in glutamate transport activity paralleled the increase of GTRAP3-18 protein level (Fig. 4a). Fluorescence microscopy indicated that this loss of transport activity was not due to changes in EAAC1 protein level (Fig. 4a) or in the cellular membrane localization of EAAC1 protein induced by retinoic acid (Fig. 4b).

To confirm that loss of transport activity was specifically due to GTRAP3-18 and not by other factors induced by retinoic acid or direct effects on EAAC1, we constructed a truncated EAAC1 cDNA, lacking the last 93 amino acids. The truncation corresponded to the region used as bait in yeast two-hybrid screening, and was not able to interact with GTRAP3-18 (Fig. 1b, lane 5). Nevertheless, after transient expression in HEK293 cells, the truncated EAAC1 transported glutamate. Retinoic acid treatment did not alter activity of the truncated EAAC1 protein; even though GTRAP3-18 protein expression was elevated markedly (Fig. 4c). Thus, the loss of transport activity caused by retinoic acid was the result of GTRAP3-18 induction. Notably, truncated EAAC1 had increased glutamate transport activity as compared with wild type. Truncated EAAC1 had a K_m of 5.4 μM, which was more than a threefold increase in affinity over that of wild-type EAAC1 (K_m = 17 μM; Fig. 4d). This might mean that endogenous EAAC1 is normally inhibited by GTRAP3-18—an effect that was eliminated in a truncated EAAC1, and that was mimicked by GTRAP3-18 antisense

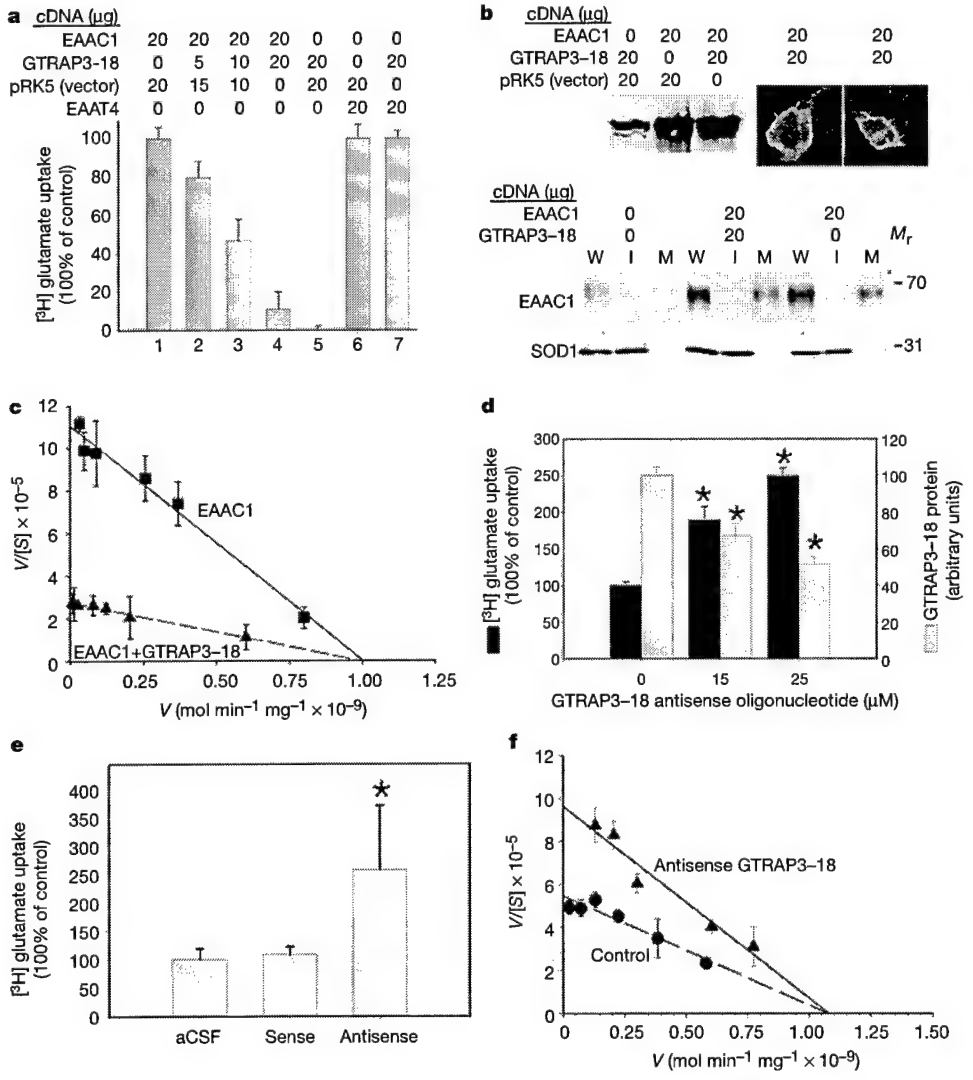

Figure 3 GTRAP3-18 negatively modulates EAAC1-mediated glutamate transport. **a**, Glutamate transport in HEK293 cells transfected with the indicated plasmids. GTRAP3-18 inhibited EAAC1-mediated transport, but had no effect on EAAT4 ($n = 6$). **b**, Western blot showed that the co-expression of GTRAP-3-18 had no effect on total EAAC1 protein expression (top, left). Analysis of HEK293 cells by confocal microscopy (top panel, right) and surface biotinylation (bottom) revealed no alteration in the membranous localization of EAAC1. I, intracellular fraction; M, cellular membrane fraction; W, whole cell. Superoxide dismutase (SOD1) was used as a control. **c**, Eadie–Scatchard plot of glutamate transport in transfected HEK293 cells showed a 4–10-fold decrease in affinity ($n = 4$). **d**, Antisense GTRAP3-18 oligomers reduced endogenous GTRAP3-18 expression in HEK293 cells and produced an increase in EAAC1 transport. Asterisks indicate statistical significance (Students t-test; $P < 0.01$) versus untreated control ($n = 4$). **e**, Intraventricular antisense delivery led to a 50% loss of cortical GTRAP3-18 levels and a significant increase in dihydrokainate-insensitive glutamate uptake. Asterisk indicates statistical significance (Students t-test; $P < 0.05$) versus artificial CSF (aCSF) control ($n = 7$). **f**, Kinetic analysis of cortical tissue from rats treated with antisense GTRAP3-18 shows an increase in apparent affinity for glutamate. All errors bars represent standard deviation.

treatment (Fig. 3f).

To test this hypothesis *in vivo*, retinoic acid was infused intraventricularly. After 4 d of treatment, cortical GTRAP3-18 protein expression was increased in a dose-dependent manner, and this was associated with a significant decrease of total glutamate uptake (Fig. 4e, top panel). This effect was specifically due to decreased EAAC1-mediated transport because it was not altered by the glutamate transport inhibitor dihydrokainic acid, at a concentration that predominantly effects GLT-1 (Fig. 4e, bottom panel)[11]. Kinetic analysis of DHK-insensitive, cortical glutamate transport from animals treated 4 d with intraventricular retinoic acid revealed a fourfold decrease in affinity over control transport (Fig. 4f)—very similar to that seen *in vitro* (Fig. 3c). In addition, retinoic acid inhibition of glutamate transport could be reversed *in vivo*; chronic intraventricular treatment with antisense GTRAP3-18 oligomer (50–100 ng d^{-1}, for 7–10 d) blocked the retinoic acid (2.5 μM)

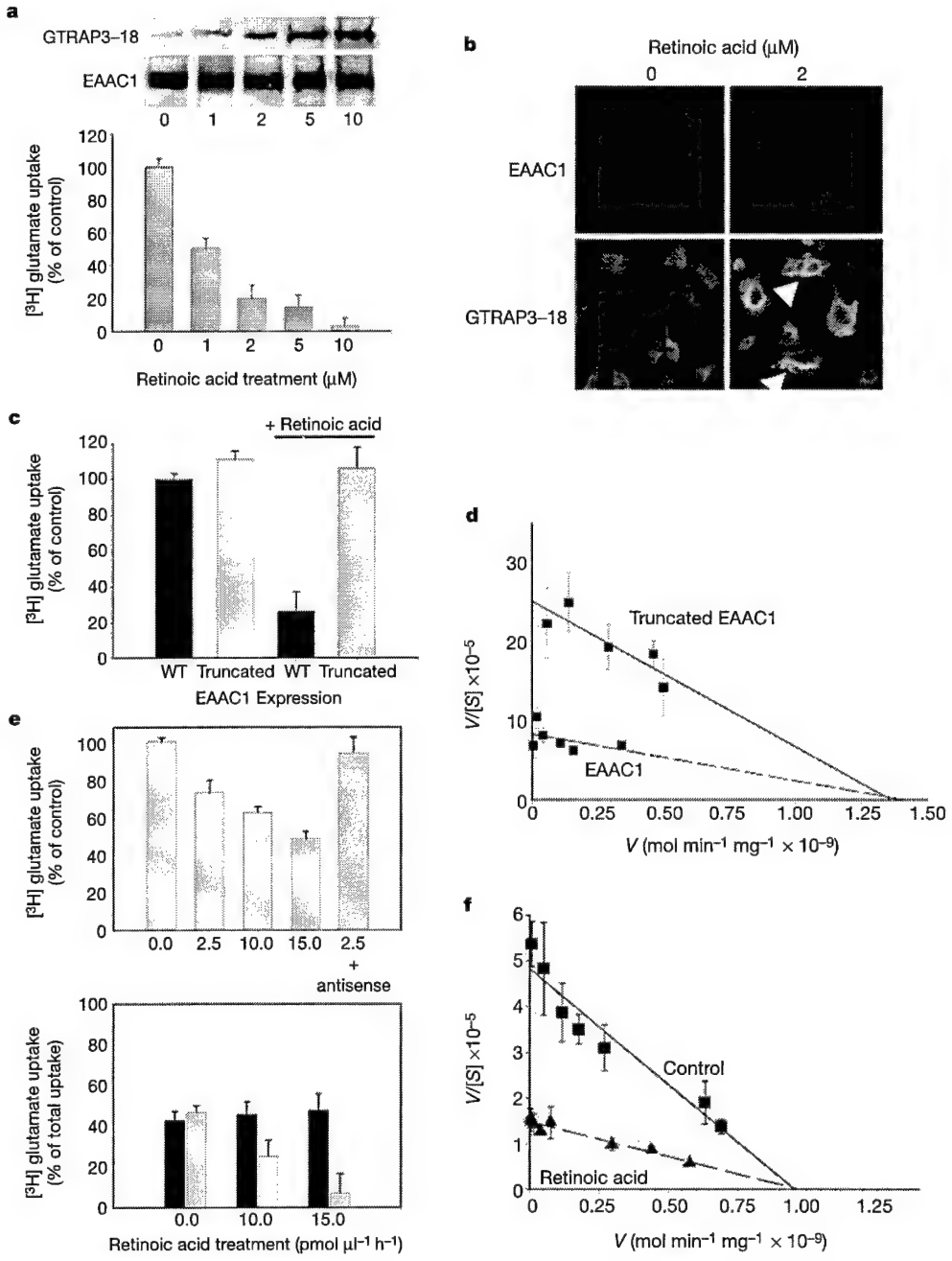

Figure 4 Retinoic acid upregulates GTRAP3-18 expression and consequently inhibits EAAC1 transport in HEK293 cells in brain. **a**, After 14 d, retinoic acid induced GTRAP3-18 expression and inhibited transport ($n = 5$) in HEK293 cells. **b**, Membrane localization of EAAC1 protein was not changed by retinoic acid, as visualized by fluorescent microscopy. GTRAP3-18 expression, particularly in a subcellular compartment, was greatly induced by retinoic acid (arrow). **c**, Glutamate transport by HEK293 cells expressing truncated EAAC1 (lacking a C-terminal interacting domain) was not inhibited by 14 d of treatment with retinoic acid (5 μM; $n = 3$). **d**, Truncated EAAC1 expressed by HEK293 cells has increased apparent affinity for glutamate compared with wild type (WT) EAAC1. **e**, Intraventricular delivery of retinoic acid (3–5 d) inhibited glutamate uptake; the effect was blocked by concomitant treatment with GTRAP3-18 antisense oligomers (5 μg $μl^{-1}$; 1 μl h^{-1}; top panel). This effect was specific for DHK-insensitive transport (bottom panel, grey bars)—a crude partial estimate of EAAC1 activity *in vivo*—but not for DHK-sensitive transport (EAAT2-mediated) (black bars; $n = 5$). **f**, Kinetic analysis of cortical uptake from rats treated with retinoic acid (2.5 pmol l^{-1} h^{-1} for 4 d) showed a large decrease in apparent affinity for glutamate ($n = 3$). All errors bars represent standard deviation.

induction of GTRAP3-18, and also blocked the inhibition of glutamate transport seen with retinoic acid treatment (Fig. 4e, top panel). Retinoic acid had no effect on glutamate transport by cells expressing GLT-1 or EAAT4.

In brain, glutamate serves as an excitatory neurotransmitter, a metabolic substrate for other neurotransmitters (that is, GABA (γ-amino butyric acid)), and an amino acid for general cellular metabolism. In brain, glutamate transporters maintain low extracellular glutamate and influence the kinetics of glutamate receptor activation[12–14]. Little is known about the molecular and protein regulation of glutamate transporters, or for neurotransmitter transporters in general. In tumour cell lines, for example, the cell-surface expression of EAAC1 appears to be regulated by pathways mediated by both protein kinase C and phosphatidylinositol-3-OH kinase, albeit through as yet unidentified proteins[7,15]. GTRAP3-18 appears to be an endogenous inhibitory regulator of EAAC1. EAAC1 is found throughout the brain on somas and dendrites of small and large pyramidal neurons[2,4]. EAAC1 is also localized to pre-synaptic GABA-containing terminals, and may have a metabolic role in providing glutamate for GABA metabolism[4,16]. Loss of brain EAAC1 expression interferes with GABA synthesis and results in epilepsy[3,17]. In kidney, EAAC1 may contribute to renal acidic amino-acid reabsorption, acid/base balance, cell volume regulation, and amino-acid metabolism[5,6]. GTRAP3-18 may have a critical role in the regulation of the neurotransmitter and metabolic functions of EAAC1. □

Methods

Yeast two-hybrid screening

The MATCHMAKER Two-Hybrid System (Clontech) was used for screening. We screened a rat brain cDNA library with a bait protein corresponding to C-terminal intracellular domain of EAAC1 (last 87 amino acids, cDNA position 1,458–1,719). The positive clones were selected and assayed for β-galactosidase activity. Plasmid DNAs were isolated from positive clones and co-transformed with bait cDNA back into yeast to reconfirm the interaction.

GST fusion proteins

The GST Gene Fusion System (Pharmacia) was used to construct and generate GST–EAAC1 and GST–GTRAP3-18 fusion proteins using pGEX–6P-1 vector.

In vitro cell-free binding assay

The TnT Coupled Reticulocyte Lysate System (Promega) was used to generate [^{35}S]methionine-labelled GTRAP3-18 protein using the pRK5–GTRAP3-18 plasmid DNA as a template, driven by SP6 RNA polymerase. GST–EAAC1 fusion proteins were expressed in *Escherichia coli* and recovered on glutathione–sepharose beads as described above. The beads were incubated with lysate which containing [^{35}S]labelled GTRAP3-18 protein for 1 h at 4 °C and then washed five times with NETN buffer (20 mM Tris pH 8.0, 100 mM NaCl, 1 mM EDTA, 0.5% NP-40). The beads were boiled in sample buffer (SB) (2% SDS, 10% glycerol, 62 mM Tris pH 6.8) and bound proteins resolved in SDS–PAGE.

Gene constructions and mammalian cell expression system

We used the eukaryotic expression vectors pcDNA3 and pRK5 for expression of cDNAs in mammalian cell lines. Full-length EAAC1 cDNA was subcloned into *Not*I, *Eco*RI sites of the pcDNA3 vector. For the truncated EAAC1, the last 279 nucleotides were removed by *Aat*II and *Eco*RI digestion in a pcDNA3/EAAC1 construct and blunt ended. For tagging GTRAP3-18 with c-Myc, GTRAP3-18 cDNA was first subcloned into downstream of *c-myc* gene (*Not*I site) in the pTYGL vector. The *Eco*RI /*Bam*HI fragment containing Myc–GTRAP3-18 fusion gene was then subcloned into pRK5. The constructed plasmid DNA was transfected into HEK293, COS-7 or C6 glioma cell lines by standard electroporation, and 72 h later cells were collected for various assays.

Immunoprecipitation, biotinylation and transport assays

For the transfected cells, cells were solubilized in 1 ml of IPB buffer (10 mM Tris pH 7.6, 5mM EDTA, 5 mM EGTA, 1 mM sodium orthovanadate, aprotinin 15 μg ml^{-1}, 0.1 mM PMSF) with 1% triton at 4 °C for 30 min with gentle rotation. Cell debris was removed (15,000*g*, 15 min), and supernatants were incubated (4 °C, 16 h) with protein A/sepharose beads (150 μl, CL-4B, Amersham) and primary antibodies (1.5 mg ml^{-1}). The immuno-bead-bound protein complexes were washed three times (IPB buffer in 1% triton X-100, 100 mM NaCl) followed by three IPB buffer washes. Immunoprecipitated proteins were boiling in SB and analysed by western blotting.

For the rat brain, coronal sections of brain were sliced at 1–2-mm intervals from the cerebellum to the olfactory bulbs. The cortex region was excised from the brain and placed in cold buffer A (50 mM Tris pH 7.5, 2 mM EDTA, 150 mM NaCl, 0.5 mM dithiothreitol). The tissue was washed three times in buffer A and then weighed. The tissue was then homogenized using a blender in 2.5 volumes of buffer B (50 mM Tris pH 7.5, 10% glycerol, 5 mM magnesium acetate, 0.2 mM EDTA, 0.5 mM dithiothreitol, 1 mM PMSF). The particulate material was removed by centrifugation at 15,000*g* for 30 min at 4 °C. The supernatant fraction was incubated with protein A/sepharose beads and primary antibodies as above.

Biotinylation was performed as described[15] with modifications. Glutamate uptake assays were done as described on either cells grown on six-well plates (up to 1 mg protein) or brain tissues (100–150 μg protein). To block GLT-1 transport activity, homogenates were pre-incubated with dihydrokainic acid (300 μM, Sigma) for 20–60 min before assay.

Blotting, immunostaining and antibodies

The methods for isolation of RNA and northern blotting, western blotting and immunostaining have been described[18]. We synthesized a synthetic peptide corresponding to an N-terminal domain of GTRAP3-18 protein NH_2-K^{14}FFPGSDRFARPDFRD^{28}-COOH and used this to generate polyclonal, affinity-purified antibodies from New Zealand White rabbits[2,19]. Confocal microscopy of transfected cells of brain sections was performed with a Zeiss LSM 510 laser scanning microscope using fluorescein (Vector, FI1000) and Texas red (Vector, TI2000) flurochromes.

Intraventricular antisense/drug administration

We used the following sequences for the new phosphodiester oligonucleotides: sense GTRAP3-18, 5′-GTGAACCTTGCCCGCTC-3′; antisense GTRAP3-18, 5′-GAGCGG GGCAAGGTTCAC-3′. Oligonucleotides (5 μg μl^{-1}), retinoic acid (1–20 μM; 0–20 pmol μl^{-1}) separately or in combination were administered intraventricularly over 3–11 d, by mini-osmotic pumps (Alza Corporation, Palo Alto, CA) as described[3].

Received 5 October; accepted 20 November 2000.

1. Kanai, Y. & Hediger, M. A. Primary structure and functional characterization of a high-affinity glutamate transporter. *Nature* **360,** 467–471 (1992).
2. Rothstein, J. D. *et al.* Localization of neuronal and glial glutamate transporters. *Neuron* **13,** 713–725 (1994).
3. Rothstein, J. D. *et al.* Knockout of glutamate transporters reveals a major role for astroglial transport in excitotoxicity and clearance of glutamate. *Neuron* **16,** 675–686 (1996).
4. He, Y., Janssen, W. G. M., Rothstein, J. D. & Morrison, J. H. Differential synaptic localization of the glutamate transporter EAAC1 and glutamate receptor subunit GluR2 in the rat hippocampus. *J. Comp. Neurol.* **418,** 255–269 (2000).
5. Shayakul, C. *et al.* Localization of the high-affinity glutamate transporter EAAC1 in rat kidney. *Am. J. Physiol. Renal Physiol.* **42,** F1023–F1029 (1997).
6. Peghini, P., Janzen, J. & Stoffel, W. Glutamate transporter EAAC-1-deficient mice develop dicarboxylic aminoaciduria and behavioral abnormalities but no neurodegeneration. *EMBO J.* **16,** 3822–3832 (1997).
7. Sims, K. D., Straff, D. J. & Robinson, M. B. Platelet-derived growth factor rapidly increases activity and cell surface expression of the EAAC1 subtype of glutamate transporter through activation of phosphatidylinositol 3-kinase. *J. Biol. Chem.* **275,** 5228–5237 (2000).
8. Hediger, M. A. & Welbourne, T. C. Introduction: glutamate transport, metabolism, and physiological responses. *Am. J. Physiol.* **277,** F477–F480 (1999).
9. Hediger, M. A. Glutamate transporters in kidney and brain. *Am. J. Physiol.* **277,** F487–F492 (1999).
10. Lin, C. G. *et al.* Aberrant RNA processing in a neurodegenerative disease: The cause for absent EAAT2 a glutamate transporter, in amyotrophic lateral sclerosis. *Neuron* **20,** 589–602 (1998).
11. Robinson, M. B. The family of sodium-dependent glutamate transporters: a focus on the GLT-1/EAAT2 subtype. *Neurochem. Int.* **33,** 479–491 (1998).
12. Bergles, D. E. & Jahr, C. E. Synaptic activation of glutamate transporters in hippocampal astrocytes. *Neuron* **19,** 1297–1308 (1997).
13. Bergles, D. E., Dzubay, J. A. & Jahr, C. E. Glutamate transporter currents in bergmann glial cells follow the time course of extrasynaptic glutamate. *Proc. Natl Acad. Sci. USA* **94,** 14821–14825 (1997).
14. Diamond, J. S. & Jahr, C. E. Transporters buffer synaptically released glutamate on a submillisecond time scale. *J. Neurosci.* **17,** 4672–4687 (1997).
15. Davis, K. E. *et al.* Multiple signaling pathways regulate cell surface expression and activity of the excitatory amino acid carrier 1 subtype of Glu transporter in C6 glioma. *J. Neurosci.* **18,** 2475–2485 (1998).
16. Conti, F., DeBiasi, S., Minelli, A., Rothstein, J. D. & Melone, M. EAAC1, a high-affinity glutamate transporter, is localized to astrocytes and gabaergic neurons besides pyramidal cells in the rat cerebral cortex. *Cereb. Cortex.* **8,** 108–116 (1998).
17. Sepkuty, J., Eccles, C. U., Lesser, R. P., Dykes-Hoberg, M. & Rothstein, J. D. Molecular knockdown of neuronal glutamate transporter EAAT3 produces epilepsy and dysregulation of GABA metabolism. *Soc. Neurosci. Abstracts* **23,** 1484 (1997).
18. Lin, C. L. G. *et al.* Molecular cloning and expression of the rat EAAT4 glutamate transporter subtype. *Mol. Brain Res.* **63,** 174–179 (1998).
19. Furuta, A., Martin, L. J., Lin, C. L. G., Dykes-Hoberg, M. & Rothstein, J. D. Cellular and synaptic localization of the neuronal glutamate transporters excitatory amino acid transporter 3 and 4. *Neuroscience* **81,** 1031–1042 (1997).

Supplementary information is available on *Nature*'s World-Wide Web site (http://www.nature.com) or as paper copy from the London editorial office of *Nature*.

Acknowledgements

We thank R. Huganir for the pRK5 vector; J. Sepkuty, R. Ganel, and W. Song for helpful suggestions and discussions; and L. Jin, C. Coccia and B. Kim for technical support.

Correspondence and requests for materials should be addressed to J.D.R. (e-mail: jrothste@welchlink.welch.jhu.edu). GenBank accession number for GTRAP3-18 is AF240182.

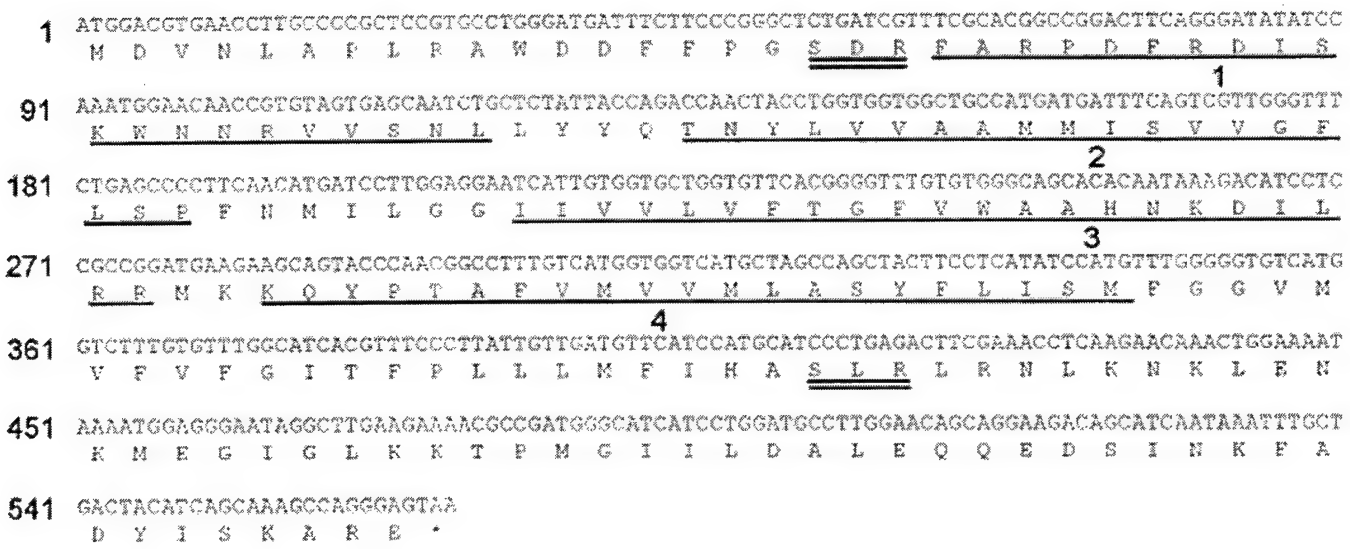

Supplement 1. Nucleotide and amino acid sequence of GTRAP3-18. Lines 1-4: putative transmembrane domains, double lines: potential protein kinase-dependent phosphorylation sites (S/T-X-K/R). GenBank accession number for GTRAP3-18 is AF240182.

Modulation of the neuronal glutamate transporter EAAT4 by two interacting proteins

Mandy Jackson*, Wei Song*, Mu-Ya Liu†, Lin Jin*, Margaret Dykes-Hoberg*, Chien-Hang G. Lin*, William J. Bowers‡, Howard J. Federoff‡, Paul C. Sternweis† & Jeffrey D. Rothstein*

** Department of Neurology and Neuroscience, Johns Hopkins University, Baltimore, Maryland 21287, USA*
† Department of Pharmacology, University of Texas Southwestern Medical Center, Dallas, Texas 75235, USA
‡ Department of Neurology, and the Center for Aging and Developmental Biology, University of Rochester School of Medicine and Dentistry, Rochester, New York 14642, USA

Glutamate is the main excitatory neurotransmitter in the mammalian central nervous system and is removed from the synaptic cleft by sodium-dependent glutamate transporters. To date, five distinct glutamate transporters have been cloned from animal and human tissue: GLAST (EAAT1), GLT-1 (EAAT2), EAAC1 (EAAT3), EAAT4, and EAAT5 (refs 1–5). GLAST and GLT-1 are localized primarily in astrocytes[6,7], whereas EAAC1 (refs 8, 9), EAAT4 (refs 9–11) and EAAT5 (ref. 5) are neuronal. Studies of EAAT4 and EAAC1 indicate an extrasynaptic localization on perisynaptic membranes that are near release sites[8–10]. This localization facilitates rapid glutamate binding, and may have a role in shaping the amplitude of postsynaptic responses in densely packed cerebellar terminals[12–15]. We have used a yeast two-hybrid screen to identify interacting proteins that may be involved in regulating EAAT4—the glutamate transporter expressed predominately in the cerebellum—or in targeting and/or anchoring or clustering the transporter to the target site. Here we report the identification and characterization of two proteins, GTRAP41 and GTRAP48 (for glutamate transporter EAAT4 associated protein) that specifically interact with the intracellular carboxy-terminal domain of EAAT4 and modulate its glutamate transport activity.

To identify proteins that interact with the C terminus of the EAAT4 protein, we used the last 77 amino acids of EAAT4 as bait to screen a rat brain complementary DNA library. We isolated two independent cDNA clones and called them GTRAP41 and GTRAP48 (for glutamate transporter-4-associated protein). Isolation of the full-length cDNAs by a series of 5′ and 3′ rapid amplification of cDNA ends (RACE) polymerase chain reactions (PCRs) showed that the largest open reading frame (ORF) for GTRAP41 is 7,164 base pairs (bp), which encodes a 2,388 amino-acid protein with a predicted relative molecular mass (M_r) of 270,958 (accession no. AF225960).

A BLAST search of the GenBank database showed that GTRAP41 possesses 87% identity with β-spectrin III (accession no. AB008567). GTRAP41 possesses seventeen 16-amino-acid spectrin repeats, two α-actinin domains and a pleckstrin homology (PH) domain (Fig. 1a). The largest ORF identified for GTRAP48 (accession no. AF225961) is 4,581 bp, which encodes a 1,527-amino-acid protein with a predicted M_r of 168,698. A BLAST search of the GenBank database showed that GTRAP48 is unique, but it possesses significant homology to the KIAA0380 cDNA encoded protein (90% identity) and RhoGEF, p115 (ref. 16). GTRAP48 possesses a PDZ domain, a regulatory G-protein-signalling sequence (LH),

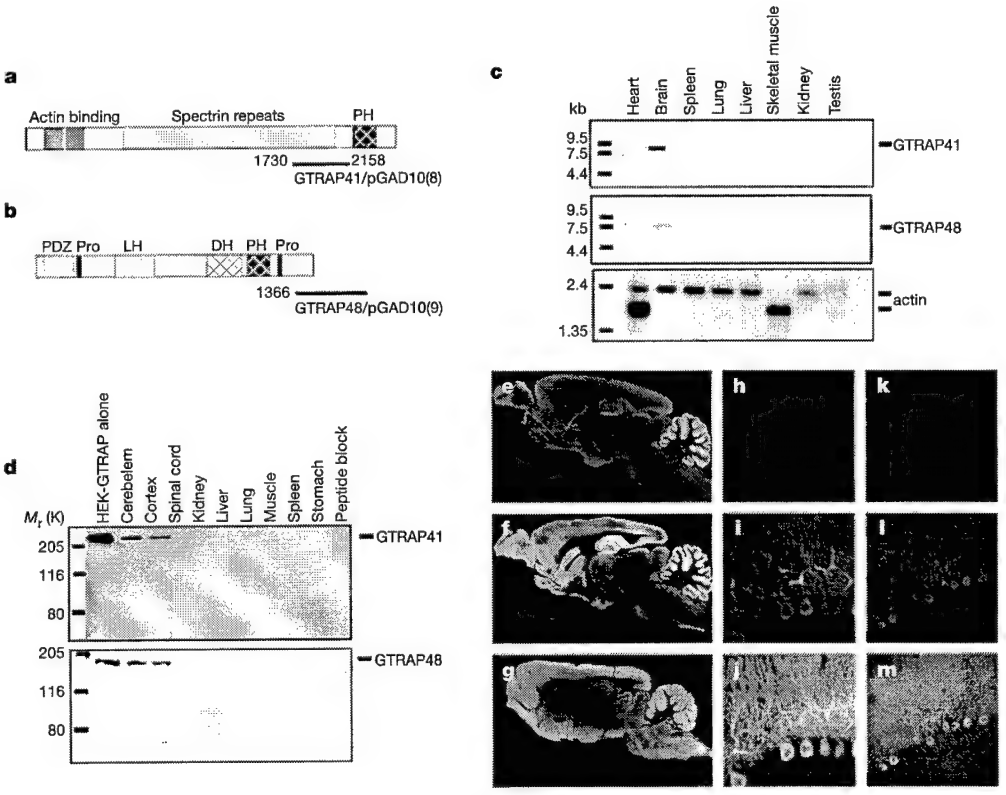

Figure 1 Structure and distribution of GTRAP41 and GTRAP48. **a**, **b**, cDNA clones GTRAP41/pGAD10 and GTRAP48/pGAD10 isolated from the yeast two-hybrid screen are shown aligned below representations of full-length GTRAP41 and GTRAP48, respectively. The number of times the clones were isolated is shown in parentheses. **c**, Multiple tissue northern (MTN; Clontech) blot probed with 3′ PCR probes of GTRAP41 and GTRAP48. **d**, Western analysis of GTRAP41 and GTRAP48. **e**–**g**, Rat brain sections stained with anti-EAAT4 (**e**), anti-GTRAP41 (**f**) and anti-GTRAP48 (**g**) antibodies. **h**–**m**, EAAT4 (**h**, **k**), GTRAP41 (**i**) and GTRAP48 (**l**) are all predominately expressed in the cell bodies and dendrites of Purkinje cells. The overlaps of GTRAP41 and GTRAP48 with EAAT4 are shown in **j** and **m**, respectively.

tandem dbl homology (DH) and pleckstrin homology (PH) domains characteristic of guanine nucleotide exchange factors for the Rho family of G proteins, and two proline-rich sequences (Fig. 1b).

Northern blot analysis detected a 8.3-kilobase (kb) GTRAP41 and a 7.5-kb GTRAP48 messenger RNA in brain tissue (Fig. 1c). Longer exposure revealed a low level of expression in liver and kidney for both GTRAP41 and GTRAP48. Anti-peptide antibodies were raised and the affinity-purified antibodies recognized a M_r 270,000 (270K) protein and a 170K protein, respectively, in HEK 293T cells transfected with full-length GTRAP41 and GTRAP48 cDNA (Fig. 1d). GTRAP41 and GTRAP48 were both selectively localized to brain, consistent with the northern blot analysis (Fig. 1d). EAAT4 is selectively localized to cerebellar Purkinje cells, although low-level expression is observed in cerebral cortex, hippocampus and striatum[9]. We found that GTRAP41 and GTRAP48 were expressed predominately in the cerebellum (Fig. 1e–g), with low-level immunoreactivity in striatum, hippocampus and thalamus. Immunofluorescence microscopy revealed that all three proteins are expressed in cerebellar Purkinje cell soma and dendrites, with little axonal staining (Fig. 1h–m).

We first confirmed the biochemical interaction between GTRAP41/GTRAP48 and EAAT4 by an *in vitro* binding assay. Full-length Myc-tagged GTRAP41 and GTRAP48 were expressed in HEK 293T cells. The solubilized cell extracts were then mixed with bead-linked glutathione *S*-transferase (GST)–EAAT4 or GST alone, and the bound proteins were eluted. GTRAP41 and GTRAP48 were retained specifically by the GST–EAAT4 fusion protein, but not by GST alone (Fig. 2a). A stable, rat EAAT4-expressing cell line was generated in HEK 293T cells (HEK-rEAT4) and transfected with cDNAs encoding Myc-tagged GTRAP41 and GTRAP48. We used antibodies directed at the amino terminus of EAAT4 to immunoprecipitate the antigen plus any associated protein. Western blot analysis using an anti-c-Myc antibody showed that GTRAP41 and GTRAP48 co-immunoprecipitated with EAAT4 (Fig. 2b).

Similarly, when the anti-c-Myc antibody was used, EAAT4 was co-immunoprecipitated with GTRAP41 and GTRAP48 (Fig. 2c). *In vivo*, GTRAP41 (Fig. 2d) and GTRAP48 (Fig. 2f) were co-immunoprecipitated with EAAT4 from brain by antibodies directed at the N terminus of EAAT4 but not by antibodies directed at the C terminus (Fig. 2d, f). As the site of interaction is within the C terminus of EAAT4, however, it is likely that the C-terminal antibodies disrupt the protein–protein interaction. Furthermore, GTRAP41 and GTRAP48 seem to interact specifically with EAAT4, as we could not co-immunoprecipitate GTRAP41 and GTRAP48 from brain with antibodies directed at other glutamate transporters (Fig. 2d, f).

Western blot analysis confirmed that the immunoprecipitating antibodies pulled down their corresponding antigen (see Supplementary Information). No co-immunoprecipitation was observed when the precipitating antibody was omitted or pre-absorbed (Fig. 2b, e, g). We next determined the region of EAAT4 that binds GTRAP41 and GTRAP48. We used a series of successively larger C-terminal deletions of the original, 77-amino-acid, C-terminal EAAT4 bait in a yeast two-hybrid screen. Residues 555–561 and 527–534 appear to be required for GTRAP41 and GTRAP48 binding, respectively.

As GTRAP48 possesses areas of homology to p115 and PDZRhoGEF, two RhoGEFs that selectively activate Rho[16,17], we investigated whether GTRAP48 interacts with the Rho family of GTPases. We measured the amount of GTP-γS that bound to GST–RhoA, GST–Cdc42 and GST–Rac in the presence of full-length GTRAP48 or p115, and found that GTRAP48, like p115, shows a specific guanine nucleotide exchange activity for Rho (Fig. 3a, b). Co-immunoprecipitation assays also showed that GTRAP48 interacts with the active form (in the presence of aluminium fluoride) but not the inactive form of the $G\alpha_{13}$ subunit and therefore, may act as a link between G-protein-coupled receptors and their downstream targets (Fig. 3c). Specificity of the $G\alpha_{13}$ antibody has been previously described[18].

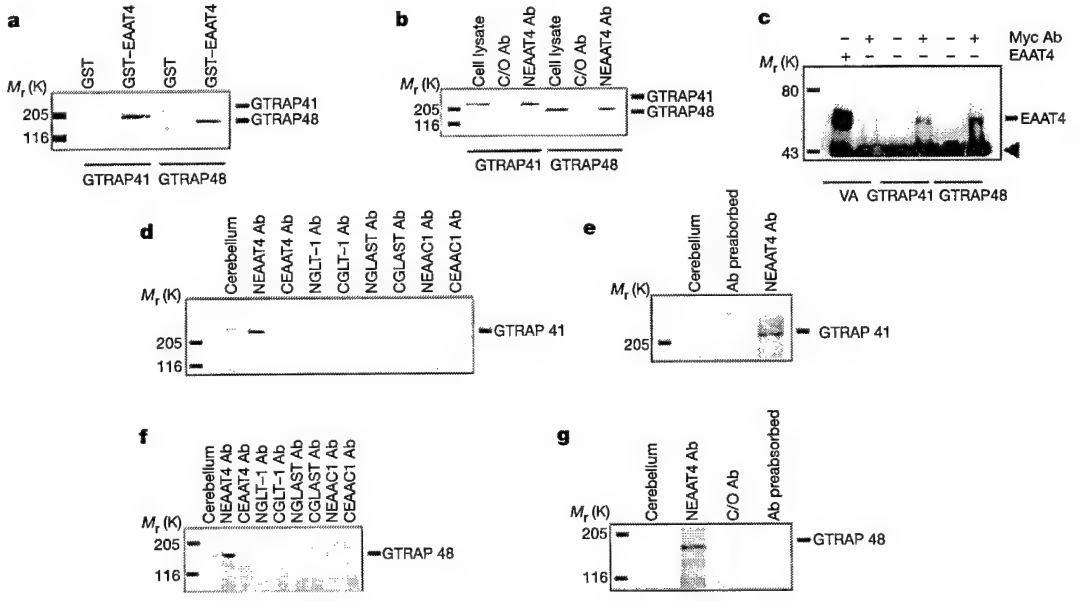

Figure 2 Interaction of GTRAP41 and GTRAP48 with EAAT4. **a**, Binding of Myc–GTRAP41 and Myc–GTRAP48 to GST–EAAT4. **b**, **c**, GTRAP41, GTRAP48 or vector alone (VA) were expressed (as indicated by the bars) in HEK-rEAAT4 cells. Immunoprecipitations were performed either with the N-terminal anti-EAAT4 antibody (**b**), or with the antibodies (Ab) indicated above the lanes (**c**). Immunoprecipitates were analysed by immunoblotting using anti-c-Myc (**b**) or C-terminal anti-EAAT4 (**c**; arrowhead indicates protein-A–Sepharose band) antibodies. **d**–**g**, Extracts of rat brain were immunoprecipitated with antibodies (**d**, **f**) directed at the N terminus and C terminus of the glutamate transporters (as indicated above the lanes), no antibody or antibody pre-absorbed with peptide (**e**, **g**). Immunoblots were probed with the anti-GTRAP41 (**d**, **e**) and the anti-GTRAP48 (**f**, **g**) antibodies.

Rho regulates the remodelling of the actin cytoskeleton through various actin-binding proteins, although the mechanism is not well characterized[19]. As GTRAP48 can activate Rho, we next determined whether the expression of GTRAP48 induced reorganization of the actin cytoskeleton and whether it altered the distribution of GTRAP41, a possible actin-binding protein. When GTRAP41 was expressed alone there was a close relationship between actin and GTRAP41 at the cell membrane, but there were very few organized actin filaments (Fig. 3d, e). Conversely, when GTRAP41 and GTRAP48 were co-expressed, GTRAP41 colocalized with actin in structures that resembled actin-stress fibres (Fig. 3f, g), a typical Rho-dependent effect. We noted that the overexpression of GTRAP48 also induced the formation of membrane ruffling and filopodia (Fig. 3h, i), suggesting some degree of cross-talk between the small GTPases, as these are typical Rac- and Cdc42-dependent effects.

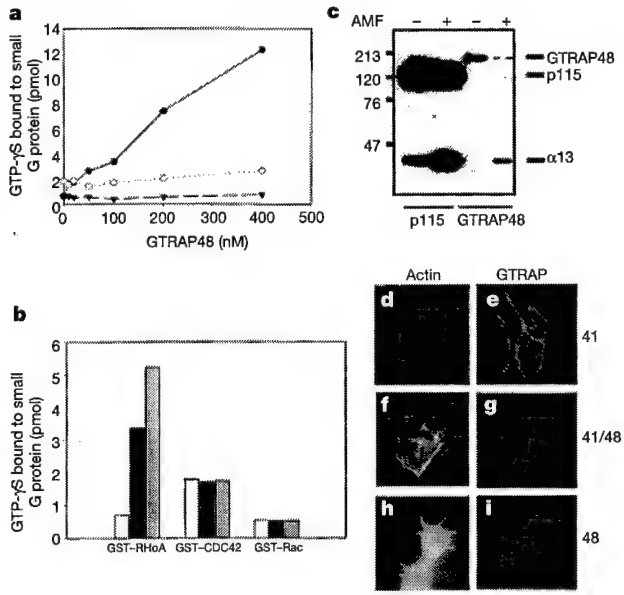

Figure 3 Guanine nucleotide exchange activity of GTRAP48. **a**, Binding of GTP-γS to GST–RhoA (filled circles), GST–CDC42 (open circles) and GST–Rac (filled triangles) was measured after 10 min at 30 °C in the presence of the indicated concentrations of full-length GTRAP48 as described in Methods. **b**, Binding of GTP-γS to the indicated GTPases in either the absence (white), or the presence of 100 nM GTRAP48 (black) or 100 nM p115-RhoGEF (grey). **c**, Binding of active $G\alpha_{13}$ to Glu-tagged (EE) GTRAP48 and p115 RhoGEF. **d–i**, HEK-rEAAT4 cells transfected with either vector alone (**d**, **e**), Myc-tagged GTRAP41 and GTRAP48 (**f**, **g**) or Myc-tagged GTRAP48 (**h**, **i**). Actin filaments were visualized with FITC- or rhodamine-conjugated phalloidin.

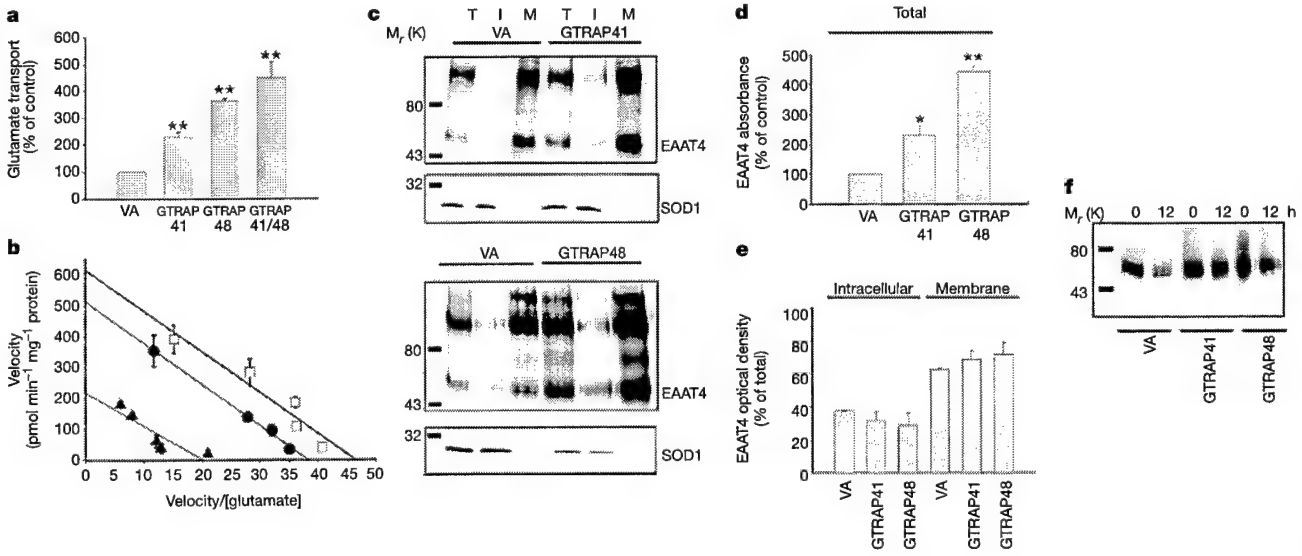

Figure 4 Effect of GTRAP41 and GTRAP48 on Na^+-dependent [^{3}H]L-glutamate uptake. **a**, GTRAP41 and GTRAP48 expression increased glutamate uptake (5 μM) significantly over cells transfected with vector alone (VA; $n = 4$; $^{**}P < 0.005$). **b**, Kinetic data showed that GTRAP41 (open squares) increased the V_{max} from 222 to 605 pmol mg^{-1} min^{-1} and increased the K_m slightly from 7 to 11 μM, as compared with EAAT4 alone (filled triangles). GTRAP48 increased the V_{max} from 208 to 512 pmol mg min^{-1} (filled circles) and increased the K_m from 10 to 13 μM. **c**, Immunoblots of total (T), intracellular (I), and biotinylated fractions (M) of HEK-rEAAT4 cells transfected with GTRAP41 and GTRAP48. **d**, Quantitation of immunoblots for total EAAT4 protein ($n = 3$; $^{**}P < 0.005$, $^{*}P < 0.05$). **e**, Ratio of membrane-bound to intracellular EAAT4. **f**, Cells transfected with GTRAP41, GTRAP48 or vector alone incubated with cycloheximide (10 μg ml^{-1}) for 12 h.

We determined whether there was a functional association between GTRAP41, GTRAP48 and EAAT4. We measured the sodium-dependent glutamate transport activity of HEK-rEAAT4 cells that had been transfected with one or both of the interacting proteins. GTRAP41 and GTRAP48 produced respective twofold and fourfold increases in glutamate transport (Fig. 4a), and their co-expression resulted in a further increase in glutamate uptake. Kinetic analysis indicated that GTRAP41 and GTRAP48 produced an increase in the V_{max} of glutamate transport activity (Fig. 4b). GTRAP41 and GTRAP48 may therefore enhance glutamate transport either through an increase in the catalytic rate of the transporter or through an increase in cell-surface availability.

To examine changes in the cell-surface levels of EAAT4, we used a cell-membrane-impermeant biotinylation reagent to label cell-surface proteins selectively. Figure 4c shows western analysis of a representative biotinylation experiment for GTRAP41 and GTRAP48. The total amount of EAAT4 increased when GTRAP41 and GTRAP48 were co-expressed (Fig. 4d); in contrast, the total amount of SOD1, a control for the total amount of protein loaded, was unaltered or decreased in the GTRAP41 or GTRAP48 samples, respectively. The percentage of total EAAT4 that was biotinylated remained the same when GTRAP41 and GTRAP48 were co-expressed, showing that most of the increase in total EAAT4 protein was located at the cell surface and not in an intracellular pool (Fig. 4e).

These results indicated that GTRAP41 and GTRAP48 stabilize and/or anchor EAAT4 at the cell membrane, making it less likely to be internalized and subsequently degraded; however, we could not rule out the possibility of increased expression of the cell's native gene. To address this issue, we treated cells with cycloheximide, an inhibitor of protein synthesis, 48 h after transfection (Fig. 4f). Densitometry showed that 12 h after treatment the EAAT4 protein in HEK-rEAAT4 cells was reduced to 54 ± 0.6% of its level before cycloheximide treatment. In contrast, 81 ± 2% and 74 ± 1.7% of the EAAT4 protein remained after 12 h when GTRAP41 and GTRAP48 were co-expressed, respectively. These results provide compelling evidence that GTRAP41 and GTRAP48 do stabilize EAAT4 at the membrane.

To determine whether the EAAT4/GTRAP48 interaction is required to mediate the increase in EAAT4 activity, we transfected HEK-rEAAT4 cells with GTRAP48 constructs lacking the last 155 amino acids, which were pulled out by EAAT4 in the yeast two-hybrid screen. The C-terminally truncated GTRAP48 had only a modest effect on stimulating EAAT4 activity, indicating that the protein–protein interaction is responsible for most of the increase in uptake activity (Fig. 5a). We also co-transfected HEK-rEAAT4 cells with GTRAP48 and a Myc-tagged cDNA construct encoding the last 77 amino acids of EAAT4, to disrupt the interaction of GTRAP48 with full-length EAAT4. We found that the co-expression of this construct inhibited the GTRAP48-mediated effect by about 25%, but co-expression of a smaller construct (residues 1,452–1,578), lacking the GTRAP48-binding domain, had no effect (Fig. 5b). Together, these results indicate that the EAAT4/GTRAP48 interaction is important in modulating EAAT4 uptake activity.

The physiological relevance of GTRAP41 and GTRAP48 on EAAT4 uptake activity *in vivo* was subsequently examined by the intra-cisternal injection of HSV amplicon vectors expressing GTRAP41 and GTRAP48. Cerebellar glutamate uptake was measured 48 h after injection, and was elevated when GTRAP41 and GTRAP48 were expressed but not when the control HSVlac amplicon vector was injected (Fig. 5c). Dihydrokainic acid (DHK), an inhibitor of GLT-1-mediated glutamate transport, had no effect on cerebellar glutamate uptake, ruling out any involvement of GLT-1. There is no method to distinguish functionally between GLAST, EAAC1 and EAAT4; but, as GTRAP41 and GTRAP48 do not interact directly with any other transporter, it is likely that the observed increase in uptake is due to an increase in EAAT4 activity. Western blot analysis confirmed an increased expression of GTRAP41 and GTRAP48 in the cerebellum after the injections. Preliminary studies of primary cultures of rat Purkinje cells indicate that EAAT4 and GTRAP41 may colocalize perisynaptically at 70% of synapses.

Glutamate transporters, through their rapid and efficient removal of glutamate from the synaptic cleft, are critical in glutamatergic plasticity and the prevention of glutamate-mediated excitotoxicity. Identifying and characterizing the glutamate transporter associated proteins GTRAP41 and GTRAP48 has begun to unravel the complex mechanism of glutamate uptake. In the modulation of EAAT4 glutamate transport, our findings implicate a role for G-protein signalling, a pathway that may involve Rho activation, and anchoring to the actin cytoskeleton (Fig. 5d). These proteins may also modulate the perisynaptic distribution of EAAT4 at glutamatergic synapses. Future studies are required to delineate the signalling pathway of GTRAP41 and GTRAP48, and how their interaction may be relevant to normal and abnormal glutamatergic neurotransmission, as altered EAAT4 function may be involved in the neurodegenerative disease spinocerebellar ataxia (SCA1)[20]. By understanding the physiological regulation of the EAAT4 transporter, we may be able to identify possible therapies for SCA1 or other toxic insults that lead to the degeneration of Purkinje cell neurons. □

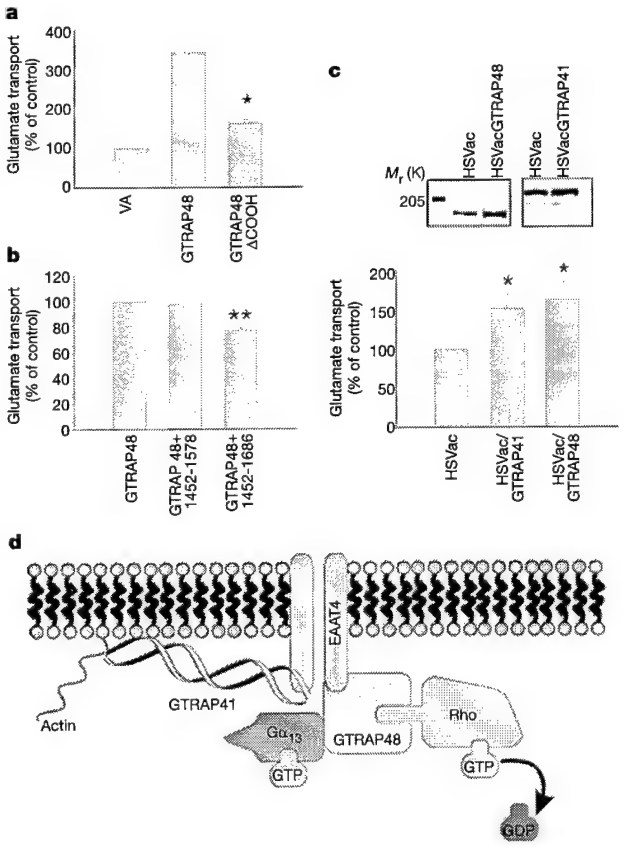

Figure 5 Modulation of EAAT4 activity. **a**, GTRAP48ΔCOOH results in a very small increase in EAAT4 uptake activity compared with full-length GTRAP48 (*$P < 0.05$). **b**, Overexpression of the EAAT4 C-terminus reduced the GTRAP48-mediated effect on EAAT4 activity (**$P < 0.005$). **c**, Intra-cisternal injection of HSVlac amplicons expressing GTRAP41 and GTRAP48 increased glutamate uptake *in vivo* ($n = 6$; *$P < 0.05$). Western blot analysis demonstrates increased expression of GTRAP41 and GTRAP48. **d**, A possible model of the coupling of EAAT4 to a Rho GTPase signal transduction cascade and to the actin cytoskeleton via GTRAP48 and GTRAP41. GDP, guanosine diphosphate; GTP, guanosine triphosphate.

Methods

Yeast two-hybrid screen

We screened a rat brain cDNA library (Clontech) using the final 77 amino acids of EAAT4 as bait (pGBT9). For the EAAT4 C-terminal domain analysis, different regions of the final 77 amino acids of EAAT4 were subcloned in-frame into the pGBT9 vector.

Cloning of full-length GTRAP41 and GTRAP48 cDNAs

Marathon cDNA amplification (CLONTECH) was used to perform both 5′- and 3′-RACE on cDNA synthesized from rat brain poly(A)$^+$ RNA.

Antibodies

Affinity-purified polyclonal antisera to EAAT4, GTRAP41 and GTRAP48 were generated as described[6]. We synthesized peptides corresponding to epitopes of EAAT4 (C-terminal, EKGASRGRGGNESA; N-terminal, KNSLFLRESGAGGGCL), rat GTRAP41 (KRGPAPSPMPQSRSSE) and rat GTRAP48 (KTPERTSPSHHRQPSD). The anti-c-Myc monoclonal antibody was from Boeringer Mannheim. For visualization of intracellular F-actin organization, the cells were probed with Texas-red-conjugated or fluorescein isothiocyanate (FITC)-conjugated phalloidin (Sigma).

Transfection and maintenance of HEK-rEAAT4 cells

The EAAT4 cDNA was subcloned into pcDNA3.1/Hygro(+) (Invitrogen) using the *Eco*RI restriction site. The plasmid was linearized with *Ssp*I and transfected into HEK 293T cells. Forty-eight hours after transfection, the cells were split to 50% confluency, and hygromycin (Invitrogen) was added at a concentration of 50 μg ml^{-1}. After about 2–3 weeks of selection, a serial dilution was carried out and cells were plated out, without selection, in a 96-well plate to obtain one cell per well. Several colonies were picked, expanded in selective medium and checked for expression by western blotting.

Fusion proteins and *in vitro* binding

Full-length EAAT4 was subcloned into the *Eco*RI site of the GST–fusion vector pGEX-6P-1 (Pharmacia). Synthesis of recombinant proteins in BL21 cells (Novagen) was induced by 0.1 mM isopropyl β-D-thiogalactoside for 2 h at 30 °C and purified according to the protocol provided by Pharmacia. HEK 293T cells were transfected with Myc-tagged GTRAP41 or GTRAP48 and gathered in ice-cold immunoprecipitation (IP) buffer. The cellular lysate was incubated with GST or GST–EAAT4 immobilized on glutathione–Sepharose-4B, and washed to remove nonspecifically bound proteins. Specifically bound proteins were eluted with 2× SDS loading buffer and analysed by immunoblotting using an anti-c-Myc antibody.

Co-immunoprecipitation

Full-length GTRAP41 and GTRAP48 cDNAs were subcloned into the *Not*I site of a Myc-tagged pRK5 vector and used to transfect HEK-rEAAT4 cells. After transfection (48–72 h), cells were solubilized with 1 ml of ice-cold IP buffer for 2 h at 4 °C with rotation and centrifuged to remove cellular debris. Antibody was added to 0.5 ml of supernatant and incubated overnight at 4 °C. We dissected and prepared the cerebellum from a Sprague-Dawley rat as described[21]. For each immunoprecipitation, 500 μg of the Triton-lysate was incubated overnight at 4 °C with 5 μg of antibody. Protein-A–Sepharose (Pharmacia) was then added for 2 h at 4 °C, washed once with IP buffer and three times with IP buffer minus Triton X-100. Bound protein was eluted by boiling in 2× SDS loading buffer, and analysed by immunoblotting.

Immunohistochemistry

Rat brain sections were stained as described[9], using the following antibodies: C-terminal anti-EAAT4 (1.5 μg ml^{-1}), anti-GTRAP41 (127 ng ml^{-1}) or anti-GTRAP48 (132 ng ml^{-1}) antibodies. Texas-red and FITC-conjugated secondary antibodies were used at dilutions of 1:200.

Guanine nucleotide exchange assay

Small G proteins GST–RhoA, GST–CDC42 and GST–Rac were expressed in bacterial cells and affinity purified to ~80% purity using a glutathione column. We incubated 20 pmoles of each protein with 100 pmoles GTP-γS for 10 min at 30 °C with varying concentrations of full-length GTRAP48 or p115. The binding reactions were filtered through BA-85 nitrocellulose and the amount of GTP-γS bound to small G protein was quantified by scintillation counting of the dried filters. Binding of $G\alpha_{13}$ to GTRAP48 was assayed as described[18].

Na^+-dependent glutamate transport activity

HEK-rEAAT4 cells transfected with GTRAP41 and GTRAP48 were grown in a monolayer on six-well plates, and assays were conducted 72 h after transfection as described[22]. We subcloned GTRAP41 and GTRAP48 into the *Eco*RI site of HSVPrPUC amplicon parent vector[23]. Amplicon vector DNA (3.6 μg) and pBAC-V2 DNA (25 μg) were used to transfect 2×10^7 baby hamster kidney cells as described[24]. Virus was collected 72 h after transfection, and titred as described[25]. Expression particles (2×10^5) were injected intracisternally into male Sprague-Dawley rats (250 g) obtained from Zivic Miller. Forty-eight hours after injection the rats were killed, synaptosomal preparations of the cerebelli were prepared using a polytron, and glutamate uptake was measured.

Biotinylation

Biotinylation of cell-surface proteins was done as described[26]. We used SOD1 to control for total protein and to determine whether the biotinylation reagent labels proteins in the intracellular compartment.

Statistics

Statistical differences were determined by Students's *t*-test for two-group comparisons.

Received 28 April; accepted 18 December 2000.

1. Storck, T., Schulte, S., Hofmann, K. & Stoffel, W. Structure, expression, and functional analysis of a Na^+-dependent glutamate/aspartate transporter from rat brain. *Proc. Natl Acad. Sci. USA* **89,** 10955–10959 (1992).
2. Kanai, Y. & Hediger, M. A. Primary structure and functional characterization of a high-affinity glutamate transporter. *Nature* **360,** 467–471 (1992).
3. Pines, G. *et al.* Cloning and expression of a rat brain L-glutamate transporter. *Nature* **360,** 464–467 (1992); erratum *ibid.* **360,** 768 (1992).
4. Fairman, W. A., Vandenberg, R. J., Arriza, J. L., Kavanaugh, M. P. & Amara, S. G. An excitatory amino-acid transporter with properties of a ligand-gated chloride channel. *Nature* **375,** 599–603 (1995).
5. Arriza, J. L., Eliasof, S., Kavanaugh, M. P. & Amara, S. G. Excitatory amino acid transporter 5, a retinal glutamate transporter coupled to a chloride conductance. *Proc. Natl Acad. Sci. USA* **94,** 4155–4160 (1997).
6. Rothstein, J. D. *et al.* Localization of neuronal and glial glutamate transporters. *Neuron* **13,** 713–725 (1994).
7. Danbolt, N. C., Storm-Mathisen, J. & Kanner, B. I. An [Na^+ + K^+]coupled L-glutamate transporter purified from rat brain is located in glial cell processes. *Neuroscience* **51,** 295–310 (1992).
8. He, Y., Janssen, W. G., Rothstein, J. D. & Morrison, J. H. Differential synaptic localization of the glutamate transporter EAAC1 and glutamate receptor subunit GluR2 in the rat hippocampus. *J. Comp. Neurol.* **418,** 255–269 (2000).
9. Furuta, A., Martin, L. J., Lin, C. L., Dykes-Hoberg, M. & Rothstein, J. D. Cellular and synaptic localization of the neuronal glutamate transporters excitatory amino acid transporter 3 and 4. *Neuroscience* **81,** 1031–1042 (1997).
10. Dehnes, Y. *et al.* The glutamate transporter EAAT4 in rat cerebellar Purkinje cells: a glutamate-gated chloride channel concentrated near the synapse in parts of the dendritic membrane facing astroglia. *J. Neurosci.* **18,** 3606–3619 (1998).
11. Nagao, S., Kwak, S. & Kanazawa, I. EAAT4, a glutamate transporter with properties of a chloride channel, is predominantly localized in Purkinje cell dendrites, and forms parasagittal compartments in rat cerebellum. *Neuroscience* **78,** 929–933 (1997).
12. Tong, G. & Jahr, C. E. Block of glutamate transporters potentiates postsynaptic excitation. *Neuron* **13,** 1195–1203 (1994).
13. Diamond, J. S. & Jahr, C. E. Transporters buffer synaptically released glutamate on a submillisecond time scale. *J. Neurosci.* **17,** 4672–4687 (1997).
14. Overstreet, L. S., Kinney, G. A., Liu, Y. B., Billups, D. & Slater, N. T. Glutamate transporters contribute to the time course of synaptic transmission in cerebellar granule cells. *J. Neurosci.* **19,** 9663–9673 (1999).
15. Barbour, B., Keller, B. U., Llano, I. & Marty, A. Prolonged presence of glutamate during excitatory synaptic transmission to cerebellar Purkinje cells. *Neuron* **12,** 1331–1343 (1994).
16. Hart, M. J. *et al.* Identification of a novel guanine nucleotide exchange factor for the Rho GTPase. *J. Biol. Chem.* **271,** 25452–25458 (1996).
17. Fukuhara, S., Murga, C., Zohar, M., Igishi, T. & Gutkind, J. S. A novel PDZ domain containing guanine nucleotide exchange factor links heterotrimeric G proteins to Rho. *J. Biol. Chem.* **274,** 5868–5879 (1999).
18. Hart, M. J. *et al.* Direct stimulation of the guanine nucleotide exchange activity of p115 RhoGEF by Gα13. *Science* **280,** 2112–2114 (1998).
19. Hall, A. Rho GTPases and the actin cytoskeleton. *Science* **279,** 509–514 (1998).
20. Lin, X., Antalffy, B., Kang, D., Orr, H. T. & Zoghbi, H. Y. Polyglutamine expansion down-regulates specific neuronal genes before pathologic changes in SCA1. *Nature Neurosci.* **3,** 157–163 (2000).
21. Blackstone, C. D. *et al.* Biochemical characterization and localization of a non-*N*-methyl-D- aspartate glutamate receptor in rat brain. *J. Neurochem.* **58,** 1118–1126 (1992).
22. Davis, K.E. *et al.* Multiple signaling pathways regulate cell surface expression and activity of the excitatory amino acid carrier 1 subtype of Glu transporter in C6 glioma. *J. Neurosci.* **18,** 2475-2485 (1998).
23. Geller, A.I., Keyomarsi, K., Bryan, J. & Pardee, A.B. An efficient deletion mutant packaging system for defective herpes simplex virus vectors: potential applications to human gene therapy and neuronal physiology. *Proc. Natl Acad. Sci. USA* **87,** 8950–8954 (1990).
24. Stavropoulos, T. A. & Strathdee, C. A. An enhanced packaging system for helper-dependent herpes simplex virus vectors. *J. Virol.* **72,** 7137–7143 (1998).
25. Bowers, W. J., Howard, D. F. & Federoff, H. J. Discordance between expression and genome transfer titering of HSV amplicon vectors: recommendation for standardized enumeration. *Mol. Ther.* **1,** 294–299 (2000).
26. Duan, S., Anderson, C. M., Stein, B. A. & Swanson, R. A. Glutamate induces rapid upregulation of astrocyte glutamate transport and cell-surface expression of GLAST. *J. Neurosci.* **19,** 10193–10200 (1999).

Supplementary information is available on *Nature*'s World-Wide Web site (http://www.nature.com) or as paper copy from the London editorial office of *Nature*.

Acknowledgements

We thank N. J. Maragakis, M. Watanabe, A. Sawa, R. Ganel, J. Llado and R. Law for discussions, advice and help. We thank R. Huganir for the pRK5 vector and D. Howard for technical assistance. This work was supported by the NIH.

Correspondence and requests for materials should be addressed to J.D.R. (e-mail: jrothste@welchlink.welch.jhu.edu). The GenBank accession numbers are AF225960 (GTRAP41) and AF225961 (GTRAP48).

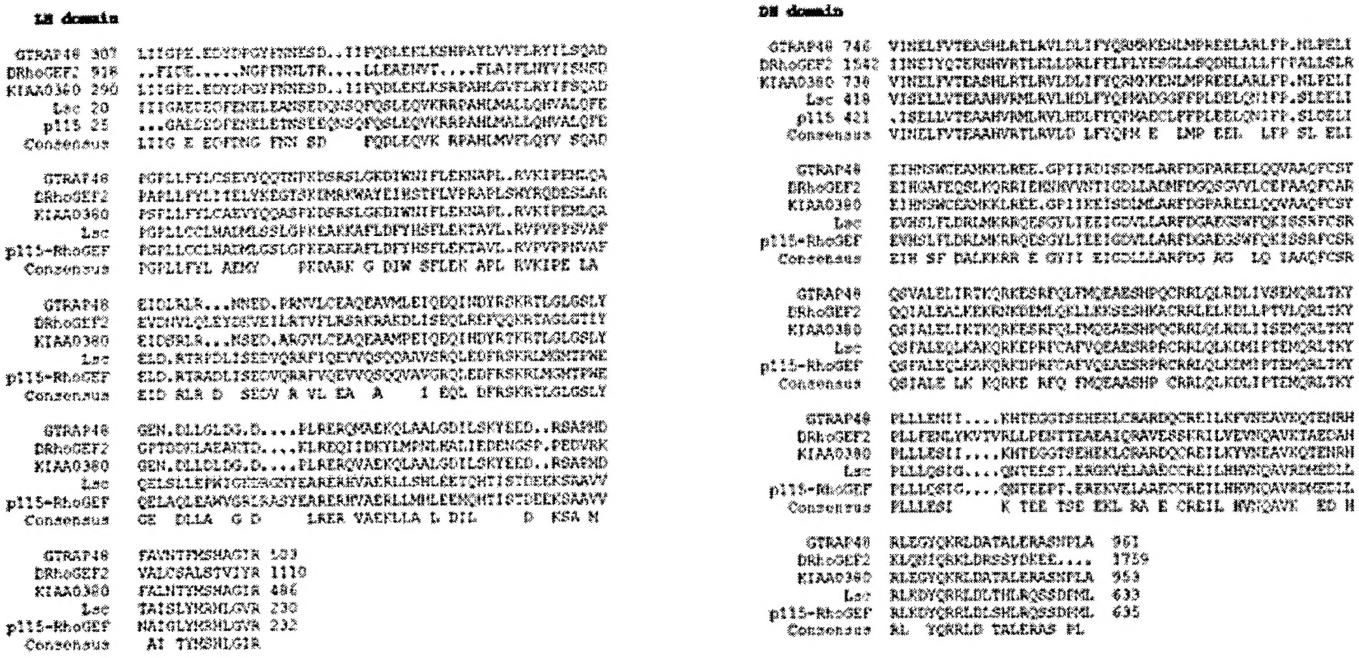

Supplemental Figure 1. Comparison of GTRAP48 with other RhoGEFs. Alignment of the LH and DH domains of GTRAP48 with KIAA0380 (AB002378), p115 (U64105), DRhoGEF2 (AF032870) and Lsc (U58203).

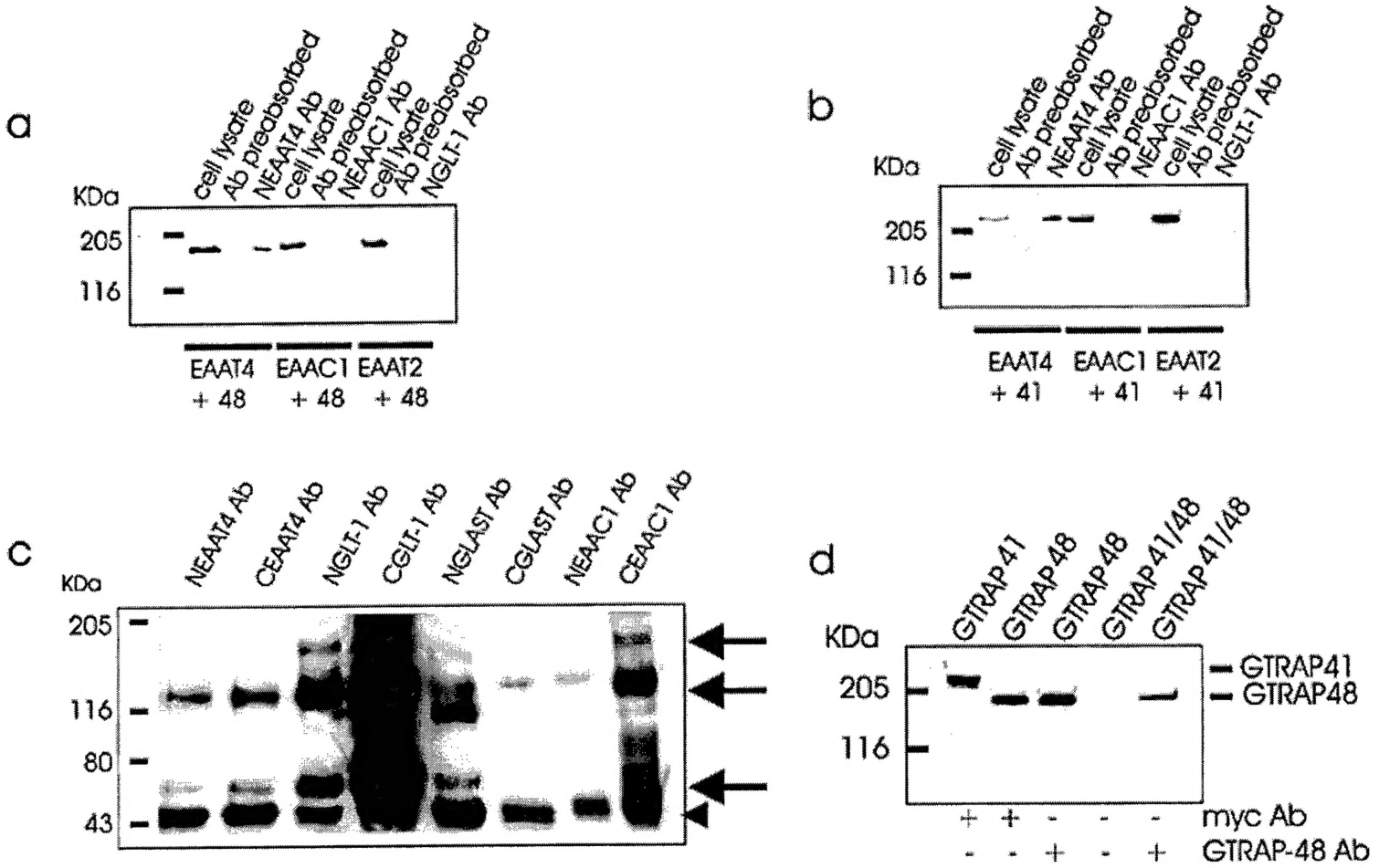

Supplemental Figure 2. Additional coimmunoprecipitation controls. HEK 293T cells were transfected with glutamate transporters and either GTRAP48 (a) or GTRAP41 (b), as indicated below the lanes. Coimmunoprecipitations were performed using antibodies directed at the transporter or antibodies preabsorbed with the corresponding peptide (as shown above the lanes), and the immunoblots were probed with an anti-c-myc antibody. c, Immunoblot probed with antibodies against the transporters shows that all the antibodies immunoprecipitated their corresponding antigen (indicated with arrows). High molecular weight bands are the multimeric forms of the transporters. Arrowhead indicates the protein-A sepharose band. d, Coimmunoprecipitation from HEK 293T cells cotransfected with myc-tagged GTRAP41 and GTRAP48 by the antibodies indicated below the lanes shows that there is probably no direct interaction between GTRAP41 and GTRAP48.

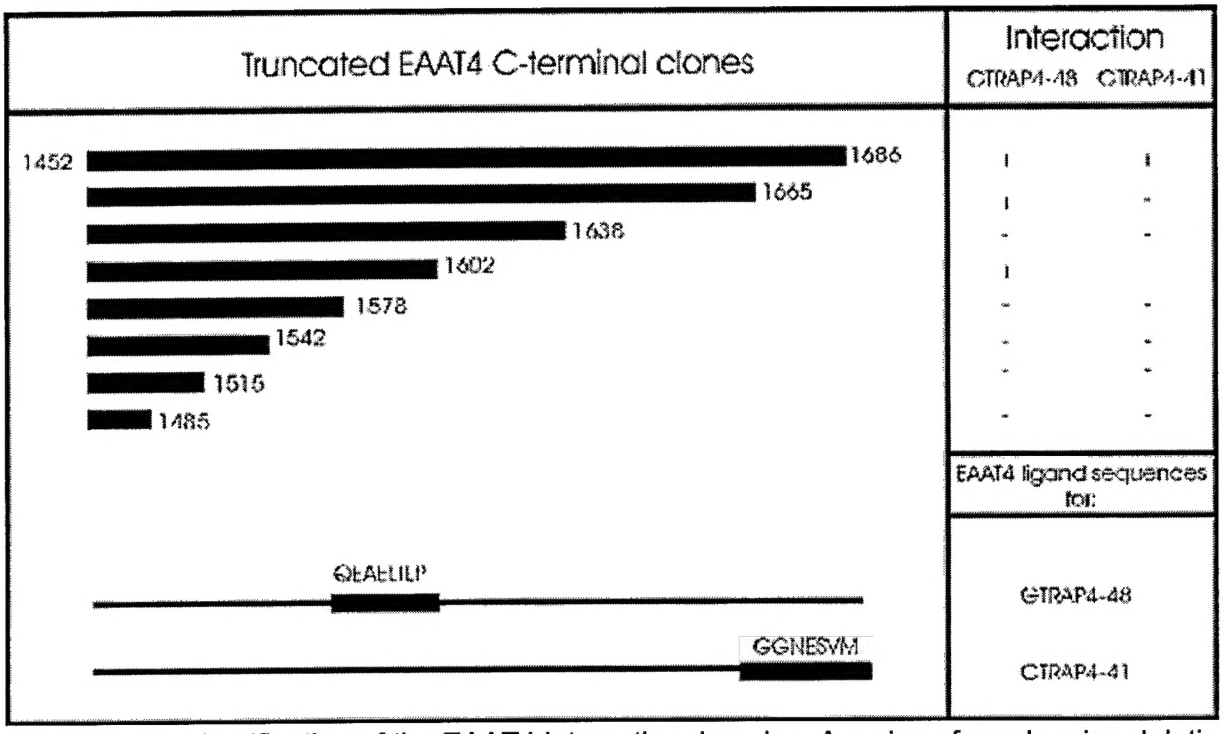

Supplemental Figure 3. Identification of the EAAT4 interacting domains. A series of overlapping deletion mutants of the C-terminus of EAAT4 were constructed using specific primers and PCR, and used in the yeast two-hybrid to determine the region of interaction. Protein-protein interaction was measured by a filter b-galactosidase assay